Université d'Ottawa · University of Ottawa

Université d'Ottawa · University of Ottawa

FACULTÉ DES ÉTUDES SUPÉRIEURES ET POSTDOCTORALES

FACULTY OF GRADUATE AND POSTDOCTORAL STUDIES

Liguo YANG

AUTEUR DE LA THÈSE - AUTHOR OF THESIS

M. A. Sc. (Electrical Engineering)

GRADE - DEGREE

Department of Electrical Engineering

FACULTÉ, ÉCOLE, DÉPARTEMENT - FACULTY, SCHOOL, DEPARTMENT

TITRE DE LA THÈSE - TITLE OF THE THESIS

Incorporation of dispersive Materials in the Envelope Finite Element (EVFE) Method

D.A. McNamara

DIRECTEUR DE LA THÈSE - THESIS SUPERVISOR

CO-DIRECTEUR DE LA THÈSE - THESIS CO-SUPERVISOR

EXAMINATEURS DE LA THÈSE - THESIS EXAMINERS

M. Yagoub

Q.J. Zhang

J.-M. De Koninck, Ph.D.

LE DOYEN DE LA FACULTÉ DES ÉTUDES SUPÉRIEURES ET POSTDOCTORALES

DEAN OF THE FACULTY OF GRADUATE AND POSTDOCTORAL STUDIES

INCORPORATION OF DISPERSIVE MATERIALS IN THE ENVELOPE FINITE ELEMENT (EVFE) METHOD

by

Liguo Yang

A thesis submitted to the

Faculty of Graduate and Post-Doctoral Studies

Master of Applied Science

in Electrical Engineering

Ottawa-Carleton Institute for Electrical and Computer Engineering

School of Information Technology and Engineering

Faculty of Engineering

University of Ottawa

May 2004

Your file Votre référence
ISBN: 0-494-01653-1
Our file Notre référence
ISBN: 0-494-01653-1

CONTENTS

ABSTRACT

In this thesis computationally efficient methods of including materials with Lorentz-type dispersion in the envelope finite-element time-domain (EVFE) method are developed and presented. A new perfectly matched layer (PML) mesh truncation scheme, which allows the PML to be applied in Lorentz-type dispersive material has also been derived. These new formulations have been implemented and applied to specific examples, and the approach validated through comparison with results obtained using alternative methods. In particular, it has been demonstrated through the examples that the method developed preserves the large-time-step advantage of the EVFE over the conventional finite-element time-domain (FETD) method.

Acknowledgments

I would like to express my gratitude to my supervisor Dr. Derek A. McNamara for his trusting of my abilities, his instruction and his encouragement. I thank Dr. Pierre Berini for providing partial financial support for this work.

I also want to thank my fellow graduate students Ms. Xiangjun Meng, Ms. Xiaowen Liu, Mr. Wei Fang, and Mr. Junjie Lu. Their discussions, suggestions, and encouragement helped me greatly.

I also want to acknowledge my parents. Although they were not here they still managed to help me in every possible way and continued to give me encouragement.

Finally, but foremost, I gratefully acknowledge my beloved wife Guangjun Liu. Without her great sacrifice and support I would not have been able to finish this thesis. It is to her that this thesis is dedicated.

CHAPTER 1

INTRODUCTION

1.1 BACKGROUND

There are a number of numerical methods available for electromagnetic modeling. In recent years, the rapid development of powerful computers and increased memory capacity has lead to direct solution of the Maxwell equations in the time-domain. This lets us obtain the transient response and wideband information in a single simulation. The finite-difference time-domain (FDTD) method [1] is the most widely used of such methods due to its numerical efficiency and the simplicity of its formulation and implementation. One difficulty is that of dealing with irregular structures using the FDTD method. An alternative (but less widely used) technique, called the finite-element time-domain (FETD) method, is able to accommodate geometrically irregular structures in a more natural way [2,3,4]. As its name implies, the FETD method applies the conventional finite-element approach [5] by expressing the spatial variation of the unknowns in a differential equation in terms of a series of selected expansion functions. The coefficients of the series expansion become the unknowns. In the FETD method these coefficients are permitted to be functions of time, and the method determines the values of the coefficients in successive time steps, through solution of a matrix equation at each time step. Although used in the civil engineering literature for many years [6], the FETD method has over the past few years started to make in-roads in electromagnetic engineering practice.

The larger the allowed time-step, the more efficient would be the FETD method, since the matrix equations would need to be solved a fewer number of times. However, accuracy considerations dictate that the time-discretisation not be too coarse. The time-domain waveform has to be sampled at a minimum of twice the highest signal frequency. In many practical applications the input signals to these structures consist of modulated RF carriers, with signals bandwidths very narrow compared to the carrier frequency. If this form of input (i.e. a time-varying envelope modulating a sinusoidal signal) is made an inherent assumption in the formulation of the FETD method itself, one arrives at the so-called envelope finite-element (EVFE) method [7]. The idea is based on similar approaches used in circuit analysis [8,9], except in the EVFE approach it is applied to Maxwell's equations instead of the Kirchoff laws. The resulting method is one in which marching-on-in-time is performed on the signal envelope (which is very much more slowly varying than the carrier itself) on top of the finite-element method used to disretise the spatial domain. As only the signal envelope needs to be sampled, much larger time-steps (i.e. a coarser sampling in time) can be used with the EVFE technique than with either the FDTD or FETD methods.

Means of incorporating many types of dispersive media in the FDTD method are relatively well-established [1]. More recently ways of doing so for plasma-type, Debye-type and Lorentz-type media have also been devised for the FETD technique [10]. Direct evaluation of the associated convolution integrals that appear in the time-stepping scheme is feasible since the time-step needed for accurate FETD results is at once also suitable for accurate evaluation of the said convolution integral.

The advantage of the EVFE method over the direct FETD method is that a much larger time step can be used. The difficulty that arises when dispersive material is present is that there is a convolution integral in the time-domain difference equation that cannot be accurately calculated if this relatively large time step is used. If the dispersive material is of the Debye-type or plasma-type, whose expressions involving the susceptibilities have only exponential terms, it is relatively easy and possible to remove the convolution integral from the time-domain difference equation [11]. However, this is not easy even is not possible for some materials that have complex susceptibilities such as Lorentz-type dispersion media. A method is developed in this thesis for applying the EVFE in the presence of Lorentz-type material without having to compute the convolution integral in the time-domain difference equation, thus preserving the ability to use the larger time step.

1.2 OVERVIEW OF THE THESIS

In Chapter 2, the use of the FETD and EVFE, in the presence of non-dispersive material, is introduced. This provides an opportunity to introduce the notation that will be used in later chapters. Before proceeding to consider the difficulties in applying either the FETD or EVFE when dispersive materials are present we briefly review the various models that exist to describe the electromagnetic behaviour of such materials. The remainder of the chapter is devoted to a discussion of how the EVFE formulation changes when material dispersion has to be accounted for, and the limitations of existing

formulations. This leads quite naturally to Chapter 3, where these limitations are removed through the development of a new technique for including quite general dispersive material (in particular Lorentz-type material).

In Chapter 3, the three methods of analyzing Lorentz media with EVFE are presented. We use as a vehicle the two-dimensional scalar formulation applicable to so-called TM problems, which will already have been encountered in Chapter 2. The first two such methods preserve the larger time step capability of the EVFE approach, and hence are the ones intended to use. The third is essentially a "brute force" application of the convolution integral, which does not preserve the larger time step advantage of the EVFE method, and is essentially included simply as a means of measuring the effectiveness of the other two approaches. Since it is necessary to truncate the solution region when using the FDTD, FETD or EVFE, Chapter 3 also introduces some straightforward changes that are needed when applying perfectly matched layers (PMLs) for this purpose when these are adjacent to dispersive material. Although not the major contribution of this thesis the results are not available elsewhere and it is useful to provide them here.

In Chapter 4 the formulations developed in Chapter 3 are applied to specific examples for which analytical solutions are available. In this way the new approaches to the inclusion of Lorentz-type materials in the EVFE method are validated.

Finally, some general conclusions are reached in Chapter 5, and the research reported herein put into perspective.

CHAPTER 2

REVIEW OF THE USE OF FINITE ELEMENT BASED METHODS IN TIME-DOMAIN COMPUTATIONAL ELETROMAGNETICS

2.1 INTRODUCTION

Although the contributions in this thesis are applicable to problem geometries of a quite general nature, the detailed discussion will center on a specific problem. In order to describe the development of a technique for including Lorentz media in the EVFE method we will consider a geometry and incident field that allows the problem to be reduced to one with a scalar unknown that is a function of two spatial variables only. Once the technique has been fully developed and validated the extension to fully three-dimensional vectorial status is relatively straightforward.

In Section 2.2 we describe the specific problem geometry around which the theoretical developments will be done, and the associated two-dimensional scalar differential equation in the frequency domain. It is initially assumed that all materials are non-dispersive. The manner in which the finite element method (*FEM*) would be applied to discretrise this differential equation and obtain a numerical solution is described in Section 2.3. Section 2.4 describes how the time-domain form of the above differential equation can be discretised – the FEM is used to discretise it with respect to the spatial

coordinates and the Newmark scheme to discretise it with respect to the time variable. This combination is referred to as the finite-element time-domain (*FETD*) method. In Section 2.5 the modification of the FETD method for the case of a modulated carrier, and which is known as the envelope finite-element time-domain (EVFE) method, is introduced. This thesis is concerned with the development of an EVFE formulation that can be used in the presence of materials exhibiting Lorentz-type dispersion. Thus Section 2.6 briefly describes various models for dispersive materials. Section 2.7 provides a literature review of existing methods to deal with material dispersion in FETD and EVFE approaches, and we are therefore able to identify (in Section 2.8) the shortcomings that are removed as a result of the contributions of this thesis.

2.2 A TWO-DIMENSIONAL ELECTROMAGNETIC FIELD FORMULATION

Consider the problem shown in Figure 2.1.

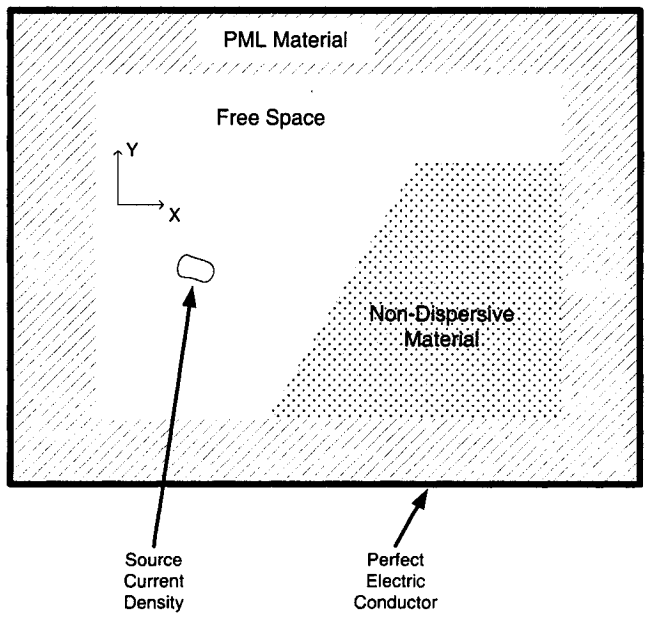

Figure 2.1 Two-Dimensional TM_z problem geometry. The outer perfectly conducting boundary is C, and S is the region inside C

Here we will use PML Boundary Condition. This is a two-dimensional geometry (that is, it is infinitely long along the z-axis), and the cross-section is shown in the figure. In addition, the impressed electric current density is also infinitely long along the z-axis, is entirely z-directed, and is not a function of the variable z. In other words, $\bar{J}(x,y,z) = \hat{z}J_z(x,y)$. As a result, the resulting electric field will be entirely z-directed and independent of the variable z. Thus for this problem we can write $\bar{E}(x,y,z) = \hat{z}E_z(x,y)$. The three-dimensional vector wave equation simplifies in this case to the two-dimensional wave equation [12]

$$\begin{aligned} &\omega^2 \underset{\sim}{\varepsilon}_0 \underset{\sim}{\mu}_0 \underset{\sim}{\varepsilon}_r \underset{\sim}{\bar{E}}_z(x,y,\omega) - \nabla\times\left(\underset{\sim}{\mu}_r^{-1}\right)\nabla\times\underset{\sim}{\bar{E}}_z(x,y,\omega) \\ &= j\omega\underset{\sim}{\mu}_0\underset{\sim}{\bar{J}}_z(x,y,\omega) \end{aligned} \tag{2.2.1}$$

where

$\underset{\sim}{E}_z$ electric field intensity
ε_r relative electric permittivity
ε_0 free-space electric permittivity
μ_r relative magnetic permeability
μ_0 free-space magnetic permeability
$\underset{\sim}{J}_z$ the source current density
$\bar{}$ denotes vector
$\underset{\sim}{}$ denotes frequency domain

Since to any vector $\bar{E}$ we have

$$\nabla\times\nabla\times\bar{E} = \nabla\nabla\cdot\bar{E} - \nabla^2\bar{E} \tag{2.2.2}$$

If we assume that there are no electric charges in the computational area, we have

$$\nabla\cdot\underset{\sim}{\bar{E}}_z(x,y,\omega) = 0 \tag{2.2.3}$$

Using (2.2.2) and (2.2.3) if $\underset{\sim}{\mu}_r^{-1}$ is position independent we can simplify (2.2.1) to be a scalar wave equation

$$\begin{aligned}&\nabla_t^2\left(\underset{\sim}{\mu}_r^{-1}\underset{\sim}{E}_z(x,y,\omega)\right)+\omega^2\,\varepsilon_0\,\underset{\sim}{\mu}_0\underset{\sim}{\varepsilon}_r\underset{\sim}{E}_z(x,y,\omega)\\&=j\omega\,\underset{\sim}{\mu}_0\underset{\sim}{J}_z(x,y,\omega)\end{aligned}\tag{2.2.4}$$

and is referred to as a TM_z type problem.

We can rewrite (2.2.4) as

$$\nabla_t^2\left(\underset{\sim}{\mu}_r^{-1}\underset{\sim}{E}_z(x,y,\omega)\right)+\frac{\omega^2}{c_0^2}\underset{\sim}{\varepsilon}_r\,\underset{\sim}{E}_z(x,y,\omega)=j\omega\mu_0\,\underset{\sim}{J}_z(x,y,\omega)\tag{2.2.5}$$

where c_0 is the velocity of the light in free space.

2.3 THE FINITE-ELEMENT METHOD (*FEM*) IN THE FREQUENCY DOMAIN

The derivation in this section follows that in [13, pp 28-29, pp 39-45, pp 100-108].using the scalar testing function T(x,y) to test the equation (2.2.5), we have:

$$\begin{aligned}&\int_S T(x,y)\nabla_t^2\left(\underset{\sim}{\mu}_r^{-1}\underset{\sim}{E}_z(x,y,\omega)\right)dS+\int_S\frac{\varepsilon_r\omega^2}{c_0^2}\,T(x,y)\,\underset{\sim}{E}_z(x,y,\omega)\,dS\\&=\int_S j\omega\mu_0\,T(x,y)\,\underset{\sim}{J}(x,y,\omega)\,dS\end{aligned}\tag{2.3.1}$$

According to the Green's theorem [14]

$$\begin{aligned}\int_S T(x,y)\,\nabla^2\left(\mu_r^{-1}\underset{\sim}{E}_z(x,y,\omega)\right)dS=&-\int_S\nabla T(x,y)\cdot\nabla\left(\mu_r^{-1}\underset{\sim}{E}_z(x,y,\omega)\right)dS\\&+\oint_C T(x,y)\,\nabla\left(\mu_r^{-1}\underset{\sim}{E}_z(x,y,\omega)\right)\cdot\hat{n}\,dC\end{aligned}\tag{2.3.2}$$

where C and S are defined in Figure 2.1, and $\hat{n}$ is the unit normal vector pointing outward from C.

If we substitute (2.3.2) into (2.3.1) we can obtain:

$$\int_S \frac{\varepsilon_r \omega^2}{c_0^2} T(x,y)\, \underset{\sim}{E}_z(x,y,\omega)\, dS - \int_S \nabla T(x,y) \cdot \nabla \left(\mu_r^{-1}\, \underset{\sim}{E}_z(x,y,\omega) \right) dS$$
$$+ \oint_C T(x,y)\ \nabla \left(\mu_r^{-1}\, \underset{\sim}{E}_z(x,y,\omega) \right) \cdot \hat{n}\, dC = \int_S j\omega\mu_0\ T(x,y)\, \underset{\sim}{J}_z(x,y,\omega)\, dS \tag{2.3.3}$$

In order to simplify the notation, in the following expressions, we will remove the subscript z from all the field and source quantities.

Next we divide the calculation region into a certain number of finite elements that are not overlapped. Then we can approximate the function $\underset{\sim}{E}(x,y,\omega)$ by $\underset{\sim}{E}^e(x,y,\omega)$ within each element, and interrelate the all functions in the various elements so that the function $\underset{\sim}{E}(x,y,\omega)$ will be continuous across the elements' boundaries. We express $\underset{\sim}{E}(x,y,\omega)$ as:

$$\underset{\sim}{E}(x,y,\omega) = \sum_{e=1}^{N} \underset{\sim}{E}^e(x,y,\omega) \tag{2.3.4}$$

where N is the number of the elements in the calculation region, and $\underset{\sim}{E}^e(x,y,\omega)$ is the function within the e-th element.

In each element we define the $\underset{\sim}{E}^e(x,y,\omega)$ as

$$\underset{\sim}{E}^e(x,y,\omega) = \sum_{j=1}^{p_j} N_j^e(x,y)\, \underset{\sim}{V}_j^e(\omega) \tag{2.3.5}$$

where $\underset{\sim}{V}_j^e(\omega)$ is a coefficient associated with the j-th node, $N_j^e(x,y)$ is an expansion function, and p_j is the number of modes associated with each element

Using (2.3.4) and (2.3.5), expression (2.3.3) can be written as

$$\sum_{e=1}^{N}\sum_{j=1}^{P}\left(\begin{array}{l}\int_s \frac{\varepsilon_r\omega^2}{c_0^2}\,T(x,y)\,N_j^e(x,y)\underset{\sim}{V}_j^e(\omega)\,ds-\int_s \nabla T(x,y)\cdot\nabla\left(\mu_r^{-1}\,N_j^e(x,y)\underset{\sim}{V}_j^e(\omega)\right)ds \\ +\oint_{C_e} T(x,y)\;\nabla\left(\mu_r^{-1}\,N_j^e(x,y)\underset{\sim}{V}_j^e(\omega)\right)\cdot\hat{n}\,dc\end{array}\right) \tag{2.3.6}$$
$$=\int_s j\omega\mu_0\;T(x,y)\,\underset{\sim}{\bar{J}}(x,y,\omega)\,ds$$

Now we choose the waiting function T(x,y) to be the same as the expansion functions in each element, namely

$$T(x,y)=\begin{cases}N_i^e(x,y) & \text{within eth element}\\ 0 & \text{else}\end{cases} \tag{2.3.7}$$

where i = 1, 2, ...P. Therefore in e-th element the equation (2.3.6) becomes

$$\sum_{j=1}^{P}\left(\begin{array}{l}\int_s \frac{\varepsilon_r\omega^2}{c_0^2}\,N_i^e(x,y)\,N_j^e(x,y)\underset{\sim}{V}_j^e(\omega)\,ds \\ -\int_s \nabla N_i^e(x,y)\cdot\nabla\left(\mu_r^{-1}\,N_j^e(x,y)\underset{\sim}{V}_j^e(\omega)\right)ds \\ +\oint_{C_e} N_i^e(x,y)\,\nabla\left(\mu_r^{-1}\,N_j^e(x,y)\underset{\sim}{V}_j^e(\omega)\right)\cdot\hat{n}\,dc\end{array}\right) \tag{2.3.8}$$
$$=\int_s j\omega\mu_0\;N_i^e(x,y)\,\underset{\sim}{\bar{J}}(x,y,\omega)\,ds$$

and hence

$$\sum_{j=1}^{P}\left(\begin{array}{l}\frac{\varepsilon_r\omega^2}{c_0^2}\underset{\sim}{V}_j^{\,e}(\omega)\int_{s_e} N_i^e(x,y)\,N_j^e(x,y)\,ds \\ -\mu_r^{-1}\underset{\sim}{V}_j^{\,e}(\omega)\int_{s_e}\left(\frac{\partial N_i^e(x,y)}{\partial x}\frac{\partial N_j^e(x,y)}{\partial x}+\frac{\partial N_i^e(x,y)}{\partial y}\frac{\partial N_j^e(x,y)}{\partial y}\right)ds \\ +\mu_r^{-1}\oint_{C_e}\left(N_i^e(x,y)\left(\hat{x}\frac{\partial \underset{\sim}{E}_j^{\,e}(x,y)}{\partial x}+\hat{y}\frac{\partial \underset{\sim}{E}_j^{\,e}(x,y)}{\partial y}\right)\right)\cdot\bar{n}\,dc\end{array}\right) \tag{2.3.9}$$
$$=j\omega\mu_0\int_{s_e} N_i^e(x,y)\,\underset{\sim}{J}(x,y,\omega)\,ds$$

We can write (2.3.9) in matrix form as

$$\frac{\varepsilon_r \omega^2}{c_0^2}[A^e]\underset{\sim}{V}^e(\omega) - \mu_r^{-1}[B^e]\underset{\sim}{V}^e(\omega) - \mu_r^{-1}[C^e]\underset{\sim}{V}^e(\omega) + \underset{\sim}{H}^e(\omega) = \underset{\sim}{f}^e(\omega) \tag{2.3.10}$$

where

$$\begin{cases} [A^e]_{ij} = \int_{s_e} N_i^e(x,y) N_j^e(x,y)\, ds \\ [B^e]_{ij} = \int_{s_e} \dfrac{\partial N_i^e(x,y)}{\partial y} \dfrac{\partial N_j^e(x,y)}{\partial y}\, ds \\ [C^e]_{ij} = \int_{s_e} \dfrac{\partial N_i^e(x,y)}{\partial x} \dfrac{\partial N_j^e(x,y)}{\partial x}\, ds \\ \underset{\sim}{H}_i^e = \mu_r^{-1} \oint_C \left(N_i^e(x,y) \left(\hat{x} \dfrac{\partial \underset{\sim}{E}_j{}^e(x,y)}{\partial x} + \hat{y} \dfrac{\partial \underset{\sim}{E}_j{}^e(x,y)}{\partial y} \right) \right) \cdot \hat{n}\, dc \\ \underset{\sim}{f}_i^e(\omega) = j\omega\mu_0 \int_{s_e} N_i^e(x,y) \underset{\sim}{J}^e(x,y,\omega)\, ds \\ \underset{\sim}{V}^e = \begin{bmatrix} \underset{\sim}{V}_1^e(\omega) \\ \underset{\sim}{V}_2^e(\omega) \\ \vdots \\ \\ \underset{\sim}{V}_P^e(\omega) \end{bmatrix} \end{cases} \tag{2.3.11}$$

Expressions for the elements of [A], [B], and [C] are given in Appendix A for the case of first-order expression functions.

After combing all the individual element equations, and enforcing the boundary condition $E_z = 0$ on the boundary C, the assembled equation will be

$$\frac{\varepsilon_r \omega^2}{c_0^2}[A]\underset{\sim}{V}(\omega) - \mu_r^{-1}[B]\underset{\sim}{V}(\omega) - \mu_r^{-1}[C]\underset{\sim}{V}(\omega) = \underset{\sim}{f}(\omega) \tag{2.3.12}$$

where [A], [B], [C], $\underset{\sim}{V}(\omega)$, and $\underset{\sim}{f}(\omega)$ are the assemblages of the corresponding individual element matrices. $\underset{\sim}{V}(\omega)$ is a column matrix of unknown coefficients obtained through solution of matrix equation (2.3.12).

We observe that although the terms $\underset{\sim}{H}_i^e$ are not zero, application of the boundary condition $E_z = 0$ may let these terms do not appear in the final assembled equation (2.3.12), as noted in [13, pp 114-118].

2.4 THE FINITE-ELEMENT TIME-DOMAIN (*FETD*) METHOD

Using the relationship [15]

$$j\omega \leftrightarrow \frac{\partial}{\partial t} \quad and \quad -\omega^2 \leftrightarrow \frac{\partial^2}{\partial^2 t} \tag{2.3.13}$$

we can transfer (2.3.12) into time domain. After some manipulation we can obtain

$$\frac{\varepsilon_r}{c_0^2}[A]\frac{d^2}{d^2t}V(t)+\mu_r^{-1}[B]V(t)+\mu_r^{-1}[C]V(t) = f(t) \tag{2.3.14}$$

where the quantity V(t) is the time domain form of $\underset{\sim}{V}(\omega)$, namely a column matrix of coefficients that vary with time. The matrices, [A], [B], and [C], are identical to those in (2.3.12), and are independent of time.

Application of the finite element technique has discretised the time-domain form of the wave equation with respect to the spatial coordinates. However, we do not have a numerical technique until we have discretised it with respect to the temporal variable as well. Thus in order to discretise (2.3.14) with respect to the time variable the so-called Newmark-Beta scheme is used in the structure-engineering context [6]:

$$\begin{cases} \dfrac{d^2}{d^2t}\Re = \dfrac{1}{\Delta t}[\Re(n+1) - 2\Re(n) + \Re(n-1)] \\ \dfrac{d}{dt}\Re = \dfrac{1}{2\Delta t}[\Re(n+1) - \Re(n-1)] \\ \Re = \alpha\Re(n+1) + (1-2\alpha)\Re(n) + \alpha\Re(n-1) \end{cases} \tag{2.3.15}$$

In (2.3.15), $\Re(n) = \Re(n\Delta t)$ is the discrete-time representation of $\Re(t)$. The quantity α is the interpolation parameter. It can be proved that when $\alpha \geq \frac{1}{4}$ the scheme (2.3.15) is unconditionally stable, and that when $\alpha = \frac{1}{4}$ we get the minimized solution error [6]. Thus in this thesis we will always use $\alpha = \frac{1}{4}$.

Using the Newmark-Beta formulations (2.3.15) we can discretise V(t) as follows:

$$\begin{cases} \frac{d^2}{d^2t}V(t) = \frac{1}{\Delta t}[V(n+1) - 2V(n) + V(n-1)] \\ \frac{d}{dt}V(t) = \frac{1}{2\Delta t}[V(n+1) - V(n-1)] \\ V(t) = \alpha V(n+1) + (1-2\alpha)V(n) + \alpha V(n-1) \end{cases} \tag{2.3.16}$$

If we substitute (2.3.16) into matrices equation (2.3.14) and solve it we can obtain the current value of V(n +1) from its previous values, V(n) and V(n – 1). By doing this at each time step, i.e. for each n, we can obtain the values of V(t) within the whole computational time period.

2.5 THE ENVELOPE FINITE-ELEMENT (EVFE) METHOD

In the FETD method the largest time step that can be used is dictated by the highest operating frequency. The higher the operating frequency the smaller the time step has to be. In many applications the input signal consists of a high frequency carrier modulated by a more slowly varying envelope. Use of the FETD method would demand that the time step be small enough to properly sample a signal at the carrier frequency. If we

could arrange matters so that we could work with the envelope only we could use much larger time steps. The EVFE method is a technique that allows one to do this.

With EVFE method the field quantities are expressed as modulated forms and then through mathematical manipulation the carrier signal is de-embedded from the time domain wave equation. Only the envelope of the signal remains and needs to be simulated. As already stated, since the envelope is much more slowly varying than the carrier a much sparser time step can be used. This leads to a higher computational efficiency than is obtained with the FETD approach.

In order to use EVFE technique, we need to define a signal envelope of the field as modulated forms [7]

$$\begin{cases} V(t) = u(t)e^{j\omega_c t} \\ J(x,y,t) = I(x,y,t)e^{j\omega_c t} \end{cases} \tag{2.5.1}$$

where ω_c is the carrier frequency. If we substitute (2.5.1) into (2.3.14), then after some manipulation we obtain

$$[T_1]\frac{d^2}{d^2t}u(t) + [T_2]\frac{d}{dt}u(t) + [T_3]u(t) = f(t) \tag{2.5.2}$$

where

$$\begin{cases} [T_1] = \dfrac{\varepsilon_r}{c_0^2}[A] \\ [T_2] = 2j\omega_c \dfrac{\varepsilon_r}{c_0^2}[A] \\ [T_3] = (j\omega_c)^2 \dfrac{\varepsilon_r}{c_0^2}[A] + \mu_r^{-1}[B] + \mu_r^{-1}[C] \end{cases} \tag{2.5.3}$$

and $f(t)$ is the assemblage of column element matrix $f^e(t)$

$$f_i^e(t) = \mu_0 \int_{s_e} N_i^e(x,y)\left(\frac{\partial}{\partial t} I^e(x,y,,t) + j\omega_c I^e(x,y,t)\right) ds \tag{2.5.4}$$

Using the Newmark-Beta scheme we can discretize (2.5.2) with respect to time as

$$\left(\frac{1}{\Delta t^2}[T_1] + \frac{1}{2\Delta t}[T_2] + \alpha[T_3]\right) u(n+1) = u_p \tag{2.5.5}$$

where u_p is the value depending on the past field and

$$\begin{aligned} u_p = {} & \frac{1}{\Delta t^2}[T]_1\left(-2u(n) + u(n-1)\right) - \frac{1}{2\Delta t}[T_2]u(n-1) \\ & + [T_3]\left((1-2\alpha)u(n) + \alpha u(n-1)\right) \\ & + \left(\alpha f(n+1) + (1-2\alpha) f(n) + \alpha f(n-1)\right) \end{aligned} \tag{2.5.6}$$

In the above equations u(n +1), u(n) and u(n-1) are different time step column matrices. Therefore we will be easily get the current value of u(n + 1) from the past values of u(n) and u(n – 1) recursively by solving equation (2.5.5).

2.6 THE MODELLING OF DISPERSIVE MEDIA

Dispersive media are characterized by the susceptibility $\chi(\omega)$, which is a function of frequency. This will lead to a frequency dependent relative permittivity. Since the relative permittivity is a function of frequency, the phase velocity of the wave is frequency dependent. Thus the individual frequency components will not maintain their original phase relationships as they propagate in dispersive media, and signal distortion will occur (eg. a pulse will broaden, which is the origin of the terminology "dispersive").

There are three kinds of dispersive media that are usually encountered in engineering practice. These are Lorentz media, Debye media, and plasma media. In Lorentz media the relative permittivity in frequency domain can be expressed as[16]

$$\underset{\sim}{\varepsilon}_r(\omega) = \varepsilon_\infty + \underset{\sim}{\chi}_e(\omega) \tag{2.6.1}$$

and

$$\underset{\sim}{\chi}_e(\omega) = \frac{\Delta\varepsilon\omega_0^2}{\omega_0^2 - \omega^2 + j\omega 2\Gamma} \tag{2.6.2}$$

and

$$\Delta\varepsilon = \varepsilon_s - \varepsilon_\infty \tag{2.6.3}$$

where ε_s is the static or zero-frequency relative permittivity, ε_∞ the relative permittivity at infinite frequency, ω_0 the resonant angular frequency, and Γ the damping coefficient.

In Debye media

$$\underset{\sim}{\varepsilon}_r(\omega) = \varepsilon_\infty + \underset{\sim}{\chi}_e(\omega) \tag{2.6.4}$$

and

$$\underset{\sim}{\chi}_e(\omega) = \frac{\Delta\varepsilon}{1 + j\omega\tau_0} \tag{2.6.5}$$

where τ_0 is the relaxation time.

In plasma media

$$\underset{\sim}{\varepsilon}_r(\omega) = 1 + \underset{\sim}{\chi}_e(\omega) \tag{2.6.6}$$

$$\underset{\sim}{\chi}_e(\omega) = \frac{\omega_p^2}{j\omega(j\omega + \nu_c)} \tag{2.6.7}$$

where ν_c is the collision frequency and ω_p is the angular plasma frequency.

In the frequency domain the electric flux density $\underset{\sim}{D}(\omega)$ and electric field intensity $\underset{\sim}{E}(\omega)$, have the relationship

$$\underset{\sim}{D}(\omega) = \underset{\sim}{\varepsilon}_r(\omega)\underset{\sim}{E}(\omega) \tag{2.6.8}$$

For Lorentz media, the time-domain susceptibility function χ (t) can be found by inverse Fourier transformation of (2.6.2) to be

$$\chi_e(t) = \frac{\Delta\varepsilon\omega_0^2}{\sqrt{\omega_0^2 - \Gamma^2}} e^{-\Gamma t} \sin\left(\sqrt{\omega_0^2 - \Gamma^2}\, t\right) U(t) \tag{2.6.9}$$

where U(t) is the unit step function.

In the same way we can obtain the time-domain susceptibility functions for Debye media as

$$\chi_e(t) = \frac{\Delta\varepsilon}{\tau_0} e^{-t/\tau_0} U(t) \tag{2.6.10}$$

and for plasma media as

$$\chi_e(t) = -\frac{\omega_p^2}{\nu_c} e^{-\nu_c t} U(t) \tag{2.6.11}$$

In the time-domain the electric flux density $D(t)$ and electric field intensity $E(t)$ are related as [1]

$$D(t) = \varepsilon_0 \varepsilon E(t) + \varepsilon_0 \int_{t'=0}^{t} E(t-t')\chi_e(t')dt' \tag{2.6.12}$$

2.7 OVERVIEW OF THE LITERATURE ON THE *FETD* AND *EVFE* IN THE PRESENCE OF DISPERSIVE MATERIALS

2.7.1 The FETD Method and Dispersive Materials

The use of the FETD method in the presence of all three types of dispersive materials mentioned in Section 2.6 has been described in [10].

2.7.2 The EVFE Method and Dispersive Materials

The use of the EVFE method in the presence of material with plasma-type dispersion has been described in [11]. The derivation is discussed in what follows. We refer to Figure 2.2 for the definition of the relevant problem geometry.

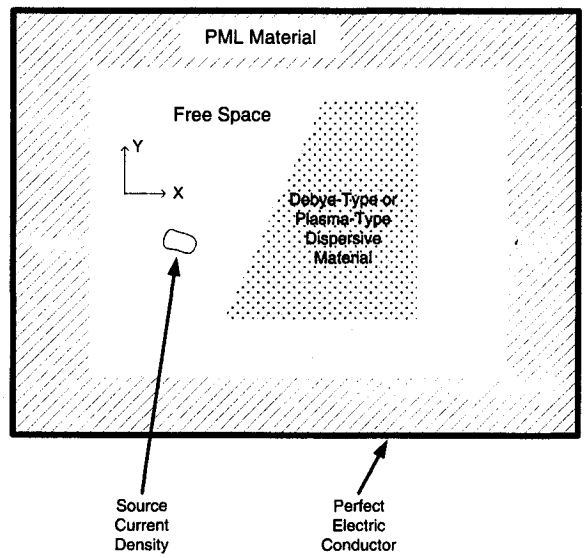

Figure 2.2 Two-Dimensional problems with Debye or plasma media

If we substitute (2.6.6) and (2.6.7) into (2.2.5) we obtain

$$\nabla_t^2\left(\underset{\sim}{\mu_r}^{-1}\underset{\sim}{E}(x,y,\omega)\right)-\frac{(j\omega)^2}{c_0^2}\underset{\sim}{E}(x,y,\omega)\ -\frac{(j\omega)\omega_p^2}{(j\omega+v_c)}\underset{\sim}{E}(x,y,\omega) \qquad (2.7.1)$$
$$= \quad j\omega\mu_0\,\underset{\sim}{J}(x,y,\omega)$$

Define

$$\underset{\sim}{\psi}(x,y,\omega)=\frac{1}{(j\omega+v_c)}\underset{\sim}{E}(x,y,\omega) \qquad (2.7.2)$$

the (2.7.1) becomes

$$\nabla_t^2\left(\underset{\sim}{\mu_r^{-1}}\underset{\sim}{E}(x,y,\omega)\right)-\frac{(j\omega)^2}{c_0^2}\underset{\sim}{E}(x,y,\omega)\;-j\omega\omega_p^2\underset{\sim}{\psi}(x,y,\omega)$$
$$=j\omega\mu_0\underset{\sim}{J}(x,y,\omega) \tag{2.7.3}$$

Using the relationship (2.3.13) we can transfer (2.7.3) into the time domain as

$$\nabla_t^2\left(\mu_r^{-1}E(x,y,t)\right)-\frac{1}{c_0^2}\frac{\partial^2}{\partial t^2}E(x,y,t)\;-\omega_p^2\frac{\partial}{\partial t}\psi(x,y,t)$$
$$=\;\frac{\partial}{\partial t}\mu_0 J(x,y,t) \tag{2.7.4}$$

where $\psi(x,y,t)$ is the time domain form of $\underset{\sim}{\psi}(x,y,\omega)$ given by

$$\psi(x,y,t)=\int_{t'=0}^{t}e^{-\nu_c(t-t')}E(x,y,t')dt' \tag{2.7.5}$$

We can rewrite (2.7.5) as

$$\psi(x,y,t)=e^{-\nu_c t}\int_{t'=0}^{t}e^{\nu_c t'}E(x,y,t')dt' \tag{2.7.6}$$

Next we differentiate both sides of (2.7.6) with respect to time, to obtain

$$\frac{\partial\psi(x,y,t)}{\partial t}=-\nu_c e^{-\nu_c t}\int_{t'=0}^{t}e^{\nu_c t'}E(x,y,t')dt'+e^{-\nu_c t}e^{\nu_c t}E(x,y,t)$$
$$=-\nu_c\psi(x,y,t)+E(x,y,t) \tag{2.7.7}$$

or in other words.

$$\frac{\partial\psi(x,y,t)}{\partial t}+\nu_c\psi(x,y,t)=\;E(x,y,t) \tag{2.7.8}$$

If we associate (2.7.4) and (2.7.8), and impose the method introduced in Sections 2.3, 2.4 and 2.5 we can simulate the electromagnetic wave in this plasma-type dispersive material using the EVFE method.

In the case of Debye media, substitution of (2.6.4) and (2.6.5) into (2.2.5) yields

$$\nabla_t^2\left(\underset{\sim}{\mu_r^{-1}}\underset{\sim}{E}(x,y,\omega)\right)-\frac{\varepsilon_\infty(j\omega)^2}{c_0^2}\underset{\sim}{E}(x,y,\omega)-\frac{(j\omega)^2\Delta\varepsilon}{(1+j\omega t_0)}\underset{\sim}{E}(x,y,\omega) \qquad (2.7.9)$$
$$= \; j\omega\mu_0\underset{\sim}{J}(x,y,\omega)$$

Define

$$\underset{\sim}{\psi'}(x,y,\omega)=\frac{\Delta\varepsilon}{(1+j\omega t_0)}\underset{\sim}{E}(x,y,\omega) \qquad (2.7.10)$$

Equation (2.7.9) becomes

$$\nabla_t^2\left(\underset{\sim}{\mu_r^{-1}}\underset{\sim}{E}(x,y,\omega)\right)-\frac{\varepsilon_\infty(j\omega)^2}{c_0^2}\underset{\sim}{E}(x,y,\omega)-(j\omega)^2\underset{\sim}{\psi'}(x,y,\omega) \qquad (2.7.11)$$
$$= \; j\omega\mu_0\underset{\sim}{J}(x,y,\omega)$$

Using (2.3.13) we transfer (2.7.11) into the time domain as

$$\nabla_t^2\left(\underset{\sim}{\mu_r^{-1}}E(x,y,t)\right)-\frac{\varepsilon_\infty}{c_0^2}\frac{\partial^2}{\partial t^2}E(x,y,t)-\frac{\partial^2}{\partial t^2}\psi'(x,y,t) \qquad (2.7.12)$$
$$= \; \frac{\partial}{\partial t}\mu_0 J(x,y,t)$$

where

$$\psi'(x,y,t)=\frac{\Delta\varepsilon}{t_0}\int_{t'=0}^{t} e^{-\frac{t-t'}{t_0}}E(x,y,t')dt' \qquad (2.7.13)$$

We once again differentiate both sides of (2.7.13) to get

$$\frac{\partial\psi'(x,y,t)}{\partial t}+\frac{\Delta\varepsilon}{t_0^2}\psi'(x,y,t)=\frac{\Delta\varepsilon}{t_0}E(x,y,t) \qquad (2.7.14)$$

If we associate (2.7.12) and (2.7.14) and apply the method introduced in Sections 2.3, 2.4 and 2.5 we can simulate the electromagnetic wave in this Debye-type dispersive material using the EVFE method.

From the above discussion we observe that it is relatively easy to incorporate materials with plasma-type or Debye-type dispersion into the EVFE method. However, for some dispersive media (such as Lorentz-type) the time-domain susceptibility expressions are more complicated, and the above "simplification" is not possible. This thesis develops computationally efficient ways of incorporating such materials in the EVFE approach.

2.8 CONCLUDING REMARKS

This chapter provided a brief background review of the FETD and EVFE methods. In Section 2.7 it was indicated that while methods of including a host of dispersive material types in the FETD method have been given, only the Debye and plasma media cases have been dealt with as far as the EVFE technique is concerned. This places a limitation on the possible EVFE applications. The principal objective of this thesis is to develop a method for incorporating Lorentz media in the EVFE method.

CHAPTER 3

THE INCORPORATION OF LORENTZ DISPERSIVE MATERIALS IN THE *EVFE* METHOD: THEORETICAL CONSIDERATIONS

3.1 PRELIMINARY REMARKS

In Section 2.7.2 we showed how material with either Debye or plasma dispersion has been included in the EVFE formulation; this enabled us to indicate why such existing methods are not directly applicable to the case of Lorentz media. In this chapter we will develop a way of doing this for the first time. Sections 3.2 through 3.5, which represent the essence of the theoretical contribution of this thesis, will describe three ways of incorporating Lorentz media in the EVFE method. In order to validate these new developments it will of course be necessary to implement these numerically, and so this will be the subject of Chapter 4. However, in order to make such an implementation possible we need a means of mesh truncation (in the presence of Lorentz material). This is discussed in Section 3.6. Section 3.7 briefly discusses how the formulations, introduced here for two-dimensional scalar problems, can be extended to three-dimensional vector problems. Section 3.8 concludes the chapter.

3.2 THE ENVELOPE-FINITE ELEMENT (EVFE) METHOD IN THE PRESENCE OF LORENTZ MEDIA

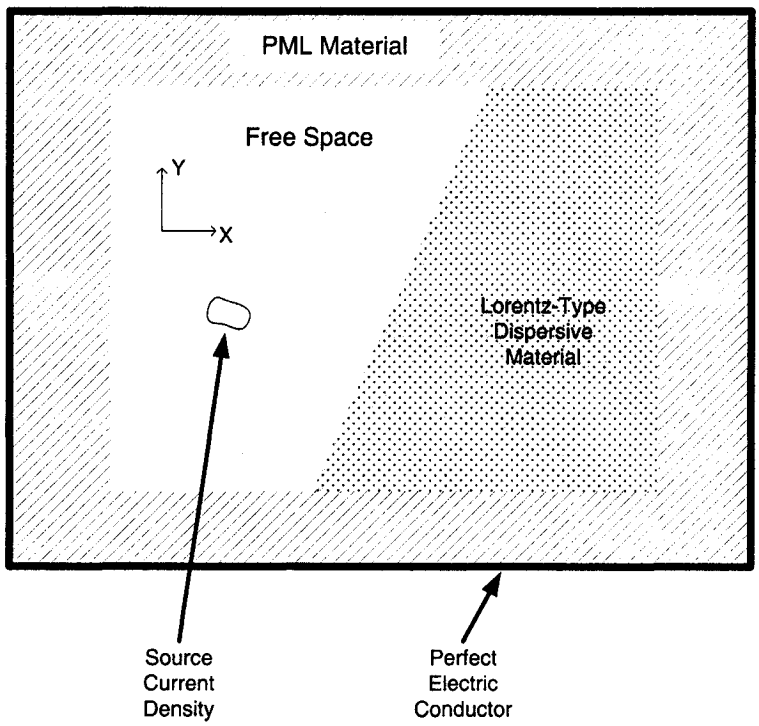

Figure 3.1 Two-dimensional problem with Loretz type dipersive material

We refer to Figure 3.1 for a definition of the problem geometry. If we substitute (2.6.1) into (2.3.10) we can obtain

$$\frac{\varepsilon_\infty \omega^2}{c_0^2}[A^e]\underset{\sim}{V}^e(\omega)+\frac{\omega^2}{c_0^2}[A^e]\underset{\sim}{\varphi}^e(\omega)-\mu_r^{-1}[B^e]\underset{\sim}{V}^e(\omega)$$
$$-\mu_r^{-1}[C^e]\underset{\sim}{V}^e(\omega)+\underset{\sim}{H}^e(\omega)=\underset{\sim}{f}^e(\omega) \tag{3.2.1}$$

where

$$\underset{\sim}{\varphi}^e(\omega)=\underset{\sim}{\chi}_e(\omega)\underset{\sim}{V}^e(\omega) \tag{3.2.2}$$

After assemble the matrices in (3.2.1) we can obtain

$$\begin{aligned}&\frac{\varepsilon_\infty \omega^2}{c_0^2}[A]\underset{\sim}{V}(\omega)+\frac{\omega^2}{c_0^2}[A]\underset{\sim}{\varphi}(\omega)-\mu_r^{-1}[B]\underset{\sim}{V}(\omega)\\&-\mu_r^{-1}[C]\underset{\sim}{V}(\omega)=\underset{\sim}{f}(\omega)\end{aligned} \tag{3.2.3}$$

We can observe that there is no assembled matrix $\underset{\sim}{H}(\omega)$ of $\underset{\sim}{H}^e(\omega)$ in the assembled equation (3.2.3). The reason is given in section 2.3.

After assemble the matrices in (3.2.2) we obtain

$$\underset{\sim}{\varphi}(\omega)=\underset{\sim}{\chi}_e(\omega)\underset{\sim}{V}(\omega) \tag{3.2.4}$$

Using the relationship (2.3.13) we can transfer (3.2.3) into time domain and after some manipulation we obtain

$$\begin{aligned}&\frac{\varepsilon_\infty}{c_0^2}[A]\frac{d^2}{dt^2}V(t)+\frac{1}{c_0^2}[A]\frac{d^2}{dt^2}\varphi(t)+\mu_r^{-1}[B]V(t)\\&+\mu_r^{-1}[C]V(t)=-f(t)\end{aligned} \tag{3.2.5}$$

To use the envelope – finite element technique, we need to define another envelope field as [11]

$$\varphi(t)=\phi(t)e^{j\omega_c t} \tag{3.2.6}$$

Substitute (3.2.6) and (2.5.1) into (3.2.5) and after some manipulation we obtain

$$\begin{aligned}&T_1\frac{d^2}{d^2t}u(t)+T_2\frac{d}{dt}u(t)+T_3u(t)+T_4\frac{d^2}{d^2t}\phi(t)+T_5\frac{d}{dt}\phi(t)+T_6\phi(t)\\&=-f(t)\end{aligned} \tag{3.2.7}$$

where

$$\begin{cases} T_1 = \frac{\varepsilon_\infty}{c_0^2}[A] \\ T_2 = 2j\omega_c \frac{\varepsilon_\infty}{c_0^2}[A] \\ T_3 = (j\omega_c)^2 \frac{\varepsilon_\infty}{c_0^2}[A] - \mu_r^{-1}[B] - \mu_r^{-1}[C] \\ T_4 = T_1 \\ T_5 = T_2 \\ T_6 = (j\omega_c)^2 \frac{\varepsilon_\infty}{c_0^2}[A] \\ f(t) = \mu_0 \int_s N_i^e(\bar{r}) \left(\frac{\partial}{\partial t} I(\bar{r},t) + j\omega_c I(\bar{r},t) \right) ds \end{cases} \tag{3.2.8}$$

Using Newmark-Beta formulations in (2.3.15) we can discretize (3.2.7) in time domain and after some manipulation we obtain

$$\left(\frac{1}{\Delta t^2} T_1 + \frac{1}{2\Delta t} T_2 + \alpha T_3 \right) u(n+1) + \left(\frac{1}{\Delta t^2} T_4 + \frac{1}{2\Delta t} T_5 + \alpha T_6 \right) \phi(n+1) = u_p \tag{3.2.9}$$

where

$$\begin{aligned} u_p = {} & \frac{1}{\Delta t^2} T_1 \left(-2u(n) + u(n-1) \right) - \frac{1}{2\Delta t} T_2 u(n-1) + \\ & T_3 \left((1-2\alpha)u(n) + \alpha u(n-1) \right) + \frac{1}{\Delta t^2} T_4 \left(-2\phi(n) + \phi(n-1) \right) \\ & - \frac{1}{2\Delta t} T_5 \phi(n-1) + T_6 \left((1-2\alpha)\phi(n) + \alpha\phi(n-1) \right) \\ & - \left(\alpha f(n+1) + (1-2\alpha) f(n) + \alpha f(n-1) \right) \end{aligned} \tag{3.2.10}$$

Therefore if we get the relationship between the field $u(t)$ and the dispersive term $\phi(t)$ we will easily calculate the field in the whole time domain recursively through solving (3.2.9) at each time step. We have three ways to get this relationship.

3.3 THE FIRST METHOD – *UTILISING THE FREQUENCY-DOMAIN MODEL OF THE DISPERSIVE MATERIAL AND INVERSE FOURIER TRANSFORM*

We refer to Figure 3.1 and note that the dispersive material may now possess Lorentz-type dispersion. In addition, through the enhancement of the PML mesh truncation scheme in Section 3.5 we will be able to allow the dispersive material to be adjacent to the PML, something that was not previously possible (and hence required the situation shown in Figure 2.2, where only non-dispersive material was adjacent to the conventional PMLs).

To be clear we rewrite the equation (3.2.4) as follow

$$\underset{\sim}{\varphi}(\omega) = \underset{\sim}{\chi}_e(\omega)\underset{\sim}{V}(\omega) \tag{3.3.1}$$

If we substitute (2.6.2) into (3.3.1) after some manipulation we obtain

$$-\omega^2\underset{\sim}{\varphi}(\omega) + j\omega 2\Gamma\underset{\sim}{\varphi}(\omega) + \omega_0^2\underset{\sim}{\varphi}(\omega) = \Delta\varepsilon\ \omega_0^2\ \underset{\sim}{V}(\omega) \tag{3.3.2}$$

Using the relationships in (2.3.13) we can transfer (3.3.2) into time domain as follow

$$\frac{d^2}{d^2t}\varphi(t) + \frac{d}{dt}2\Gamma\varphi(t) + \omega_0^2\varphi(t) = \Delta\varepsilon\ \omega_0^2\ V(t) \tag{3.3.3}$$

If we substitute (3.2.6) and (2.5.1) into (3.3.3) we can obtain the envelope equation of (3.3.3)

$$\begin{aligned}&\frac{d^2}{d^2t}\phi(t) + 2\left(j\omega_c + \Gamma\right)\frac{d}{dt}\phi(t) + \left(\left(\varepsilon_s - \varepsilon_\infty\right)\omega_0^2 - \omega_c^2 + 2\Gamma j\omega_c\right)\phi(t)\\ &= \Delta\varepsilon\ \omega_0^2\ u(t)\end{aligned} \tag{3.3.4}$$

Now using Newmark–Beta to discretize (3.3.4) we can obtain

$$C_{f1}\,\phi(n+1) = C_{f2}u(n+1) + \phi_{fp} \tag{3.3.5}$$

where

$$C_{f1} = \frac{1}{\Delta t^2} + \frac{1}{\Delta t}\left(j\omega_c + \Gamma\right) + \alpha(\omega_p^2 - \omega_c^2 + 2\Gamma j\omega_c \tag{3.3.6}$$

$$C_{f2} = \alpha\Delta\varepsilon\omega_0^2 u(n+1) \tag{3.3.7}$$

$$\begin{aligned}\phi_{fp} &= (\varepsilon_s - \varepsilon_\infty)\omega_0^2\left(u(n) + \alpha u(n-1)\right) + \frac{1}{\Delta t^2}\left(2\phi(n) - \phi(n-1)\right) \\ &+ \frac{1}{\Delta t}\left(j\omega_c + \Gamma\right)\phi(n-1) - \left(\omega_p^2 - \omega_c^2 + 2\Gamma j\omega_c\right)\left((1-2\alpha)\phi(n) - \alpha\phi(n-1)\right)\end{aligned} \tag{3.3.8}$$

where ϕ_{fp} depends on only the past value of the fields.

Solve the equations (3.3.5) and (3.2.9) we can obtain the recursive expression of the field

$$u(n+1) = \left(\begin{array}{l}\frac{1}{\Delta t^2}T_1 + \frac{1}{2\Delta t}T_2 + \alpha T_3 \\ + \frac{C_{f2}}{C_{f1}}\left(\frac{1}{\Delta t^2}T_4 + \frac{1}{2\Delta t}T_5 + \alpha T_6\right)\end{array}\right)^{-1}\left(\begin{array}{l}u_p - \frac{1}{C_{f1}}\phi_{fp} \times \\ \left(\frac{1}{\Delta t^2}T_4 + \frac{1}{2\Delta t}T_5 + \alpha T_6\right)\end{array}\right) \tag{3.3.9}$$

Now we can see that all the values on the left of (3.3.9) depend on the past values of the field. So we can recursively calculate the current field value by using its previous values through (3.3.9).

3.4 THE SECOND METHOD – *UTILISING THE TIME-DOMAIN MODEL OF THE DISPERSIVE MATERIAL AND CONVOLUTION THEORY*

Rewrite the time-domain Lorentz media susceptibility expression (2.6.9)

$$\chi_e(t) = \frac{\Delta\varepsilon\omega_0^2}{\sqrt{\omega_0^2 - \Gamma^2}}e^{-\Gamma t}\sin\left(\sqrt{\omega_0^2 - \Gamma^2}t\right)U(t) \tag{3.3.10}$$

Define

$$\beta = \sqrt{\omega_0^2 - \Gamma^2} \quad and \quad \gamma = \frac{\Delta\varepsilon\omega_0^2}{\beta} \tag{3.3.11}$$

we can rewrite (3.3.10) as:

$$\chi_e(t) = \gamma e^{-\Gamma t} \sin(\beta t) U(t) \tag{3.3.12}$$

According to convolution theory from (3.3.1) we can get the expression of φ in time domain

$$\varphi(t) = \int_{-\infty}^{\infty} \chi_e(t - t')V(t')\,dt' \tag{3.3.13}$$

If we substitute (3.3.12) into (3.3.13) we can obtain

$$\varphi(t) = \int_0^t \gamma e^{-\Gamma(t-t')} \sin(\beta(t-t'))V(t')\,dt' \tag{3.3.14}$$

To obtain difference equation without convolution integral in it we define another expression

$$\varphi'(t) = \int_0^t \gamma e^{-\Gamma(t-t')} \cos(\beta(t-t'))V(t')\,dt' \tag{3.3.15}$$

Rewrite (3.3.15) as

$$\begin{aligned} \varphi'(t) = {} & \gamma e^{-\Gamma t} \cos(\beta t) \int_0^t e^{\Gamma t'} \cos(\beta t')V(t')\,dt' \\ & + \gamma e^{-\Gamma t} \sin(\beta t) \int_0^t e^{\Gamma t'} \sin(\beta t')V(t')\,dt' \end{aligned} \tag{3.3.16}$$

If we do differentiate on both sides of (3.3.16) we obtain

$$\begin{aligned}\frac{d}{dt}\varphi'(t) &= \frac{d}{dt}\left(\gamma e^{-\Gamma t}\cos(\beta t)\right)\int_0^t e^{\Gamma t'}\cos(\beta t')V(t')\,dt' \\ &+ \left(\gamma e^{-\Gamma t}\cos(\beta t)\right)\frac{d}{dt}\int_0^t e^{\Gamma t'}\cos(\beta t')V(t')\,dt' \\ &+ \frac{d}{dt}\left(\gamma e^{-\Gamma t}\sin(\beta t)\right)\int_0^t e^{\Gamma t'}\sin(\beta t')V(t')\,dt' \\ &+ \left(\gamma e^{-\Gamma t}\sin(\beta t)\right)\frac{d}{dt}\int_0^t e^{\Gamma t'}\sin(\beta t')V(t')\,dt' \qquad (3.3.17) \\ &= \left(-\gamma\Gamma e^{-\Gamma t}\cos(\beta t) - \gamma\beta e^{-\Gamma t}\sin(\beta t)\right)\int_0^t e^{\Gamma t'}\cos(\beta t')V(t')\,dt' \\ &+ \left(\gamma e^{-\Gamma t}\cos(\beta t)\right)e^{\Gamma t}\cos(\beta t)V(t) \\ &+ \left(-\gamma\Gamma e^{-\Gamma t}\sin(\beta t) + \gamma\beta e^{-\Gamma t}\cos(\beta t)\right)\int_0^t e^{\Gamma t'}\sin(\beta t')V(t')\,dt' \\ &+ \left(\gamma e^{-\Gamma t}\sin(\beta t)\right)e^{\Gamma t}\sin(\beta t)V(t)\end{aligned}$$

Rearrange (3.3.17) we obtain

$$\frac{d}{dt}\varphi'(t) = \beta V(t) - \beta\varphi(t) - \Gamma\varphi'(t) \qquad (3.3.18)$$

With the same way from (3.3.14) we can get

$$\frac{d}{dt}\varphi(t) = \beta\varphi'(t) - \Gamma\varphi(t) \qquad (3.3.19)$$

To use envelope method we define

$$\varphi'(t) = \phi'(t)e^{j\omega_c t} \qquad (3.3.20)$$

If we substitute (3.2.6) and (3.3.20) into (3.3.18) and (3.3.19) respectively we can obtain

$$\frac{d}{dt}\phi(t) + (j\omega_c + \Gamma)\phi(t) - \beta\phi'(t) = 0 \qquad (3.3.21)$$

and

$$\frac{d}{dt}\phi'(t) + (j\omega_c + \Gamma)\phi'(t) + \beta\phi(t) = \gamma u(t) \qquad (3.3.22)$$

Using Newmark–Beta formulations (2.3.15) to discretize (3.3.21) and (3.3.22) we obtain

$$\frac{1}{2\Delta t}\left(\phi(n+1)-\phi(n-1)\right)+(j\omega_c+\Gamma)\begin{pmatrix}\alpha\phi(n+1)+(1-2\alpha)\phi(n)\\+\alpha\phi(n-1)\end{pmatrix}\\-\beta\left(\alpha\phi'(n+1)+(1-2\alpha)\phi'(n)+\alpha\phi'(n-1)\right)=0 \tag{3.3.23}$$

and

$$\frac{1}{2\Delta t}\left(\phi'(n+1)-\phi'(n-1)\right)+(j\omega_c+\Gamma)\begin{pmatrix}\alpha\phi'(n+1)+(1-2\alpha)\phi'(n)\\+\alpha\phi'(n-1)\end{pmatrix}\\+\beta\left(\alpha\phi(n+1)+(1-2\alpha)\phi(n)+\alpha\phi(n-1)\right)\\=\gamma\left(\alpha u(n+1)+(1-2\alpha)u(n)+\alpha u(n-1)\right) \tag{3.3.24}$$

Solve (3.3.23) and (3.3.24) together we can obtain:

$$\phi'(n+1)=\frac{1}{\beta\alpha}\left(\left(\frac{1}{2\Delta t}+\alpha(j\omega_c+\Gamma)\right)\phi(n+1)+\phi'_p\right) \tag{3.3.25}$$

and

$$\phi(n+1)=C_t u(n+1)+\phi_{tp} \tag{3.3.26}$$

where

$$C_t=\alpha\gamma\left(\frac{1}{\alpha\beta}\left(\frac{1}{2\Delta t}+\alpha(j\omega_c+\Gamma)\right)^2+\alpha\beta\right)^{-1} \tag{3.3.27}$$

$$\phi_{tp}=-\left(\frac{1}{\alpha\beta}\left(\frac{1}{2\Delta t}+\alpha(j\omega_c+\Gamma)\right)^2+\alpha\beta\right)^{-1}\cdot\\\begin{pmatrix}\frac{1}{\alpha\beta}\left(\frac{1}{2\Delta t}+\alpha(j\omega_c+\Gamma)\right)\phi'_p+(j\omega_c+\Gamma)(1-2\alpha)\phi'(n)\\+\left(\alpha(j\omega_c+\Gamma)-\frac{1}{2\Delta t}\right)\phi'(n-1)+\beta(1-2\alpha)\phi(n)+\alpha\beta\phi(n-1)\\-\gamma(1-2\alpha)u(n)-\alpha\gamma u(n-1)\end{pmatrix} \tag{3.3.28}$$

and

$$\phi_p' = (j\omega_c + \Gamma)(1-2\alpha)\phi(n) + \left(\alpha(j\omega_c + \Gamma) - \frac{1}{2\Delta t}\right)\phi(n-1) - \beta(1-2\alpha)\phi'(n) - \alpha\beta\phi'(n-1) \tag{3.3.29}$$

From the above we observe that the value of ϕ_{tp} *and* ϕ_p' depends on the past field values and C_t is a constant.

Now solve (3.2.9) and (3.3.26) we can obtain the recursive expression of the field as

$$u(n+1) = \begin{pmatrix} \frac{1}{\Delta t^2}T_1 + \frac{1}{2\Delta t}T_2 + \alpha T_3 \\ + C_t\left(\frac{1}{\Delta t^2}T_4 + \frac{1}{2\Delta t}T_5 + \alpha T_6\right) \end{pmatrix}^{-1} \left(u_p - \phi_{tp}\left(\frac{1}{\Delta t^2}T_4 + \frac{1}{2\Delta t}T_5 + \alpha T_6\right)\right) \tag{3.3.30}$$

Now all the values on the left side of (3.3.30) depend on the past field values. So with (3.3.30), (3.3.25) and (3.3.26) we can recursively calculate the current field value using the past field values in whole computational time domain.

3.5 THE THIRD METHOD – *A DIRECT CONVOLUTION INTEGRAL METHOD*

This method might be called the "brute force" approach. In practice it would not be the one we would want to use since it does not preserve the larger time step advantage of the EVFWE method. Nevertheless, it provides a means of measuring the effectiveness of the other two approaches.

From (3.3.14) we can obtain

$$\varphi(t) = \gamma e^{-\Gamma t}\begin{pmatrix} \sin(\beta t)\int_0^t e^{\Gamma t'}\cos(\beta t')V(t')\,dt' \\ -\cos(\beta t)\int_0^t e^{\Gamma t'}\sin(\beta t')V(t')\,dt' \end{pmatrix} \tag{3.3.31}$$

In order to use the EVFE method we substitute (3.2.6) into (3.3.31) and obtain

$$\phi(t) = \gamma\left(\sin(\beta t)I_2 - \cos(\beta t)I_1\right) \tag{3.3.32}$$

where

$$I_1(t) = e^{-(\Gamma+\omega_c)t}\int_0^t e^{\Gamma t'}\sin(\beta t')V(t')\,dt' \tag{3.3.33}$$

and

$$I_2(t) = e^{-(\Gamma+\omega_c)t}\int_0^t e^{\Gamma t'}\cos(\beta t')V(t')\,dt' \tag{3.3.34}$$

Define $I_1(n) = I_1(nt)$ *and* $I_2(n) = I_2(nt)$ to be the discrete time representations of $I_1(t)$ *and* $I_2(t)$ respectively. And then we have:

$$I_1(n) = e^{-(\Gamma+j\omega_c)n\Delta t}\sum_{m=1}^{n}\int_{(m-1)\Delta t}^{m\Delta t} e^{\Gamma t'}\sin(\beta t')V(t')\,dt' \tag{3.3.35}$$

and

$$I_2(n) = e^{-(\Gamma+j\omega_c)n\Delta t}\sum_{m=1}^{n}\int_{(m-1)\Delta t}^{m\Delta t} e^{\Gamma t'}\cos(\beta t')V(t')\,dt' \tag{3.3.36}$$

In order to use EVFE method we substitute $V(t) = u(t)e^{j\omega_c t}$ into (3.3.35) and (3.3.36) and obtain:

$$I_1(n) = e^{-(\Gamma+j\omega_c)n\Delta t}\sum_{m=1}^{n}\int_{(m-1)\Delta t}^{m\Delta t} e^{\Gamma t'}\sin(\beta t')u(t')e^{j\omega_c t'}dt' \tag{3.3.37}$$

and

$$I_2(n) = e^{-(\Gamma+j\omega_c)n\Delta t}\sum_{m=1}^{n}\int_{(m-1)\Delta t}^{m\Delta t} e^{\Gamma t'}\cos(\beta t')u(t')e^{j\omega_c t'}dt' \tag{3.3.38}$$

Obviously (3.3.37) and (3.3.38) have recursive property. So we can rewrite them in recursive forms as follow:

$$I_1(n) = e^{-(\Gamma+j\omega_c)\Delta t}I_1(n-1) + e^{-(\Gamma+j\omega_c)n\Delta t}\int_{(n-1)\Delta t}^{n\Delta t} e^{\Gamma t'}\sin(\beta t')u(t')e^{j\omega_c t'}dt' \tag{3.3.39}$$

and

$$I_2(n) = e^{-(\Gamma + j\omega_c)\Delta t} I_2(n-1) + e^{-(\Gamma + j\omega_c)n\Delta t} \int_{(n-1)\Delta t}^{n\Delta t} e^{\Gamma t'} \cos(\beta t') u(t') e^{j\omega_c t'} dt' \quad (3.3.40)$$

In time-step interval $(m\Delta t, (m+1)\Delta t)$, with interpolation method the approximate value of $u(t')$ can be expressed as [1]

$$u(t') = u(m) + \left(\frac{u(m+1) - u(m)}{\Delta t} \right)(t' - m\Delta t) \quad (3.3.41)$$

According to (3.3.41), (3.3.39) and (3.3.40) can be written as

$$I_1(n) = e^{-(\Gamma + j\omega_c)\Delta t} I_1(n-1) + e^{-(\Gamma + j\omega_c)n\Delta t} \int_{(n-1)\Delta t}^{n\Delta t} e^{\Gamma t'} \sin(\beta t') \left(u(n-1) + \left(\frac{u(n) - u(n-1)}{\Delta t} \right)(t' - (n-1)\Delta t) \right) e^{j\omega_c t'} dt' \quad (3.3.42)$$

and

$$I_2(n) = e^{-(\Gamma + j\omega_c)\Delta t} I_2(n-1) + e^{-(\Gamma + j\omega_c)n\Delta t} \int_{(n-1)\Delta t}^{n\Delta t} e^{\Gamma t'} \cos(\beta t') \left(u(n-1) + \left(\frac{u(n) - u(n-1)}{\Delta t} \right)(t' - (n-1)\Delta t) \right) e^{j\omega_c t'} dt' \quad (3.3.43)$$

Rearrange (3.3.42) and (3.3.43) we can obtain

$$\begin{aligned} I_1(n) = e^{-(\Gamma + j\omega_c)\Delta t} I_1(n-1) &+ \left(nu(n-1) - (n-1)u(n) \right) \chi_1(n) \\ &+ \left(u(n) - u(n-1) \right) \xi_1(n) \end{aligned} \quad (3.3.44)$$

and

$$\begin{aligned} I_2(n) = e^{-(\Gamma + j\omega_c)\Delta t} I_2(n-1) &+ \left(nu(n-1) - (n-1)u(n) \right) \chi_2(n) \\ &+ \left(u(n) - u(n-1) \right) \xi_2(n) \end{aligned} \quad (3.3.45)$$

where

$$\chi_1(n) = e^{-(\Gamma + j\omega_c)n\Delta t} \int_{(n-1)\Delta t}^{n\Delta t} \sin(bt') e^{at'} dt' \quad (3.3.46)$$

$$\xi_1(n) = \frac{1}{\Delta t} e^{-(\Gamma + j\omega_c)n\Delta t} \int_{(n-1)\Delta t}^{n\Delta t} t' \sin(bt') e^{at'} dt' \quad (3.3.47)$$

$$\chi_2(n) = e^{-(\Gamma + j\omega_c)n\Delta t} \int_{(n-1)\Delta t}^{n\Delta t} \cos(bt')\, e^{at'} dt' \tag{3.3.48}$$

$$\xi_2(n) = \frac{1}{\Delta t} e^{-(\Gamma + j\omega_c)n\Delta t} \int_{(n-1)\Delta t}^{n\Delta t} t'\cos(bt')\, e^{at'} dt' \tag{3.3.49}$$

with

$$\begin{cases} a = \Gamma + j\omega_c \\ b = \beta \end{cases} \tag{3.3.50}$$

After integration we can obtain the results of (3.3.46) and(3.3.48) as follow respectively

$$\begin{aligned} \chi_1(n) = {} & \frac{1}{a^2 + b^2}\left(a\sin(bn\Delta t) - b\cos(bn\Delta t)\right) \\ & - \frac{e^{-a\Delta t}}{a^2 + b^2}\left(a\sin(b(n-1)\Delta t) - b\cos(b(n-1)\Delta t)\right) \end{aligned} \tag{3.3.51}$$

and

$$\begin{aligned} \chi_2(n) = {} & \frac{1}{a^2 + b^2}\left(a\cos(bn\Delta t) + b\sin(bn\Delta t)\right) \\ & - \frac{e^{-a\Delta t}}{a^2 + b^2}\left(a\cos(b(n-1)\Delta t) + b\sin(b(n-1)\Delta t)\right) \end{aligned} \tag{3.3.52}$$

From (3.3.47) we have

$$\begin{aligned} \xi_1(n) &= \frac{1}{a\Delta t} e^{-an\Delta t} \int_{(n-1)\Delta t}^{n\Delta t} t'\sin(bt')\, de^{at'} \\ &= \frac{1}{a\Delta t} e^{-an\Delta t}\left(t'\sin(bt')e^{at'}\Big|_{(n-1)\Delta t}^{n\Delta t} - \int_{(n-1)\Delta t}^{n\Delta t} e^{at'} d\left(t'\sin(bt')\right)\right) \\ &= \frac{1}{a\Delta t} e^{-an\Delta t}\left(\begin{array}{l} t'\sin(bt')e^{at'}\Big|_{(n-1)\Delta t}^{n\Delta t} - \int_{(n-1)\Delta t}^{n\Delta t} \sin(bt')\, e^{at'} dt' \\ -b\int_{(n-1)\Delta t}^{n\Delta t} t'\cos(bt')\, e^{at'} dt' \end{array}\right) \\ &= \frac{1}{a\Delta t}\left(\begin{array}{l} n\Delta t\sin(bn\Delta t) - (n-1)\Delta t\sin(b(n-1)\Delta t)e^{-a\Delta t} \\ -\chi_1(n) \end{array}\right) \\ &\quad - \frac{b}{a}\xi_2(n) \end{aligned} \tag{3.3.53}$$

From (3.3.49) we can obtain

$$\begin{aligned}
\xi_2(n) &= \frac{1}{a\Delta t} e^{-an\Delta t} \int_{(n-1)\Delta t}^{n\Delta t} t'\cos(bt')\, de^{at'} \\
&= \frac{1}{a\Delta t} e^{-an\Delta t} \left(t'\cos(bt') e^{at'} \Big|_{(n-1)\Delta t}^{n\Delta t} - \int_{(n-1)\Delta t}^{n\Delta t} e^{at'} d\left(t'\cos(bt')\right) \right) \\
&= \frac{1}{a\Delta t} e^{-an\Delta t} \left(\begin{array}{l} t'\cos(bt') e^{at'} \Big|_{(n-1)\Delta t}^{n\Delta t} - \int_{(n-1)\Delta t}^{n\Delta t} \cos(bt')\, e^{at'} dt' \\ + b\int_{(n-1)\Delta t}^{n\Delta t} t'\sin(bt')\, e^{at'} dt' \end{array} \right) \\
&= \frac{1}{a\Delta t} \left(\begin{array}{l} n\Delta t\cos(bn\Delta t) - (n-1)\Delta t\cos(b(n-1)\Delta t) e^{-a\Delta t} \\ - \chi_2(n) \end{array} \right) \\
&\quad + \frac{b}{a}\xi_1(n)
\end{aligned} \tag{3.3.54}$$

Solve (3.3.53) and (3.3.54) we can obtain

$$\xi_1(n) = \frac{\left(\begin{array}{l} \frac{1}{a\Delta t}\left(n\Delta t\sin(bn\Delta t) - (n-1)\Delta t\sin(b(n-1)\Delta t) e^{-a\Delta t} - \chi_1(n)\right) \\ -\frac{b}{a^2\Delta t}\left(n\Delta t\cos(bn\Delta t) - (n-1)\Delta t\cos(b(n-1)\Delta t) e^{-a\Delta t} - \chi_2(n)\right) \end{array} \right)}{1 + \frac{b^2}{a^2}} \tag{3.3.55}$$

$$\xi_2(n) = \frac{\left(\begin{array}{l} \frac{1}{a\Delta t}\left(n\Delta t\cos(bn\Delta t) - (n-1)\Delta t\cos(b(n-1)\Delta t) e^{-a\Delta t} - \chi_1(n)\right) \\ +\frac{b}{a^2\Delta t}\left(n\Delta t\sin(bn\Delta t) - (n-1)\Delta t\sin(b(n-1)\Delta t) e^{-a\Delta t} - \chi_2(n)\right) \end{array} \right)}{1 + \frac{b^2}{a^2}} \tag{3.3.56}$$

So using (3.3.51), (3.3.52), (3.3.55), and (3.3.56) we can obtain any instant time moment values of χ_1, χ_2, ξ_1, *and* ξ_2. Therefore from (3.3.44) and (3.3.45) we can calculate the values of $I_1(n), I_1(n-1),\ I_2(n),$ *and* $I_2(n-1)$.

Substitute $I_1(n), I_1(n-1),\ I_2(n),$ *and* $I_2(n-1)$ into (3.3.32) we can get $\phi(n)$ *and* $\phi(n-1)$. For time step t = (n + 1) Δt from (3.3.44) and (3.3.45) we have:

$$I_1(n+1) = e^{-a\Delta t} I_1(n) + \big((n+1)u(n) - nu(n+1)\big)\chi_1(n+1) + \big(u(n+1) - u(n)\big)\xi_1(n+1) \tag{3.3.57}$$

and

$$I_2(n+1) = e^{-a\Delta t} I_2(n) + \big((n+1)u(n) - n\,u(n+1)\big)\chi_2(n+1) + \big(u(n+1) - u(n)\big)\xi_2(n+1) \tag{3.3.58}$$

From (3.3.32) we have

$$\phi(n+1) = \gamma\big(\sin\big(\beta(n+1)\big)I_2(n+1) - \cos\big(\beta(n+1)\big)I_1(n+1)\big) \tag{3.3.59}$$

Substitute (3.3.57) and (3.3.58) into (3.3.59) and after some manipulation we obtain

$$\phi(n+1) = C_c u(n+1) + \phi_{cp} \tag{3.3.60}$$

where

$$C_c = \gamma\sin\big(\beta(n+1)\Delta t\big)\big(\xi_2(n+1) - n\chi_2(n+1)\big) - \gamma\cos\big(\beta(n+1)\Delta t\big)\big(\xi_1(n+1) - n\chi_1(n+1)\big) \tag{3.3.61}$$

$$\phi_{cp} = \gamma\sin\big(\beta(n+1)\Delta t\big)\big((n+1)\chi_2(n+1) - \xi_2(n+1)\big)u(n) + e^{1a\Delta t} I_2(n) - \gamma\cos\big(\beta(n+1)\Delta t\big)\big((n+1)\chi_1(n+1) - \xi_1(n+1)\big)u(n) + e^{1a\Delta t} I_1(n) \tag{3.3.62}$$

Solve (3.3.60) and (3.2.9) we obtain

$$u(n+1) = \left(\begin{array}{l} \dfrac{1}{\Delta t^2}T_1 + \dfrac{1}{2\Delta t}T_2 + \alpha T_3 \\ + C_c\left(\dfrac{1}{\Delta t^2}T_4 + \dfrac{1}{2\Delta t}T_5 + \alpha T_6\right) \end{array}\right)^{-1} \left(u_p - \phi_{cp}\left(\frac{1}{\Delta t^2}T_4 + \frac{1}{2\Delta t}T_5 + \alpha T_6\right)\right) \tag{3.3.63}$$

Now using (3.3.63) we can recursively obtain the field value at any instant time.

3.6 MESH TRUNCATION USING A PERFECTLY-MATCHED LAYER (*PML*) ADJACENT TO A LORENTZ MEDIUM

In the PML region, the permittivity and permeability are expressed as (Appendix C)

$$[\underset{\sim}{\varepsilon}] = \varepsilon_0 \underset{\sim}{\varepsilon_r} [\wedge] \tag{3.6.1}$$

$$[\underset{\sim}{\varepsilon}] = \underset{\sim}{\mu_0} \underset{\sim}{\mu_r} [\wedge] \tag{3.6.2}$$

where

$$[\wedge] = \begin{pmatrix} \frac{s_y s_z}{s_x} & 0 & 0 \\ 0 & \frac{s_z s_x}{s_y} & 0 \\ 0 & 0 & \frac{s_x s_y}{s_z} \end{pmatrix} \tag{3.6.3}$$

In this two-D case

$$s_z = 1 \tag{3.6.4}$$

In the two-dimensional situation with which we are concerned in this chapter the coordinates are as shown in Fig.3.2.

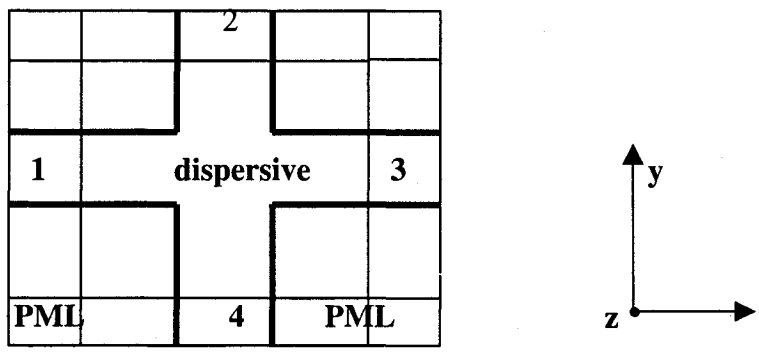

Figure 3.2: Two dimensional problem with PML boundary condition

Suppose that PML is a sourceless region. Accordingly (2.2.1) should be modified as

$$\frac{\varepsilon_r \omega^2}{c_0^2}[\wedge]\ \underset{\sim}{\bar{E}}(x,y,\omega) - \nabla\times\left((\mu_r[\wedge])^{-1}\nabla\times\underset{\sim}{\bar{E}}(x,y,\omega)\right)=0 \tag{3.6.5}$$

If we substitute (2.6.1) into (3.6.5) we obtain the wave equation in dispersive midea as

$$\begin{aligned}&\frac{\varepsilon_\infty \omega^2}{c_0^2}[\wedge]\ \underset{\sim}{\bar{E}}(x,y,\omega) + \frac{\omega^2}{c_0^2}[\wedge]\,\underset{\sim}{\chi_e}(\omega)\underset{\sim}{\bar{E}}(x,y,\omega)\\ &-\nabla\times\left((\mu_r[\wedge])^{-1}\nabla\times\underset{\sim}{\bar{E}}(x,y,\omega)\right)=0\end{aligned} \tag{3.6.6}$$

Considering this TM case and there are only z direction vectors in the equation we can test (3.6.6) by scalar function $T(x,y)$

$$\begin{aligned}&\int_s \frac{\varepsilon_\infty \omega^2}{c_0^2}T(x,y)[\wedge]\underset{\sim}{\bar{E}}(x,y,\omega)\,ds + \int_s \frac{\omega^2}{c_0^2}T(x,y)[\wedge]\ \underset{\sim}{\chi_e}(\omega)\underset{\sim}{\bar{E}}(x,y,\omega)ds\\ &+\int_s \nabla T(x,y)\times\left((\mu_r[\wedge])^{-1}\ \nabla\times\underset{\sim}{\bar{E}}(x,y,\omega)\right)ds=0\end{aligned} \tag{3.6.7}$$

In PML regions adjacent to the dipersive region, substitute (3.6.3) and (3.6.4) into (3.6.7) and with the same way as introduced in section 2.3 and 3.2, in each element we can derive

$$\begin{aligned}&\frac{\varepsilon_\infty \omega^2}{c_0^2}s_x s_y[A^e]\underset{\sim}{V^e} + \frac{\omega^2}{c_0^2}s_x s_y[A^e]\underset{\sim}{\varphi^e} + (\mu_r)^{-1}\frac{s_x}{s_y}[B^e]\underset{\sim}{V^e}\\ &+(\mu_r)^{-1}\frac{s_y}{s_x}[C]\underset{\sim}{V^e} - \frac{s_y}{s_x}\underset{\sim}{H^e}=0\end{aligned} \tag{3.6.8}$$

If we time the both sides of (3.6.8) with $\frac{s_x}{s_y}$ we obtain

$$\begin{aligned}&\frac{\varepsilon_\infty \omega^2}{c_0^2}s_x^2[A^e]\underset{\sim}{V^e} + \frac{\omega^2}{c_0^2}s_x^2[A^e]\underset{\sim}{\varphi^e} + (\mu_r)^{-1}\frac{s_x^2}{s_y^2}[B^e]\underset{\sim}{V^e}\\ &+(\mu_r)^{-1}[C]\underset{\sim}{V^e} - \underset{\sim}{H^e}=0\end{aligned} \tag{3.6.9}$$

After assemble the matrices in (3.6.9) we get the equation in whole computational area as:

$$\frac{\varepsilon_\infty \omega^2}{c_0^2} s_x^2 [A] \underset{\sim}{V} + \frac{\omega^2}{c_0^2} s_x^2 [A] \underset{\sim}{\varphi} + (\mu_r)^{-1} \frac{s_x^2}{s_y^2} [B] \underset{\sim}{V} + (\mu_r)^{-1} [C] \underset{\sim}{V} = 0 \tag{3.6.10}$$

Define

$$\underset{\sim}{\Phi} = \frac{\underset{\sim}{V}}{(-\omega^2 s_y^2)} \tag{3.6.11}$$

Substituting (3.6.11) into (3.6.10) results in

$$\frac{\varepsilon_\infty \omega^2}{c_0^2} s_x^2 [A] \underset{\sim}{V} + \frac{\omega^2}{c_0^2} s_x^2 [A] \underset{\sim}{\varphi} - (\mu_r)^{-1} (-\omega^2) s_x^2 [B] \underset{\sim}{\Phi} + (\mu_r)^{-1} [C] \underset{\sim}{V} = 0 \tag{3.6.12}$$

Define

$$\begin{cases} s_x = \alpha + \dfrac{\sigma_x}{j\omega\varepsilon_0} \\ s_y = \alpha + \dfrac{\sigma_y}{j\omega\varepsilon_0} \end{cases} \tag{3.6.13}$$

If we substitute (3.6.13) into (3.6.12) we obtain

$$-\frac{\varepsilon_\infty}{c_0^2}\left(-\omega^2 + \frac{2\sigma_x}{\varepsilon_0} j\omega + \frac{\sigma_x^2}{\varepsilon_0^2}\right)[A] \underset{\sim}{V} - \frac{1}{c_0^2}\left(-\omega^2 + \frac{2\sigma_x}{\varepsilon_0} j\omega + \frac{\sigma_x^2}{\varepsilon_0^2}\right)[A] \underset{\sim}{\varphi} - (\mu_r)^{-1}\left(-\omega^2 + \frac{2\sigma_x}{\varepsilon_0} j\omega + \frac{\sigma_x^2}{\varepsilon_0^2}\right)[B] \underset{\sim}{\Phi} + (\mu_r)^{-1} [C] \underset{\sim}{V} = 0 \tag{3.6.14}$$

Using relationship in (2.3.13) we can transfer (3.6.14) from frequency domain into time domain as:

$$-\frac{\varepsilon_\infty}{c_0^2}[A]\left(\frac{d^2}{dt^2}+\frac{2\sigma_x}{\varepsilon_0}\frac{d}{dt}+\frac{\sigma_x^2}{\varepsilon_0^2}\right)V(t)-\frac{1}{c_0^2}[A]\left(\frac{d^2}{dt^2}+\frac{2\sigma_x}{\varepsilon_0}\frac{d}{dt}+\frac{\sigma_x^2}{\varepsilon_0^2}\right)\varphi(t)$$
$$-(\mu_r)^{-1}[B]\left(\frac{d^2}{dt^2}+\frac{2\sigma_x}{\varepsilon_0}\frac{d}{dt}+\frac{\sigma_x^2}{\varepsilon_0^2}\right)\Phi(t)+(\mu_r)^{-1}[C]V(t)=0 \tag{3.6.15}$$

In order to use EVFE we define

$$\Phi(t)=\psi(t)e^{j\omega_c t} \tag{3.6.16}$$

If we substitute (3.6.16), (2.5.1)and (3.2.6) into (3.6.15) and after some manipulation we obtain an envelope equation

$$G_1\frac{d^2}{d^2t}u(t)+G_2\frac{d}{dt}u(t)+G_3u(t)+G_4\frac{d^2}{d^2t}\phi(t)+G_5\frac{d}{dt}\phi(t)+G_6\phi(t)$$
$$+G_7\frac{d^2}{d^2t}\psi(t)+G_8\frac{d}{dt}\psi(t)+G_9\psi(t)=-h(t) \tag{3.6.17}$$

where

$$\begin{cases}
G_1=\dfrac{1}{c_0}[A] \\
G_2=\dfrac{2}{c_0}[A](j\omega_c+\dfrac{\sigma_x}{\varepsilon_0}) \\
G_3=\dfrac{1}{c_0^2}[A](j\omega_c+\dfrac{\sigma_x}{\varepsilon_0})^2+\dfrac{1}{\mu_r}[C] \\
G_4=G_1 \\
G_5=G_2 \\
G_6=\dfrac{1}{c_0^2}[A](j\omega_c+\dfrac{\sigma_x}{\varepsilon_0})^2 \\
G_7=\dfrac{1}{\mu_r}[B] \\
G_8=\dfrac{2}{\mu_r}[B](j\omega_c+\dfrac{\sigma_x}{\varepsilon_0}) \\
G_9=\dfrac{1}{\mu_r}[B](j\omega_c+\dfrac{\sigma_x}{\varepsilon_0})^2
\end{cases} \tag{3.6.18}$$

Using Newmark-Beta formulations we can discretize (3.6.17) in time domain as:

$$\left(\frac{1}{\Delta t^2}G_1+\frac{1}{2\Delta t}G_2+\alpha G_3\right)u(n+1)+\left(\frac{1}{\Delta t^2}G_4+\frac{1}{2\Delta t}G_5+\alpha G_6\right)\phi(n+1)$$
$$+\left(\frac{1}{\Delta t^2}G_7+\frac{1}{2\Delta t}G_8+\alpha G_9\right)\psi(n+1)=u_m \tag{3.6.19}$$

where

$$\begin{aligned}
u_m=&\frac{1}{\Delta t^2}G_1\left(-2u(n)+u(n-1)\right)-\frac{1}{2\Delta t}G_2u(n-1)+\\
&G_3\left((1-2\alpha)u(n)+\alpha u(n-1)\right)+\frac{1}{\Delta t^2}G_4\left(-2\phi(n)+\phi(n-1)\right)\\
&-\frac{1}{2\Delta t}G_5\phi(n-1)+G_6\left((1-2\alpha)\phi(n)+\alpha\phi(n-1)\right)\\
&+\frac{1}{\Delta t^2}G_7\left(-2\psi(n)+\psi(n-1)\right)\\
&-\frac{1}{2\Delta t}G_8\psi(n-1)+G_9\left((1-2\alpha)\psi(n)+\alpha\psi(n-1)\right)\\
&-\left(\alpha h(n+1)+(1-2\alpha)h(n)+\alpha h(n-1)\right)\\
&-\left(\alpha F(n+1)+(1-2\alpha)F(n)+\alpha F(n-1)\right)
\end{aligned} \tag{3.6.20}$$

Now rewrite (3.6.11) as:

$$s_y^2\left(-\omega^2\right)\underset{\sim}{\Phi}=\underset{\sim}{V} \tag{3.6.21}$$

If we substitute (3.6.13) into (3.6.21) we obtain

$$\left(-\omega^2+\frac{2\sigma_y}{\varepsilon_0}j\omega+\frac{\sigma_y^2}{\varepsilon_0^2}\right)\underset{\sim}{\Phi}=\underset{\sim}{V} \tag{3.6.22}$$

Using relationship $-\omega^2\leftrightarrow\frac{d^2}{dt^2}$ *and* $j\omega\leftrightarrow\frac{d}{dt}$ we can transfer (3.6.22) from frequency domain into time domain as:

$$\left(\frac{d^2}{dt^2}+\frac{2\sigma_y}{\varepsilon_0}\frac{d}{dt}+\frac{\sigma_y^2}{\varepsilon_0^2}\right)\Phi(t)=V(t) \tag{3.6.23}$$

To use EVFE we substitute $\Phi(t)=\psi(t)e^{j\omega_c t}$ *and* $V(t)=u(t)e^{j\omega_c t}$ into (3.6.23) and after some manipulation we can get:

$$\frac{d^2}{dt^2}\psi(t)+2\left(j\omega_c+\frac{\sigma_y}{\varepsilon_0}\right)\frac{d}{dt}\psi(t)+\left(j\omega_c+\frac{\sigma_y}{\varepsilon_0}\right)^2\psi(t)=u(t) \tag{3.6.24}$$

Using Newmark-Beta formulations again we can discretize (3.6.24). And after some manipulation we can get expression

$$\psi(n+1)=\frac{K_2}{K_1}u(n+1)+\frac{K_3}{K_1} \tag{3.6.25}$$

where

$$\begin{cases} K_1=\dfrac{1}{\Delta t^2}+\dfrac{1}{\Delta t}\left(j\omega_c+\dfrac{\sigma_y}{\varepsilon_0}\right)+\alpha\left(j\omega_c+\dfrac{\sigma_y}{\varepsilon_0}\right)^2 \\ K_2=\alpha \\ K_3=(1-2\alpha)u(n)+\alpha u(n-1)+\dfrac{1}{\Delta t^2}\left(2\psi(n)-\psi(n-1)\right) \\ \qquad +\dfrac{1}{\Delta t}\left(j\omega_c+\dfrac{\sigma_y}{\varepsilon_0}\right)\psi(n-1)-\left(j\omega_c+\dfrac{\sigma_y}{\varepsilon_0}\right)^2\left((1-2\alpha)\psi(n)+\alpha\psi(n-1)\right) \end{cases} \tag{3.6.26}$$

If we substitute (3.6.25) into (3.6.19) and after some manipulation we obtain

$$\begin{aligned} &\left(\frac{1}{\Delta t^2}G_1+\frac{1}{2\Delta t}G_2+\alpha G_3+\frac{K_2}{K_1}\left(\frac{1}{\Delta t^2}G_7+\frac{1}{2\Delta t}G_8+\alpha G_9\right)\right)u(n+1) \\ &+\left(\frac{1}{\Delta t^2}G_4+\frac{1}{2\Delta t}G_5+\alpha G_6\right)\phi(n+1)=u_m-\frac{K_3}{K_1} \end{aligned} \tag{3.6.27}$$

First we solve (3.6.27) and (3.3.5) in section 3.3 we can obtain

$$u(n+1)=\left(\begin{array}{l}\frac{1}{\Delta t^2}G_1+\frac{1}{2\Delta t}G_2+\alpha G_3\\ +\frac{C_{f2}}{C_{f1}}\left(\frac{1}{\Delta t^2}G_4+\frac{1}{2\Delta t}G_5+\alpha G_6\right)\\ +\frac{K_2}{K_1}\left(\frac{1}{\Delta t^2}G_7+\frac{1}{2\Delta t}G_8+\alpha G_9\right)\end{array}\right)^{-1}\left(\begin{array}{l}u_m-\frac{1}{C_{f1}}\phi_{fp}\times\\ \left(\frac{1}{\Delta t^2}G_4+\frac{1}{2\Delta t}G_5+\alpha G_6\right)\\ -\frac{K_3}{K_1}\times\\ \left(\frac{1}{\Delta t^2}G_7+\frac{1}{2\Delta t}G_8+\alpha G_9\right)\end{array}\right) \quad (3.6.28)$$

Therefore using (3.3.5), (3.6.25) and (3.6.28) we can recursively obtain the field values at whole computational time domain with the first method in section 3.3.

Secondly, we solve (3.6.27) and (3.3.26) in section 3.4 we can obtain

$$u(n+1)=\left(\begin{array}{l}\frac{1}{\Delta t^2}G_1+\frac{1}{2\Delta t}G_2+\alpha G_3\\ +\frac{C_{t2}}{C_{t1}}\left(\frac{1}{\Delta t^2}G_4+\frac{1}{2\Delta t}G_5+\alpha G_6\right)\\ +\frac{K_2}{K_1}\left(\frac{1}{\Delta t^2}G_7+\frac{1}{2\Delta t}G_8+\alpha G_9\right)\end{array}\right)^{-1}\left(\begin{array}{l}u_m-\frac{1}{C_{t1}}\phi_{fp}\times\\ \left(\frac{1}{\Delta t^2}G_4+\frac{1}{2\Delta t}G_5+\alpha G_6\right)\\ -\frac{K_3}{K_1}\times\\ \left(\frac{1}{\Delta t^2}G_7+\frac{1}{2\Delta t}G_8+\alpha G_9\right)\end{array}\right) \quad (3.6.29)$$

Therefore using (3.3.26), (3.6.29) and (3.6.25) we can recursively obtain the field values in whole computational time domain with the second way in section 3.4.

Thirdly, we solve (3.6.27) and (3.3.60) in section 3.5 we can obtain

$$u(n+1)=\left(\begin{array}{l}\frac{1}{\Delta t^2}G_1+\frac{1}{2\Delta t}G_2+\alpha G_3\\ +C_c\left(\frac{1}{\Delta t^2}G_4+\frac{1}{2\Delta t}G_5+\alpha G_6\right)\\ +\frac{K_2}{K_1}\left(\frac{1}{\Delta t^2}G_7+\frac{1}{2\Delta t}G_8+\alpha G_9\right)\end{array}\right)^{-1}\left(\begin{array}{l}u_m-\phi_{cp}\times\\ \left(\frac{1}{\Delta t^2}G_4+\frac{1}{2\Delta t}G_5+\alpha G_6\right)\\ -\frac{K_3}{K_1}\times\\ \left(\frac{1}{\Delta t^2}G_7+\frac{1}{2\Delta t}G_8+\alpha G_9\right)\end{array}\right) \quad (3.6.30)$$

Therefore using (3.3.60), (3.6.30) and (3.6.25) we can recursively obtain the field values within whole computational time domain with the third way in section 3.5.

3.7 **CONCLUDING REMARKS**

In this chapter, three methods of incorporating Lorentz media into the EVFE method have been presented for the first time. The first two methods preserve the larger-time-step advantage of the EVFE over the FETD and are the ones to be used in practice. The third method, intended as a reference method for the development work against which to measure the clear time-step size advantages of the EVFE, does not possess the said advantage. This is to be expected since it evaluates the convolution integrals directly, which have to be evaluated using a time-step appropriate for the carrier rather than the envelope. We note that the first method can also be used for materials with dispersive characteristics other than the Loretz type (although this has not been implemented in the thesis); this fact represents an additional generalization of the existing EVFE techniques. In order to validate these new developments it will of course be necessary to implement these numerically, and so this will be the subject of Chapter 4.

CHAPTER 4

THE INCORPORATION OF LORENTZ DISPERSIVE MATERIALS IN THE *EVFE* METHOD : COMPUTATIONAL ASPECTS & VALIDATION

4.1 INTRODUCTORY COMMENTS

A complete two-dimensional formulation of the EVFE method in the presence of Lorentz-type dispersive material has been given in Chapter 3. In order to test the validity of any computational method it is desirable to compare its predictions to those obtained from analytical solutions. Usually analytical solutions are only known for certain simplified geometries. Nevertheless, these serve as validity tests of the computational method, even though the latter can be applied to more complicated geometries. Indeed, this is the reason so much effort is put into developing computational methods in the first place.

Unfortunately, analytical solutions do not appear to be available for two-dimensional problem geometries which include Lorentz-type dispersive material. Thus in order to validate the formulation of Chapter 3 we will apply it to one-dimensional problems for which analytical solutions are easily obtained. We will for convenience refer to these as the "validation problems". The contention is that if the EVFE formulation developed in Chapter 3 is successful when applied to the one-dimensional problems then its correctness for two-dimensional applications is at once validated as well.

In Section 4.2 we will define the two validation problems that will be discussed in this chapter. Section 4.3 will describe the manner in which the incident field is applied. Section 4.4 tests the effectiveness of the PMLs when they are used to truncate regions of non-dispersive material. This is immediately followed by a discussion of the first validation problem in Section 4.5. There we will observe the effectiveness of the PMLs when they are use to truncate regions of Lorentz-type dispersive material, and also note the broadening of the field envelope as it moves through the dispersive material. The computed results will be compared to those obtained using a semi-analytical method. In Section 4.6 we consider reflection of a Gaussian pulse-modulated plane wave incident on the interface between dispersive and non-dispersive material, and the correctness of the interesting results discussed. Some concluding remarks are given in Section 4.7.

4.2 VALIDATION PROBLEMS FOR COMPARISON WITH SEMI-ANALYTICAL SOLUTIONS

4.2.1 Preliminary Remarks

The geometry considered consists of an incident plane wave in non-dispersive or dispersive material. The coordinate system is so chosen that the wave propagates in the x-direction and the electric field is z-polarised. Thus the incident electric field is of the form $\vec{E}(x, y, z) = \hat{z}\, E_z(x)$ in the frequency-domain form, and $\vec{E}(x, y, z, t) = \hat{z}\, E_z(x,t)$ in the time-domain form. The structure is infinite along the z-direction and along the y-direction. We note that the incident electric field can be described by the one-dimensional scalar function $E_z(x)$.

The dispersive material will always be such that its electromagnetic properties are functions of x only, and not of y or z. Thus any inhomogeneity is along the x-direction (i.e. the propagation direction) only. This means that if only x-travelling plane waves are incident on the material, then only x-travelling plane waves will be excited by the material inhomogeneities. This means that the total electric field (and not only the incident electric field) will always be entirely z-directed, and a function of x only (and not y or z). Thus all derivatives with respect to either the y-variable or the z-variable are zero. The latter fact can be used in the formulation of Chapter 3 to make it directly applicable to the one-dimensional validation problems under consideration here.

4.2.2 First Validation Problem

The first validation problem is shown in Figure 4.1. There is a single piece of Lorentz-type dispersive material (of thickness L). In order to apply the EVFE method the solution region has to be truncated to be of finite size, and so the above-mentioned material is bounded by PML layers which are terminated in perfect electric conductors. There is an impressed electric current source density located at $x = x_s$ in the dispersive material. As pointed out in Section 4.2.1, this is a one-dimensional scalar problem.

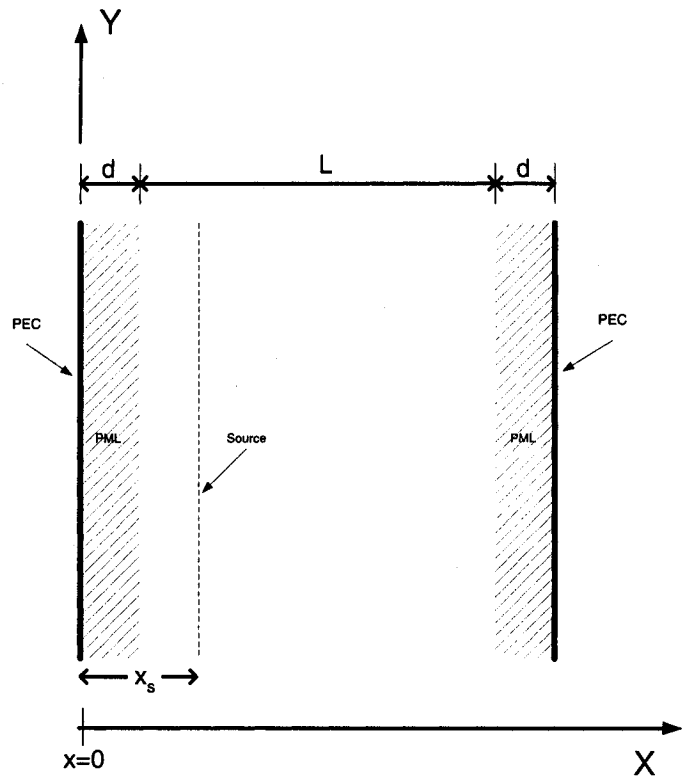

Figure 4.1 : The First Validation Problem

4.2.3 Second Validation Problem

The second validation problem is shown in Figure 4.2. There are two pieces of material of length L_1 and L_2, respectively. The first piece of length L_1 is non-dispsersive material; it need not be but is chosen to be so for this validation problem. The second piece of material, of length L_2, has Lorentz-type dispersion. Once again, in order to apply the EVFE method the solution region has to be truncated to be of finite size, and so the above-mentioned material is bounded by PML layers which are terminated in perfect electric conductors. There is an impressed electric current source density located at $x = x_s$ in the dispersive material. As pointed out in Section 4.2.1, this is a one-dimensional scalar problem.

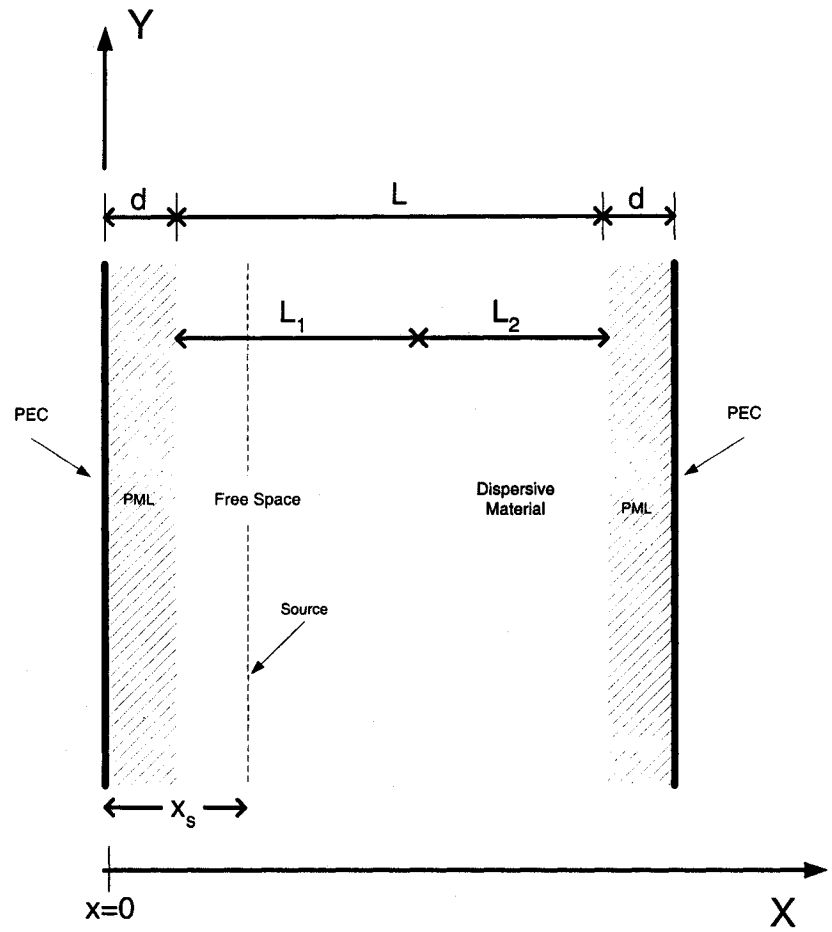

Figure 4.2 : The Second Validation Problem

4.3 SPEFICATION OF SOURCES IN THE VALIDATION PROBLEM

In order to generate a plane wave we use a sheet of current density at x = x_s given by

$$\underset{\sim}{J}_z(x,y,\omega) = \hat{z}\underset{\sim}{J}_0(x,y,\omega)\delta(x-x_s) \tag{4.3.1}$$

This source can generate a plane wave both in the +x direction and –x direction [17]

$$\underset{\sim}{E}_z(x,y,\omega) = -\frac{\eta J_0(x,y,\omega)}{2}\begin{cases} e^{-\gamma(x-x_s)} & x > x_s \\ e^{+\gamma(x-x_s)} & x < x_s \end{cases} \tag{4.3.2}$$

where η is the wave impedance and

$$\eta = \frac{j\omega\mu}{\gamma} \tag{4.3.3}$$

where γ is the wave propagation constant. At the source plane (4.3.1) and (4.3.2) will take the following forms respectively

$$\underset{\sim}{J}_z(x = x_s, y, \omega) = \hat{z}\underset{\sim}{J}_0(x = x_s, y, \omega) \tag{4.3.4}$$

$$\underset{\sim}{E}_z(x = x_s, y, \omega) = \frac{\eta J_0(x = x_s, y, \omega)}{2} \tag{4.3.5}$$

In order to generate a modulated Gaussian pulse at the source plane

$$E_z(t) = \hat{z}e^{\frac{(t-3\sigma_t)}{2\sigma_t^2}} e^{j\omega_c t} \tag{4.3.6}$$

we chose

$$J_0(x = x_s, y, \omega) = \frac{2}{\eta}\left(-\frac{j}{\sqrt{2\pi}\left(\omega_c - \omega + j\frac{1}{2\sigma_t^2}\right)} e^{\frac{3}{2\sigma_t}} \right) \tag{4.3.7}$$

where ω_c is the carrier frequency.

Through the above we observe that if we substitute (4.3.7) into (4.3.5) and use Fourier transformation we can obtain a modulated Gaussian pulse at the source plane the same as (4.3.6).

If we substitute (4.3.4) into $f_i^e(\omega)$ expression in (2.3.11) we have

$$\underset{\sim}{f}_i^e(x = x_s, \omega) = \mathrm{j}\omega\mu_0 \int_{s_e} N_i^e(x = x_s, y)\underset{\sim}{J}_i^e(x = x_s, y, \omega)\, ds \tag{4.3.8}$$

According to (4.3.4) and (4.3.5) we can rewrite the (4.3.8) as

$$\underset{\sim}{f}_{zi}^{e}(x=x_s,\omega) = j\omega\mu_0\frac{2}{\eta}\int_{s_e} N_i^e(x=x_s,y)\,\underset{\sim}{E}_{zi}^{e}(x=x_s,y,\omega)\,ds \tag{4.3.9}$$

If we substitute (4.3.3) into (4.3.9) we can obtain

$$\underset{\sim}{f}_{zi}^{e}(x=x_s,\omega) = 2\mu_r^{-1}\gamma\int_{S_e}\left(N_i^e(x=x_s,y,\omega)\,\underset{\sim}{E}_{zi}^{e}(x=x_s,y,\omega)\right)dS \tag{4.3.10}$$

Since the incident field is a plane wave on the incident plane the incident field will not change with the position. Therefore at incident plane (4.3.10) can be written as

$$\underset{\sim}{f}_{zi}^{e}(x=x_s,\omega) = 2\mu_r^{-1}\gamma\underset{\sim}{E}_{zi}^{e}(x=x_s,\omega)\int_{S_e} N_i^e(x=x_s,y,\omega)dS \tag{4.3.11}$$

Define

$$D_i^e(x=x_s) = \int_{s_e} N_i^e(x=x_s,y)ds \tag{4.3.12}$$

The value of D_i is given in Appendix A. So we can rewrite (4.3.11) as

$$\underset{\sim}{f}_{zi}^{e}(x=x_s,\omega) = 2\mu_r^{-1}\gamma\underset{\sim}{E}_{zi}^{e}(x=x_s,\omega)D_i^e(x=x_s) \tag{4.3.13}$$

In Lorentz media the propagation constant

$$\begin{aligned}\gamma = j\omega\sqrt{\varepsilon\mu} &= j\omega\left(\varepsilon_0\mu_0\left(\varepsilon_\infty + \frac{(\varepsilon_s-\varepsilon_\infty)\omega_0^2}{\omega_0^2-\omega^2+2j\omega\Gamma}\right)\right)^{\frac{1}{2}} \\ &= j\omega(\varepsilon_0\mu_0)^{\frac{1}{2}}\left(\varepsilon_\infty + \frac{(\varepsilon_s-\varepsilon_\infty)\omega_0^2}{\omega_0^2-\omega^2+2j\omega\Gamma}\right)^{\frac{1}{2}}\end{aligned} \tag{4.3.14}$$

If we substitute (4.3.14) into (4.3.11) we obtain

$$\underset{\sim}{f}_{zi}^{e}(x=x_s,\omega) = 2j\omega\mu_r^{-1}(\varepsilon_0\mu_0)^{\frac{1}{2}}L_\gamma(\omega)\underset{\sim}{E}_{zi}^{e}(x=x_s,\omega)D_i^e(x=x_s) \tag{4.3.15}$$

where

$$L_\gamma(\omega)=\left(\varepsilon_\infty+\frac{(\varepsilon_s-\varepsilon_\infty)\omega_0^2}{\omega_0^2-\omega^2+2j\omega\Gamma}\right)^{\frac{1}{2}} \tag{4.3.16}$$

For narrow band, $L_\gamma(\omega)$ can be linearized using Taylor series expansion about carrier frequency ω_c as follow [18]

$$\begin{aligned}L_\gamma(\omega)=L_\gamma(\omega_c)+\left.\frac{dL_\gamma(\omega)}{dt}\right|_{\omega=\omega_c}(\omega-\omega_c)\\+\frac{1}{2}\left.\frac{d^2L_\gamma(\omega)}{dt^2}\right|_{\omega=\omega_c}(\omega-\omega_c)^2+\cdots\cdots\end{aligned} \tag{4.3.17}$$

Retaining the first three terms and define

$$\begin{cases}L_1=\left.\dfrac{df_\gamma(\omega)}{dt}\right|_{\omega=\omega_c}\\ L_2=\left.\dfrac{d^2f_\gamma(\omega)}{dt^2}\right|_{\omega=\omega_c}\\ L_0=f_\gamma(\omega_c)\end{cases} \tag{4.3.18}$$

We can rewrite (4.3.17) as

$$L_\gamma(\omega)=\frac{1}{2}L_2\omega^2+(L_1-\omega_c)\omega+\left(L_0-L_1\omega_c+\frac{1}{2}L_2\omega_c^2\right) \tag{4.3.19}$$

If we substitute (4.3.19) into (4.3.15) we obtain

$$\begin{aligned}\underset{\sim}{f}_{zi}^e(x=x_s,\omega)&=-2j\omega\mu_r^{-1}(\varepsilon_0\mu_0)^{\frac{1}{2}}\begin{pmatrix}\frac{1}{2}L_2\omega^2+(L_1-\omega_c)\omega\\+\left(L_0-L_1\omega_c+\frac{1}{2}L_2\omega_c^2\right)\end{pmatrix}\underset{\sim}{E}_{zi}^e(x=x_s,\omega)D_i^e(x=x_s)\\&=-2\mu_r^{-1}(\varepsilon_0\mu_0)^{\frac{1}{2}}D_i^e(x=x_s)\begin{pmatrix}-\frac{1}{2}L_2(j\omega)^3-(L_1-\omega_c)j(j\omega)^2\\+\left(L_0-L_1\omega_c+\frac{1}{2}L_2\omega_c^2\right)(j\omega)\end{pmatrix}\underset{\sim}{E}_{zi}^e(x=x_s,\omega)\end{aligned} \tag{4.3.20}$$

Now using the relationship

$$j\omega \leftrightarrow \frac{d}{dt} \quad (j\omega)^2 \leftrightarrow \frac{d^2}{dt^2} \quad (j\omega)^3 \leftrightarrow \frac{d^3}{dt^3} \tag{4.3.21}$$

we can transfer (4.3.20) into the time domain as

$$f_{zi}^e(x=x_s,t) = -2\mu_r^{-1}(\varepsilon_0\mu_0)^{\frac{1}{2}} D_i^e(x=x_s)\left(\begin{array}{l} -\frac{1}{2}L_2\frac{d^3E_{zi}^e(x=x_s,t)}{dt^3} - (L_1-\omega_c)j\frac{d^2E_{zi}^e(x=x_s,t)}{dt^2} \\ +\left(l_0 - L_1\omega_c + \frac{1}{2}L_2\omega_c^2\right)\frac{dE_{zi}^e(x=x_s,t)}{dt} \end{array}\right) \tag{4.3.22}$$

where $E_{zi}^e(x=x_s,t)$ is the incident field shown in(4.3.6) and $f_{zi}^e(x=x_s,t)$ is the time domain function of $\underset{\sim}{f}_{zi}^e(x=x_s,\omega)$.

Thus we can use equation (4.3.22) to calculate $f_{zi}^e(x=x_s,t)$ for any time step.

4.4 THE PERFORMANCE OF PML WITH NON-DISPERSIVE MATERIAL

In order to test the performance of the PML with nondispersive material we choose the problem shown in Figure 4.1 and let the material in the region of thickness L be free space (and hence non-dispersive). The specific dimensions are listed in Table 4.1.

Table 4.1 Parameters for the Problem Geometry of Figure 4.1

Quantity	*Description*	*Value*
L	Length of Region Between the PMLs	90mm
d	Thickness of Each PML Layer	15mm
x_{left}	Location of Left PML Face	15mm
x_{right}	Location of Right PML Face	75mm
x_s	Location of Source	17mm
Δx	Length of Finite Element	0.1mm
f_c	Carrier Frequency	291 GHz
σ_t	Width of the Gaussian Envelope of the Source Located at $x = x_s$	0.03 ns

In order to reduce the discretization error we use a spatially varying PML electric conductivity along the normal axis given by [11]

$$\sigma_x = \frac{\sigma_{\max} |x - x_0|^m}{\sqrt{\varepsilon_r}\, d^m} \tag{4.1}$$

The quantity m is the order of the polynomial describing this conductivity variation, and in this case we will use $m = 2$, and $x_o = x_{left}$ (x_{right}) for the PML on the left (right) in Figure 4.1. In order to determine how well the PML is performing we wish to compute the input reflection coefficient of the PML at x=d+L. Thus we need to know what the incident field is at x=d+L over the time period (say during the period $0 \le t \le T_P$) during which the Guassian envelope strikes the PML until it is fully reflected. The EVFE will always provide only the total field at x=d+L, and thus we need to compute the incident

field $E_z^{inc}(x = d + L, t)$ up to t = T_P using a supplementary problem. In this supplementary problem we simply make L larger (150mm in this case) so that no reflected field reaches the point x=d+L during the period $0 \le t \le T_P$. Then the total field obtruded by the EVFE at x=d+L over the period $0 \le t \le T_P$ will be the incident field there for the actual problem. Figure 4.3 shows this incident field envelope $u^{inc}(x,\ t)$ throughout the region $0 \le x \le 2d + L$ at time t = 0.18ns. Observe that, as expected, there is an envelope that moves in the +x direction (to the right) and one that moves in the –x direction (to the left). The one to the left is quickly dissipated by the PML, and hence its amplitude is small, as can be observed in the figure. Furthermore, we note that the amplitude of the envelope remains constant, as expected in non-dispersive material.

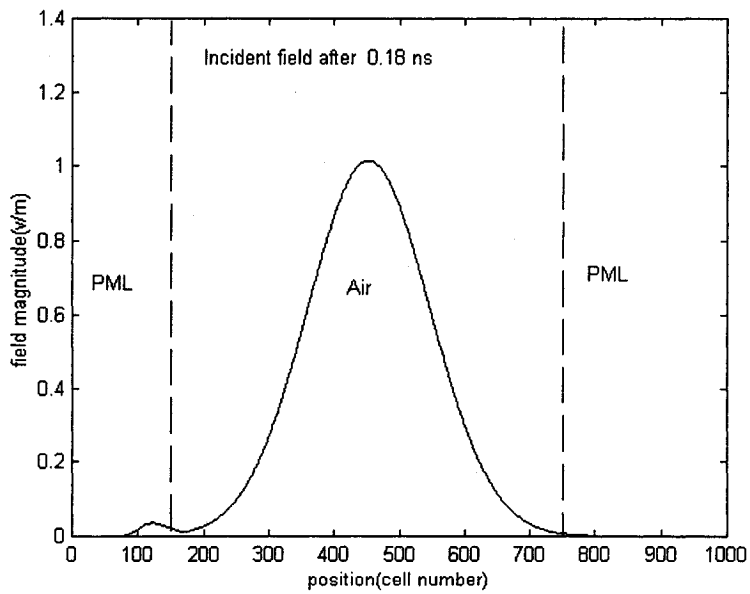

Figure 4.3 : The Incident Field Envelope $|u^{inc}|(x, t = 0.18ns)$ for the First Validation Problem

Figures 4.4 through 4.6 show such "snapshots" of the Gaussian envelope of the incident fields at later times t =0.24 ns, t = 0.27 ns and t = 0.315ns, respectively.

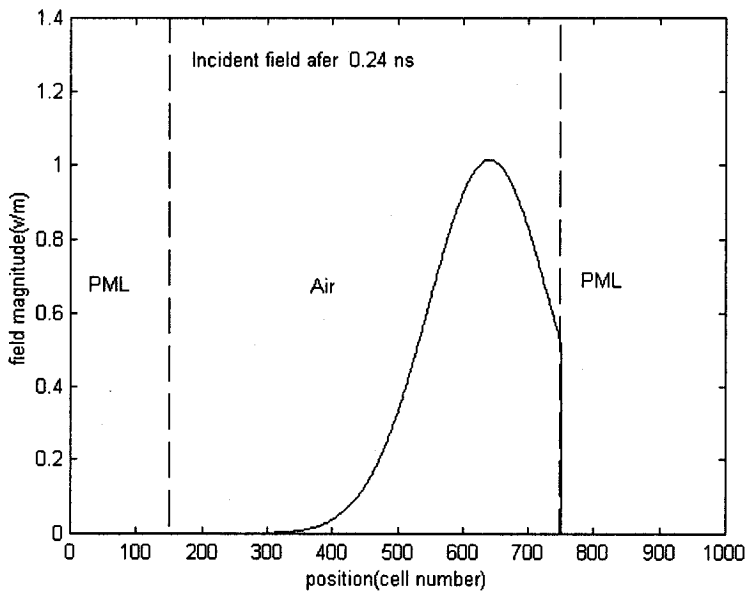

Figure 4.4 : The Incident Field Envelope $|u^{inc}|(x,t=0.24ns)$ **for the First Validation Problem**

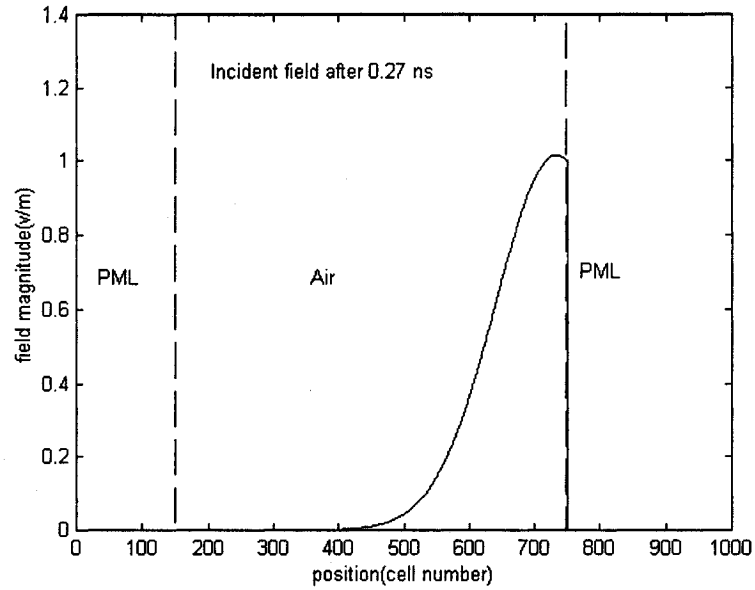

Figure 4.5 : The Incident Field Envelope $|u^{inc}|(x,t=0.27ns)$ for the First Validation Problem

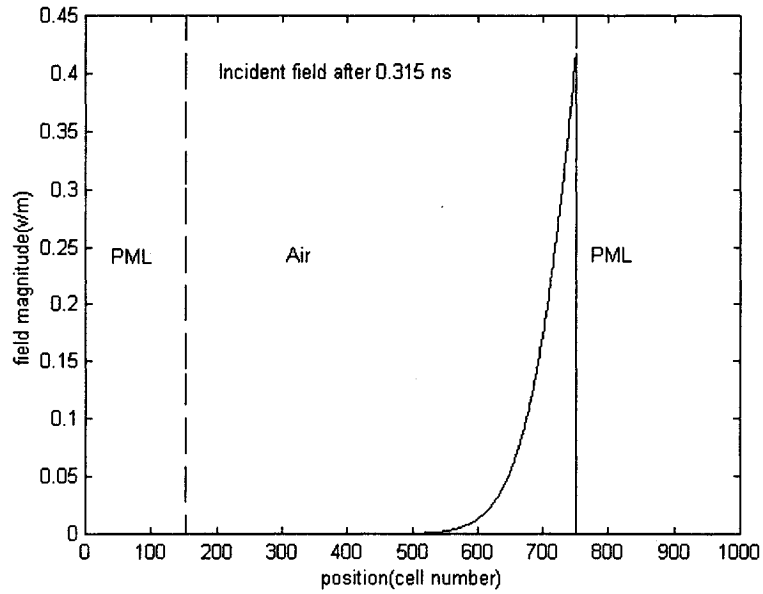

Figure 4.6 : The Incident Field Envelope $|u^{inc}|(x,t=0.315ns)$ for the First Validation Problem

Returning to the original problem, we use the EVFE to compute the envelope of the total field $V^{total}(x,\ t)$. Since we already know the incident field $V^{inc}(x,\ t)$ from the supplementary problem, we can compute the reflected field envelope as $u^{reflected}(x,\ t) = u^{total}(x,\ t) - u^{inc}(x,\ t)$. Figures 4.7 through 4.10 show the "snapshots' of the reflected field envelope at t = 0.24 ns, t = 0.27 ns, t = 0.315 ns and t = 0.375 ns, respectively. We observe that the reflected field envelope is Gaussian pulse, as expected, but that its amplitude is several orders of magnitude smaller (roughly 88dB smaller) than that of the incident field. This is indicative of the fact that the reflection coefficient at the interface between free space and the dissipative PML material is very low.

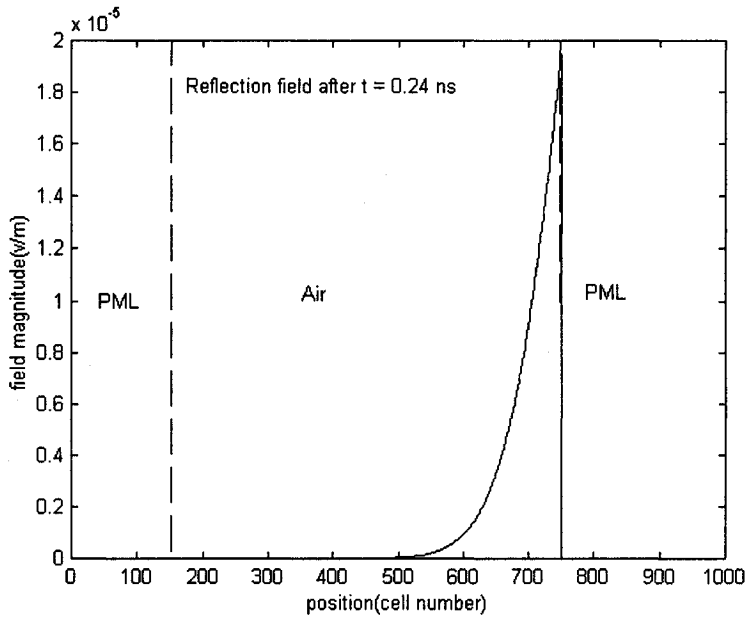

Figure 4.7 : The Reflected Field Envelope $|u^{reflected}|(x, t = 0.24ns)$ for the First Validation Problem

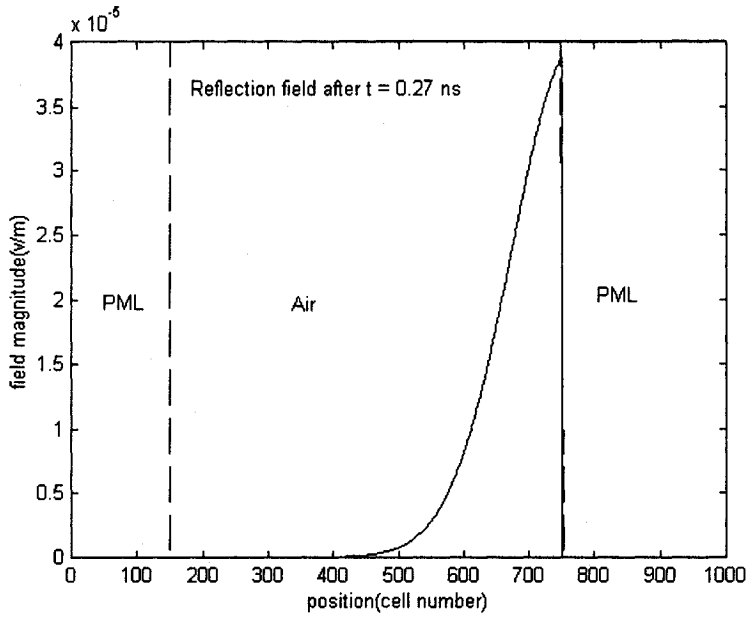

Figure 4.8 : The Reflected Field Envelope $|u^{reflected}|(x, t = 0.27ns)$ for the First Validation Problem

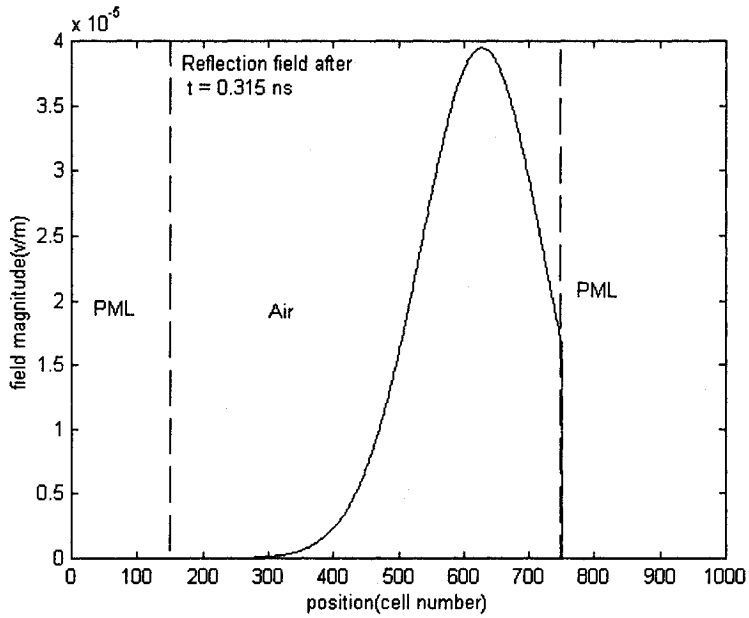

Figure 4.9 : The Reflected Field Envelope $|\mu^{reflected}|(x, t = 0.315ns)$ for the First Validation Problem

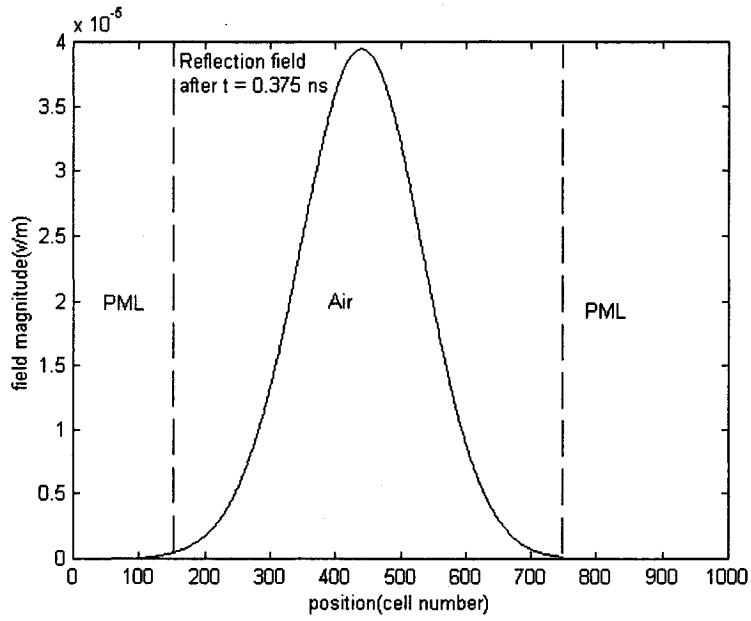

Figure 4.10 : The Reflected Field Envelope $|u^{reflected}|(x,t=0.375ns)$ for the First Validation Problem

We next wish to estimate the performance of the PML on the individual frequency components of the incident field. We denote by *FFT{f(t)}* the Fourier transform of the signal *f(t)* as computed using the fast Fourier transform routine available in the *MATLAB* package [19]. The input reflection coefficient "looking into" the PML at x = d+L can be computed as

$$\Gamma_{PML}(\omega) = \frac{FFT\{E_z^{reflected}(x=d+L,t)\}}{FFT\{E_z^{inc}(x=d+L,t)\}} = \frac{FFT\{u^{reflected}(x=d+L,t)\ \ \cos(2\pi\ \ f_c t)\}}{FFT\{u^{inc}(x=d+L,t)\ \ \cos(2\pi\ \ f_c t)\}}$$

The quantity $20\log|\Gamma_{PML}(\omega)|$ is plotted in Figure 4.11, and is seen to be better than –86dB over the bandwidth of the incident field.

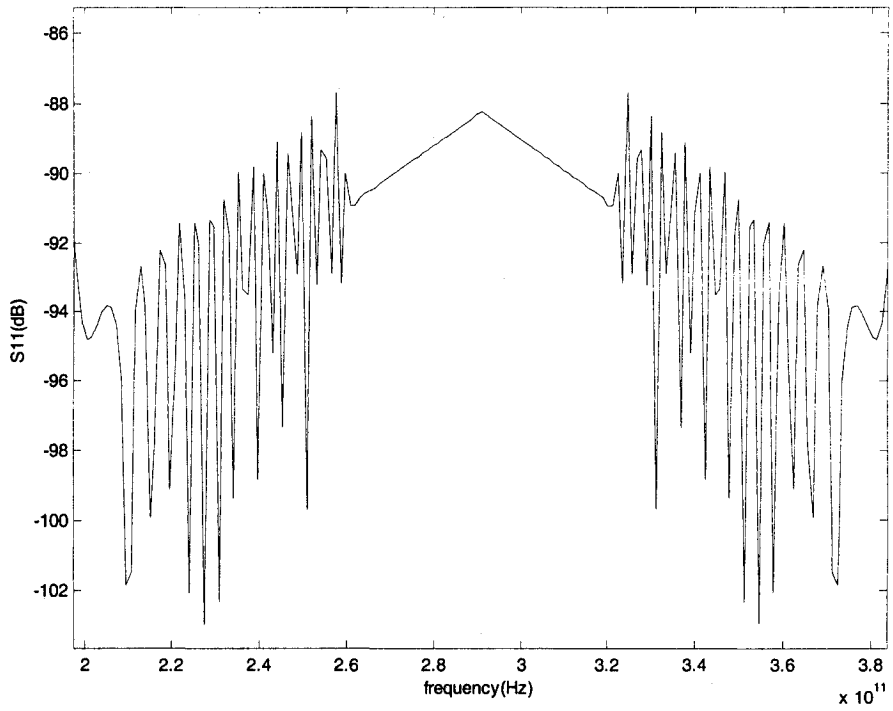

Figure 4.11 : The Reflection Coefficient $\Gamma_{PML}(\omega)$ "Looking Into" the PML at x=d+L

4.5 PROPAGATION OF THE ENVELOPE-MODULATED PLANE WAVE IN DISPERSIVE MATERIAL : PERFORMANCE OF THE PML & ENVELOPE BROADENING

4.5.1 Present Goals

In Section 4.4 we tested the effectiveness of the PML by using it in the EVFE computations of a Gaussian pulse-modulated plane wave in non-dispersive material. This analysis is repeated in Section 4.5.2, for the same dimensions as were used in Section 4.4, except that the material in the region of thickness L is replaced by dispersive material whose properties are provided in Table 4.2. We will continue to examine this problem in

Section 4.5.3, where we compare the results obtained using the EVFE method (with different time-step sizes Δt) to those obtained using a semi-analytical method.

4.5.2 Performance of the PMLs

Figures 4.12 through 4.15 show such "snapshots" of the Gaussian envelope of the incident field at times t = 0.30 ns, t = 0.72 ns, t = 0.9ns and t = 1.08, respectively. This was determined using the supplementary problem approach discussed in Section 4.4. We immediately observe that, due to the dispersive nature of the material, the envelope of the incident field becomes broader and of lower amplitude as it propagates to the right. Figures 4.16 through 4.19 show "snapshots' of the reflected field envelope at t = 0.72ns, t = 0.90ns, t = 1.08ns and t = 1.50ns, respectively. We observe that the reflected field envelope also broadens and decreases in amplitude as it propagates to the left, as expected. The quantity $20\log\left|\Gamma_{PML}(\omega)\right|$, determined in the same way as in Section 4.4, plotted in Figure 4.20, and is seen to be better than –83dB over the bandwidth of the incident field. These results show that the PMLs developed in Section 3.6 for use adjacent to Lorentz-type dispersive material do indeed work well.

Table 4.2 Parameters for the First Validation Problem of Figure 4.1 as Used in Section 4.5.2

Quantity	*Description*	*Value*
L	Length of Region Between the PMLs	90mm
d	Thickness of Each PML Layer	15mm
x_{left}	Location of left PML Face	15mm
x_{right}	Location of right PML Face	75mm
x_s	Location of Source	17mm
Δx	Length of Finite Element	0.1mm
f_c	Carrier Frequency	291 GHz
σ_t	Width of the Gaussian Envelope of the Source Located at $x = x_s$	0.03 ns
$\omega_o / 2\pi$	Resonance Frequency of the Lorentz-Type Material in the Region $d \leq x \leq d+L$	195 GHz
$\Gamma / 2\pi$	Damping Frequency of the Lorentz-Type Material in the Region $d \leq x \leq d+L$	1.17 GHz
ε_∞	Relative Permittivity at Infinite Frequency of the Lorentz-Type Material in the Region $d \leq x \leq d+L$	1.5
ε_s	Relative Permittivity at Zero Frequency of the Lorentz-Type Material in the Region $d \leq x \leq d+L$	3.0

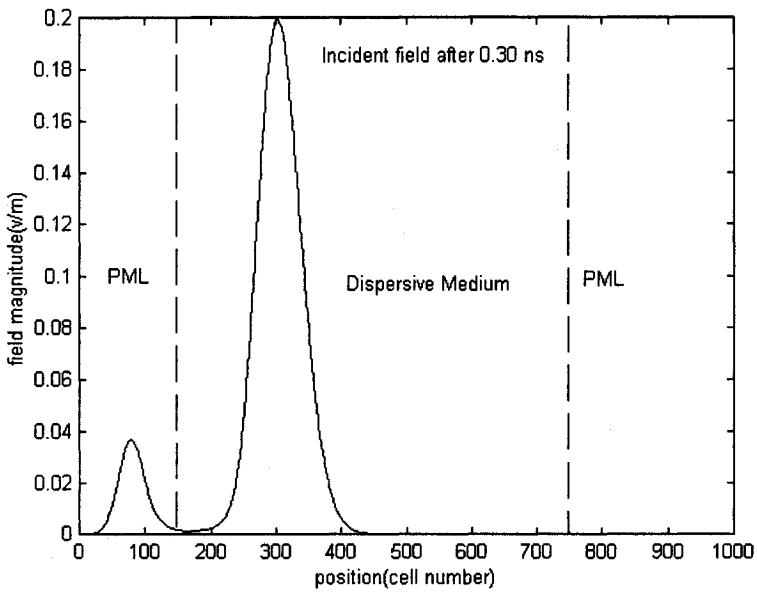

Figure 4.12 : The Incident Field Envelope $|u^{reflected}|(x,t=0.3ns)$ for the First Validation Problem

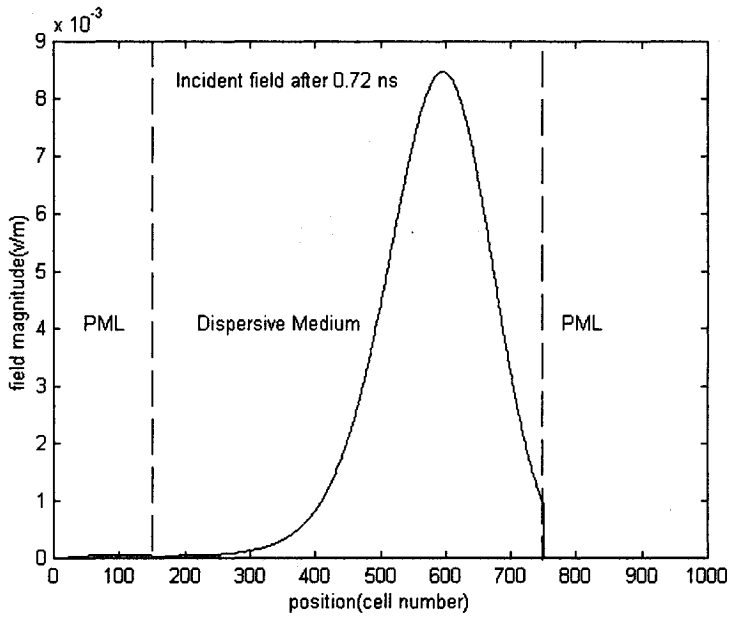

Figure 4.13: The Incident Field Envelope $|u^{reflected}|(x,t=0.72ns)$ for the First Validation Problem

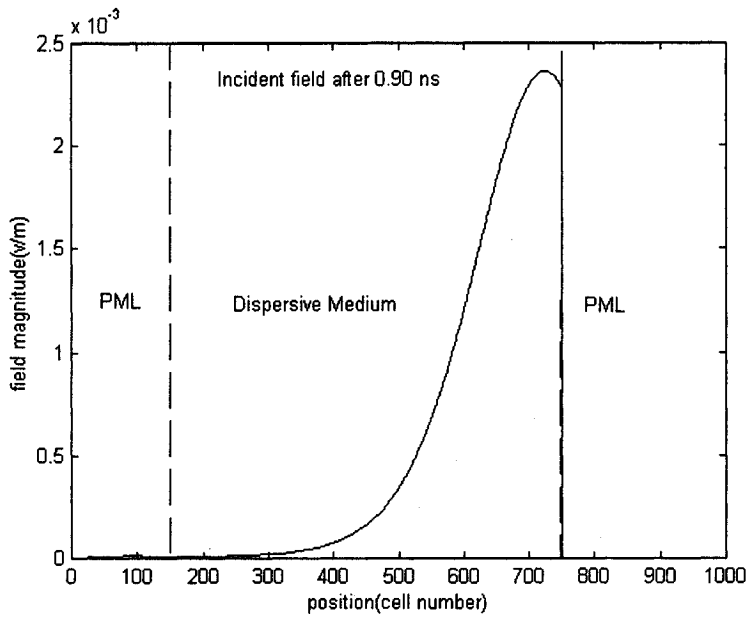

Figure 4.14 : The Incident Field Envelope $|u^{reflected}|(x, t = 0.9ns)$ for the First Validation Problem

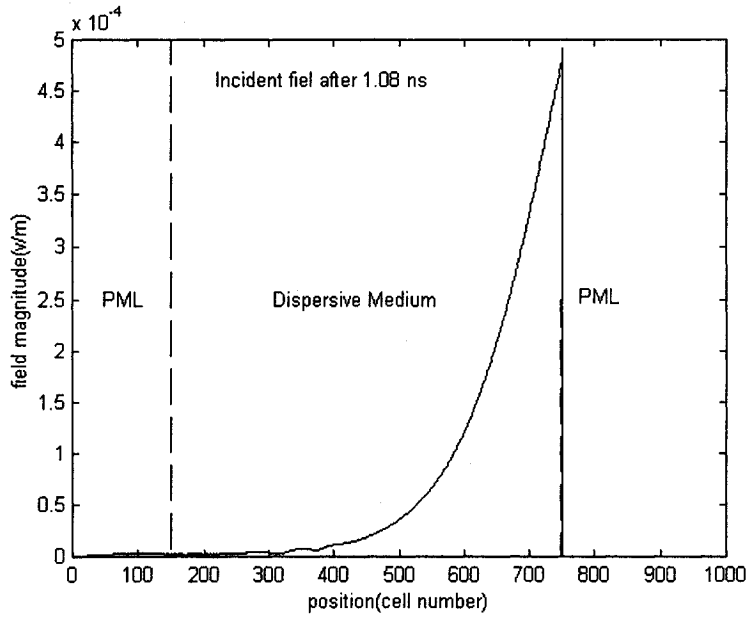

Figure 4.15 : The Incident Field Envelope $|u^{reflected}|(x, t = 1.08ns)$ for the First Validation Problem

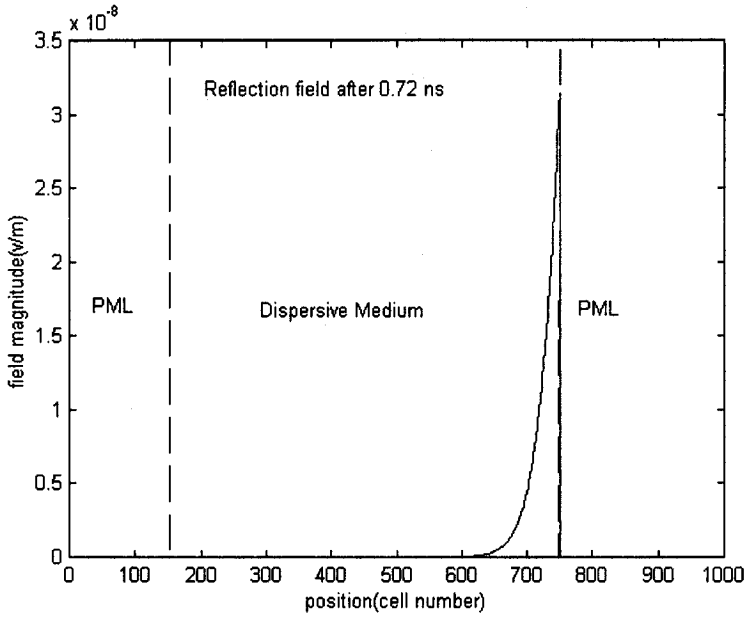

Figure 4.16: The Reflected Field Envelope $|u^{reflected}|(x,t=0.72ns)$ for the First Validation Problem

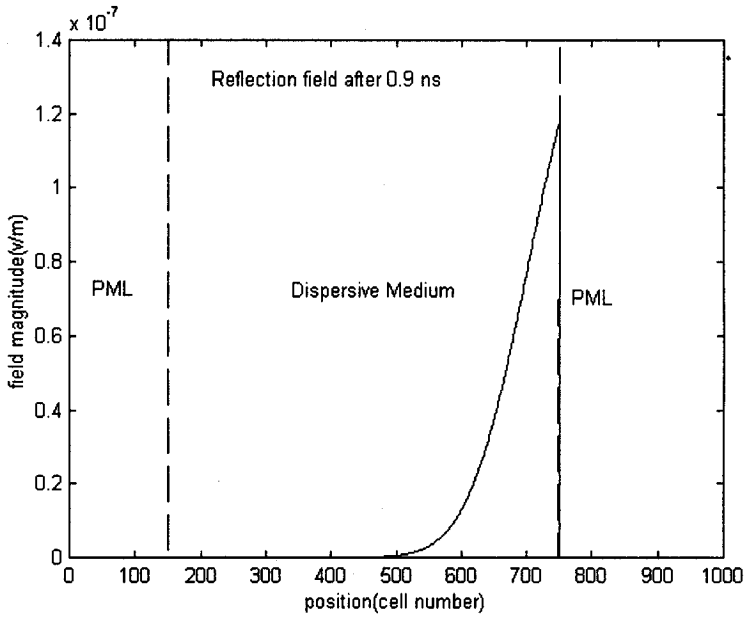

Figure 4.17 : The Reflected Field Envelope $|u^{reflected}|(x,t=0.90ns)$ for the First Validation Problem

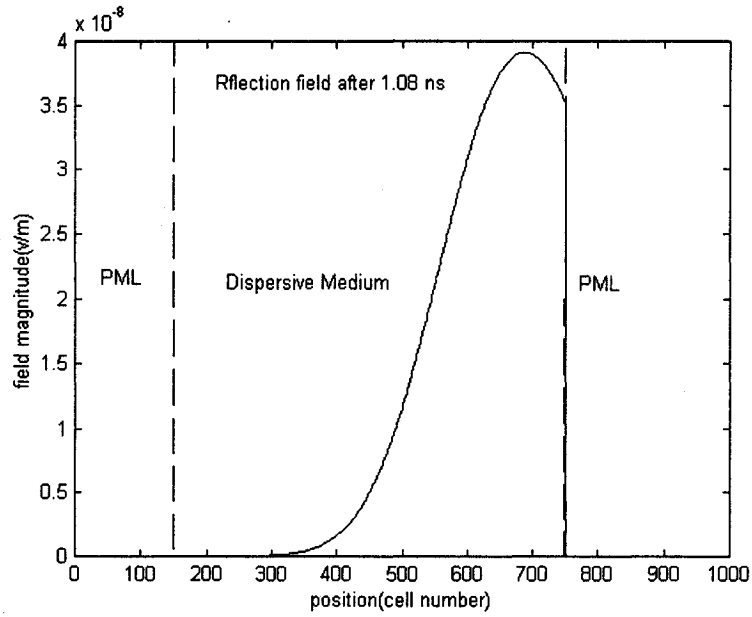

Figure 4.18 : The Reflected Field Envelope $|u^{reflected}|(x,t=1.08ns)$ for the First Validation Problem

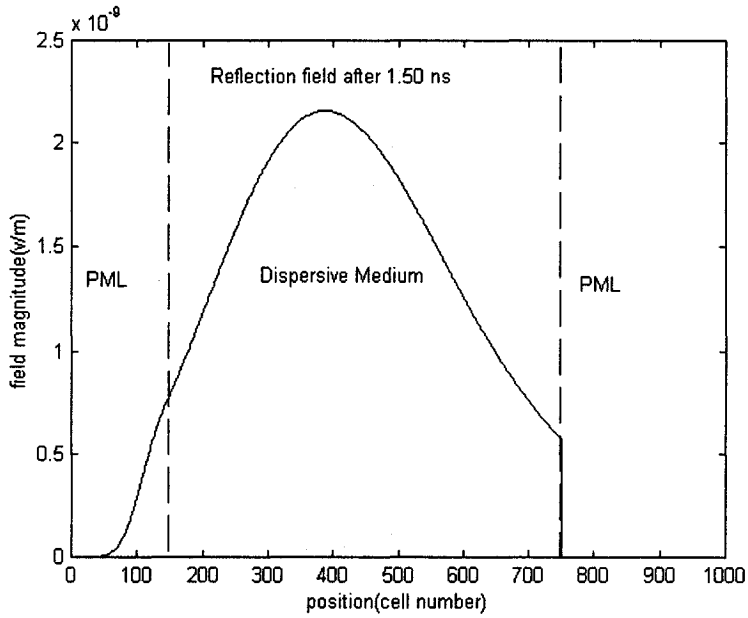

Figure 4.19: The Reflected Field Envelope $|u^{reflected}|(x,t=1.50ns)$ for the First Validation Problem

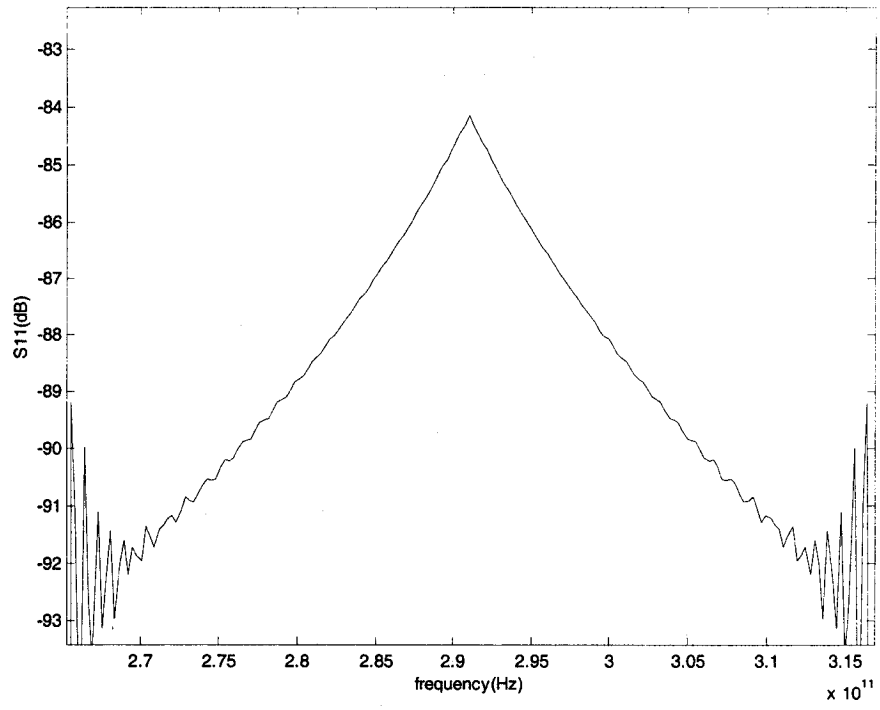

Figure 4.20 : The Reflection Coefficient $\Gamma_{PML}(\omega)$ "Looking Into" the PML at x=d+L

4.5.3 Comparison of the EVFE Results to Semi-Analytical Results

In this case the situation is the same as that in Section 4.5.2, except that the length L has been altered, as well as the element length Δx. Their values, as well as those of all the other parameters, are for completeness summarised in Table 4.3. The semi-analytical results referred to in this section were obtained using the technique described in Section E.1 of Appendix E.

Table 4.3 Parameters for the First Validation Problem of Figure 4.1 as Used in Section 4.5.3

Quantity	*Description*	*Value*
L	Length of Region Between the PMLs	120mm
d	Thickness of Each PML Layer	15mm
x_{left}	Location of left PML Face	15mm
x_{right}	Location of right PML Face	105mm
x_s	Location of Source	17mm
Δx	Length of Finite Element	0.1mm
f_c	Carrier Frequency	291 GHz
σ_t	Width of the Gaussian Envelope of the Source Located at $x = x_s$	0.03 ns
$\omega_o / 2\pi$	Resonance Frequency of the Lorentz-Type Material in the Region $d \leq x \leq d+L$	195 GHz
$\Gamma / 2\pi$	Damping Frequency of the Lorentz-Type Material in the Region $d \leq x \leq d+L$	1.17 GHz
ε_∞	Relative Permittivity at Infinite Frequency of the Lorentz-Type Material in the Region $d \leq x \leq d+L$	1.5
ε_s	Relative Permittivity at Zero Frequency of the Lorentz-Type Material in the Region $d \leq x \leq d+L$	3.0

A. *Validation of Method#1 of Section 3.3*

Figures 4.21 and 4.22 show "snapshots" of the envelope of the total field at times t = 0.35 ns and t = 0.975 ns, respectively, when the method of Section 3.3 is used to account for the presence of the dispersive material. The results are shown for three different values of the time step, namely $\Delta t = 0.0025$ ns, $\Delta t = 0.0050$ ns, and $\Delta t = 0.0075$ ns.

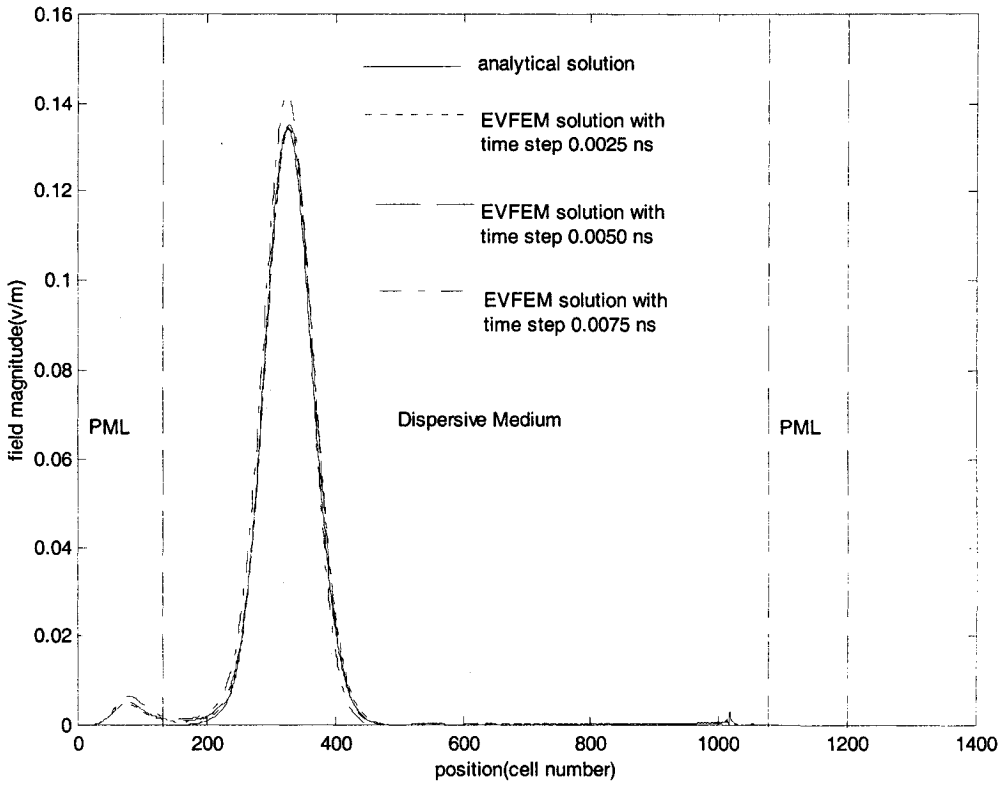

Figure 4.21 : The Total Electric Field Envelope $|u^{total}|(x, t = 0.35ns)$ for the First Validation Problem

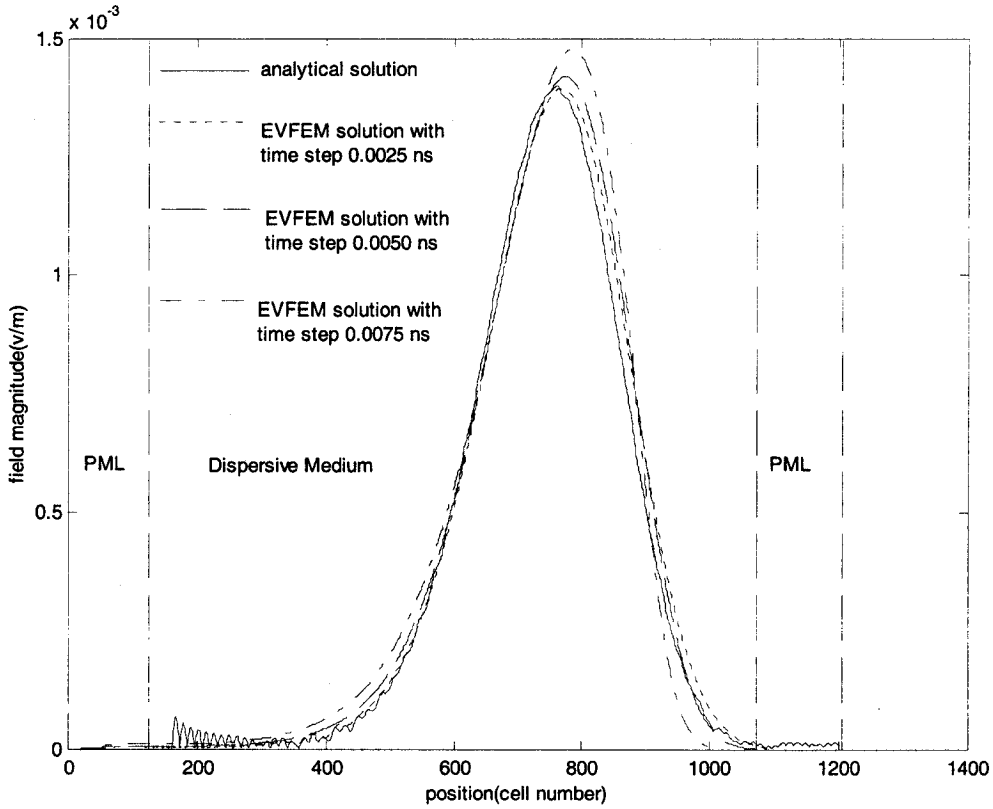

Figure 4.22 : The Total Electric Field Envelope $|u^{total}|(x,t=0.975ns)$ for the First Validation Problem

We observe that when $\Delta t = 0.0025$ ns the EVFE result is almost identical to that obtained using the semi-analytical method. If $\Delta t = 0.0050$ ns is used the agreement is initially good, but deteriorates as time progresses. With $\Delta t = 0.0075$ ns the agreement is unsatisfactory. The broadening of the envelope as it propagates is observed as expected.

B. Validation of Method#2 of Section 3.4

Figures 4.23 and 4.24 show "snapshots" of the envelope of the total field at times t = 0.35 ns and t = 0.975 ns, respectively, when the method of Section 3.4 is used to account

for the presence of the dispersive material. The results are shown for three different values of the time step, namely $\Delta t = 0.0025$ ns, $\Delta t = 0.0050$ ns, and $\Delta t = 0.0075$ ns. We observe that when $\Delta t = 0.0025$ ns the EVFE result is almost identical to that obtained using the semi-analytical method. If $\Delta t = 0.0050$ ns is used the agreement is initially good, but deteriorates as time progresses. With $\Delta t = 0.0075$ ns the agreement is unsatisfactory. Thus the performance of Methos#1 and Method#2 are similar.

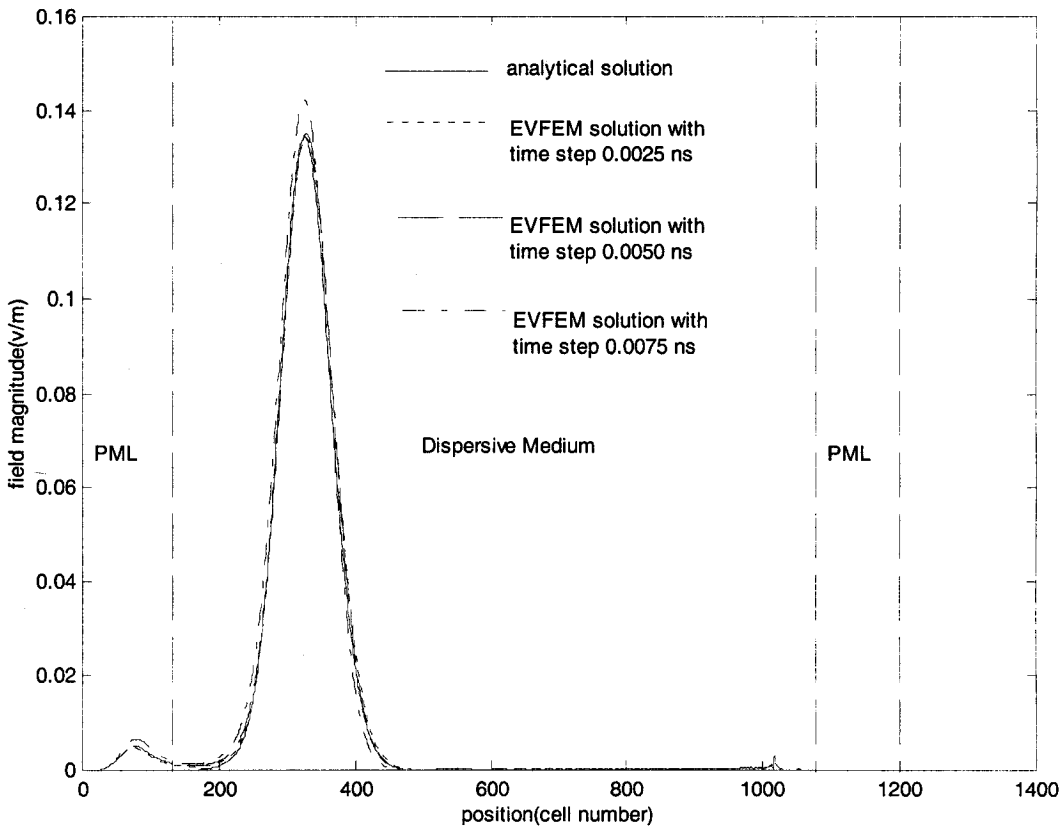

Figure 4.23 : The Total Electric Field Envelope $|u^{total}|(x,t=0.35ns)$ for the First Validation Problem

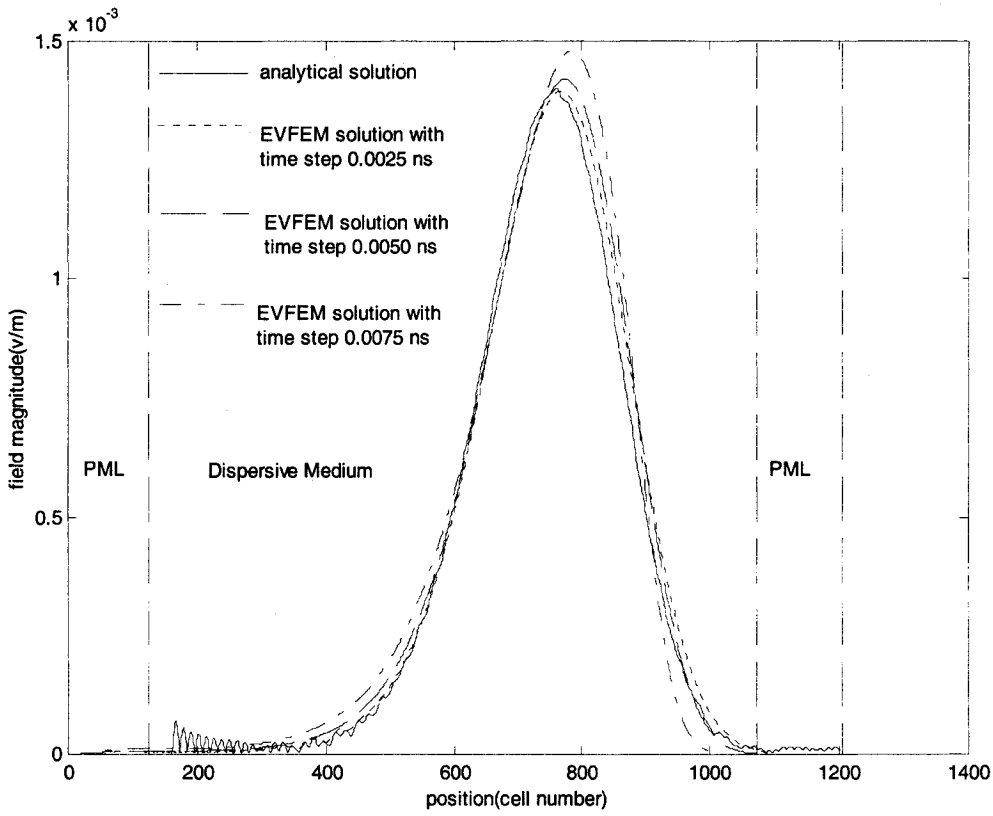

Figure 4.24 : The Total Electric Field Envelope $|u^{total}|(x,t=0.975ns)$ for the First Validation Problem

C. Validation of Method#3 of Section 3.5

Figures 4.25 and 4.26 show "snapshots" of the envelope of the total field at times t = 0.35 ns and t = 0.975 ns, respectively, when the method of Section 3.5 is used to account for the presence of the dispersive material. It was observed that for $\Delta t > 0.0022$ ns entirely incorrect results are obtained. Thus the results are shown for $\Delta t = 0.0022$ ns and $\Delta t = 0.0010$ ns. Clearly the results with $\Delta t = 0.0022$ ns are worse than those obtained using Method#1 and Method#2 with $\Delta t = 0.0025$ ns. In other words, with Method#3, it is necessary to go as small as $\Delta t = 0.0010$ ns to get acceptable results, and even these are

seen to deteriorate as time progresses. Thus Method#3 does not allow the advantage of larger Δt offered by the EVFE method to be exploited when using Lorentz-type dispersive material. As stated in Section 3.5, this is due to the fact that Method#3 attempts to evaluate the convolution integral directly, and this evaluation becomes imprecise if Δt is not small.

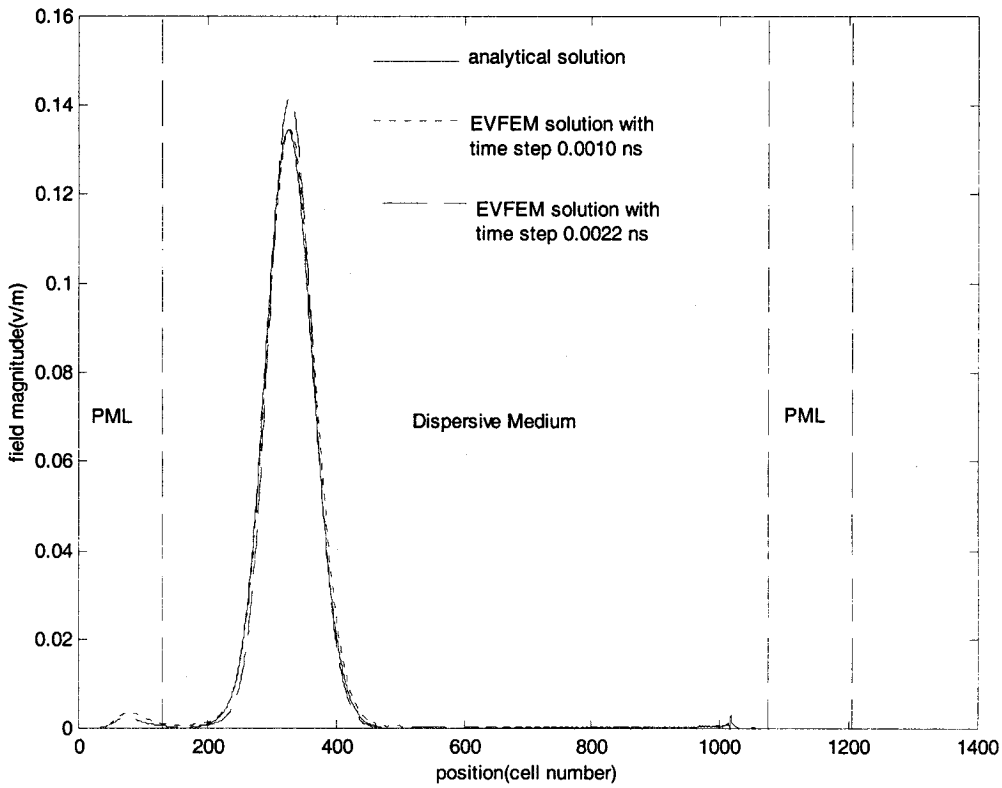

Figure 4.25 : The Total Electric Field Envelope $|u^{total}|(x,t=0.35ns)$ for the First Validation Problem

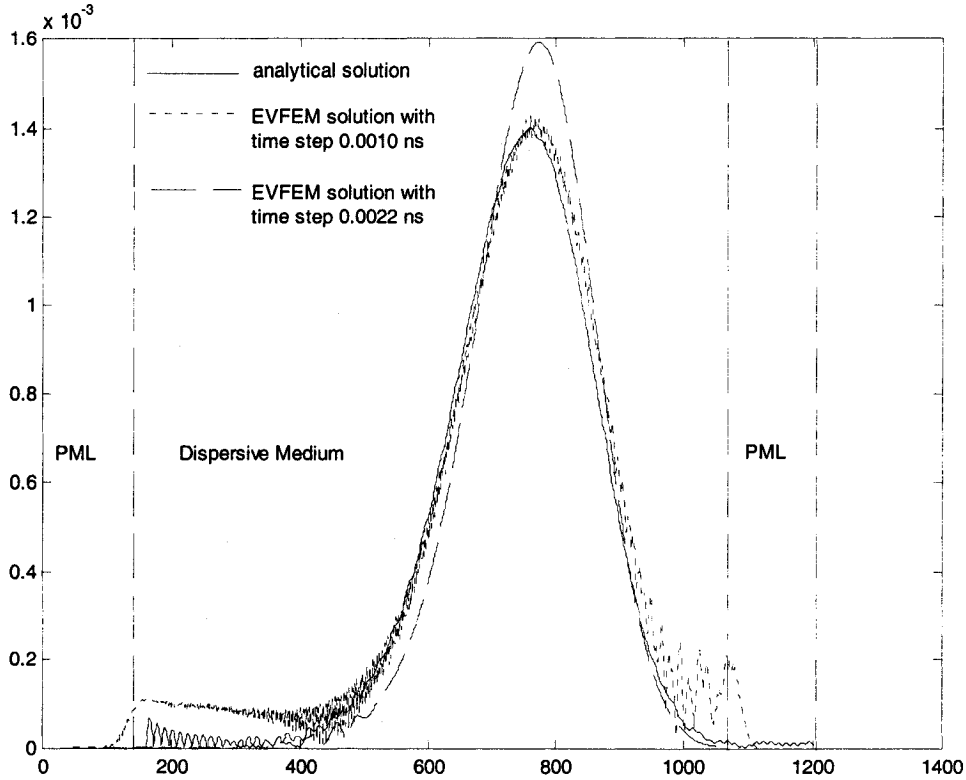

Figure 4.26 : The Total Electric Field Envelope $|u^{total}|(x,t=0.975ns)$ for the First Validation Problem

4.6 REFLECTION OF A PLANE WAVE AT THE PLANAR INTERFACE BETWEEN NON-DISPERSIVE AND DISPERSIVE MATERIAL

4.6.1 Preliminary Comments

In this section we consider reflection of a Gaussian pulse-modulated plane wave incident on the interface between dispersive and non-dispersive material. This is the second validation problem mentioned in Section 4.2, and is shown in Figure 4.2. In order to establish the correctness of the interesting results obtained we will compare them to those obtained for the same problem but using a semi-analytical method.

4.6.2 Details of the Second Validation Problem

In this case the situation is the same as that in Section 4.5.2, except that the length L has been altered, as well as the element length Δx. Their values, as well as those of all the other parameters, are for completeness summarised in Table 4.3. The semi-analytical results referred to in this section were obtained using the technique described in Section E.2 of Appendix E.

Table 4.3 Parameters for the Second Validation Problem of Figure 4.2

Quantity	*Description*	*Value*
L	Length of Region Between the PMLs	150mm
d	Thickness of Each PML Layer	15mm
L_1	Length of Non-Dispersive Region	50mm
L_2	Length of the Dispersive Region	70 mm
x_{left}	Location of left PML Face	15mm
x_{right}	Location of right PML Face	135mm
x_s	Location of Source	17mm
Δx	Length of Finite Element	0.005mm
f_c	Carrier Frequency	291 GHz
σ_t	Width of the Gaussian Envelope of the Source Located at $x = x_s$	0.03 ns
$\omega_o / 2\pi$	Resonance Frequency of the Lorentz-Type Material in the Region $d \leq x \leq d+L$	195 GHz
$\Gamma / 2\pi$	Damping Frequency of the Lorentz-Type Material in the Region $d \leq x \leq d+L$	1.17 GHz
ε_∞	Relative Permittivity at Infinite Frequency of the Lorentz-Type Material in the Region $d \leq x \leq d+L$	1.5
ε_s	Relative Permittivity at Zero Frequency of the Lorentz-Type Material in the Region $d \leq x \leq d+L$	3.0

The "snapshots' of the incident field envelope at times 0.185 ns, 0.248 ns, and 0.310 ns are shown in Figures 4.27 through 4.29, respectively. The "snapshots" of the total field after 0.248 ns, and 0.310 ns are shown in Figures 4.30 and 4.31, respectively. The "fuzzy" portions on the plots in the latter three figures are those regions where the unsynchronized incident and reflected envelopes overlap.

In order to be able to compare the EVFE calculated envelopes of the field reflected at the interface, and transmitted through the interface, with the semi-analytical results provided in Section E.2 of Appendix E, it is convenient to subtract the incident field from the total field. This enables us to view the reflected and transmitted field envelopes separately. These are shown in Figures 4.32 through 4.36 after increasingly longer time lapses. In each of these figures the EVFE results are shown for different values of time step Δt. The semi-analytical results are also shown in each case. Clearly, for $\Delta t \leq$ 0.0025ns the EVFE results agree excellently with the semi-analytical ones. Furthermore, we observe that the reflected wave envelope does not broaden or decrease in amplitude as it moves to the left in the non-dispersive lossless material. The transmitted wave envelope, on the other hand, which travels in the dispersive material, does indeed broaden.

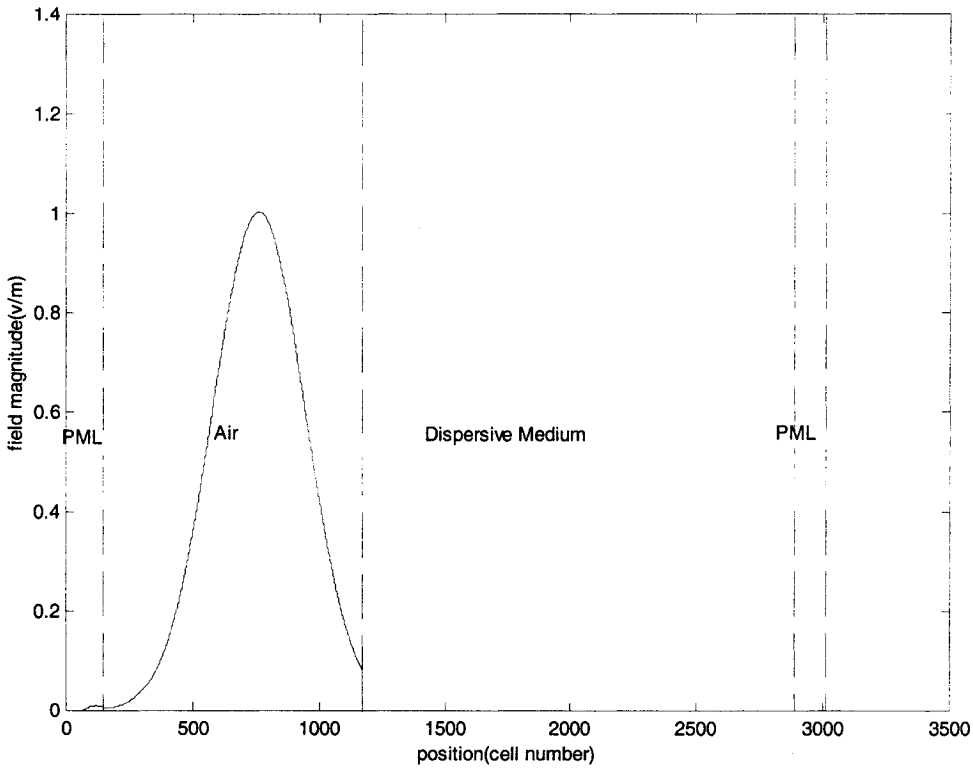

Figure 4.27 : The Incident Field Envelope $|u^{inc}|(x, t = 0.185ns)$ for the Second Validation Problem

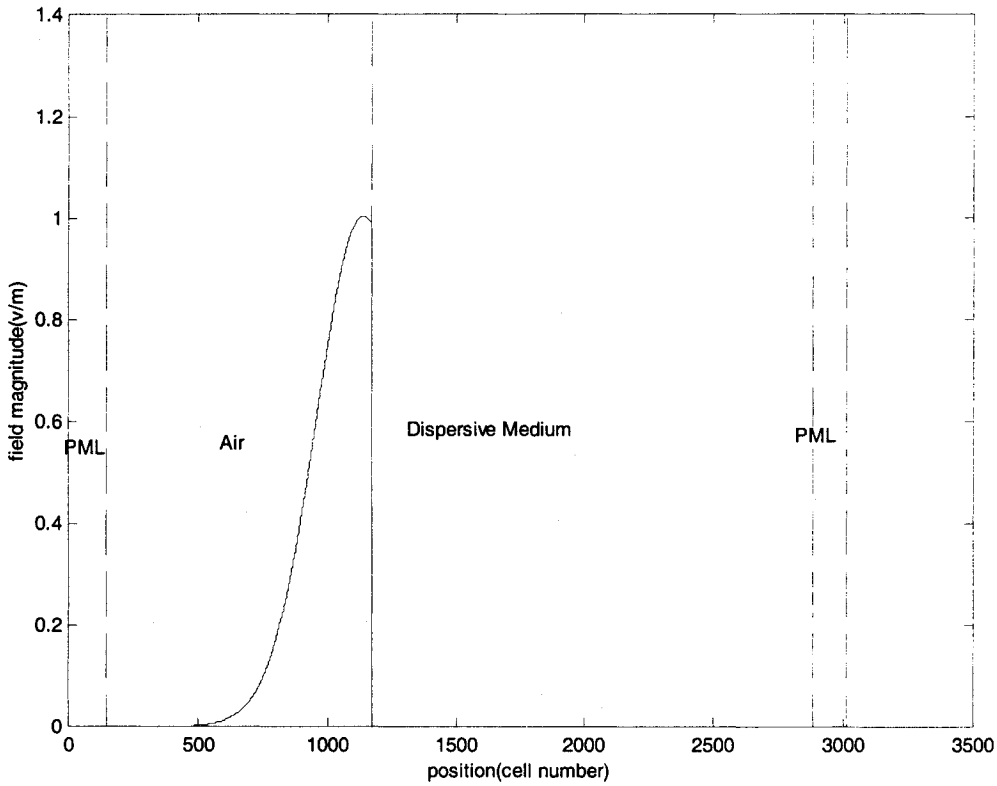

Figure 4.28 : The Incident Field Envelope $|u^{inc}|(x, t = 0.248ns)$ for the Second Validation Problem

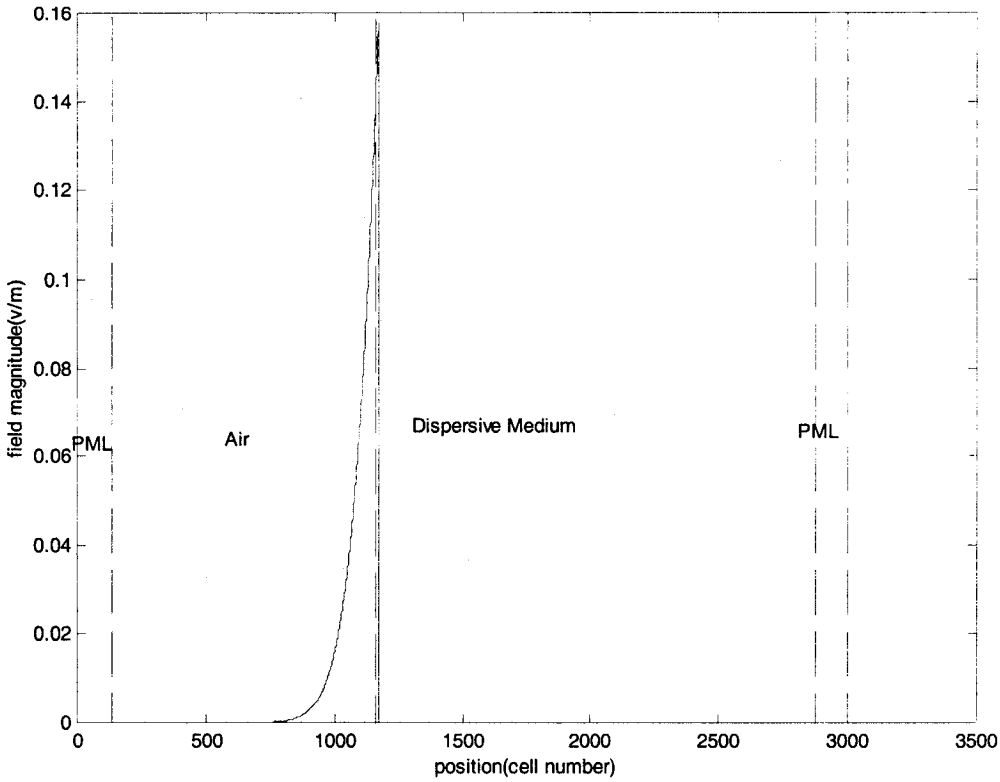

Figure 4.29 : The Incident Field Envelope $|u^{inc}|(x, t = 0.310ns)$ for the Second Validation Problem

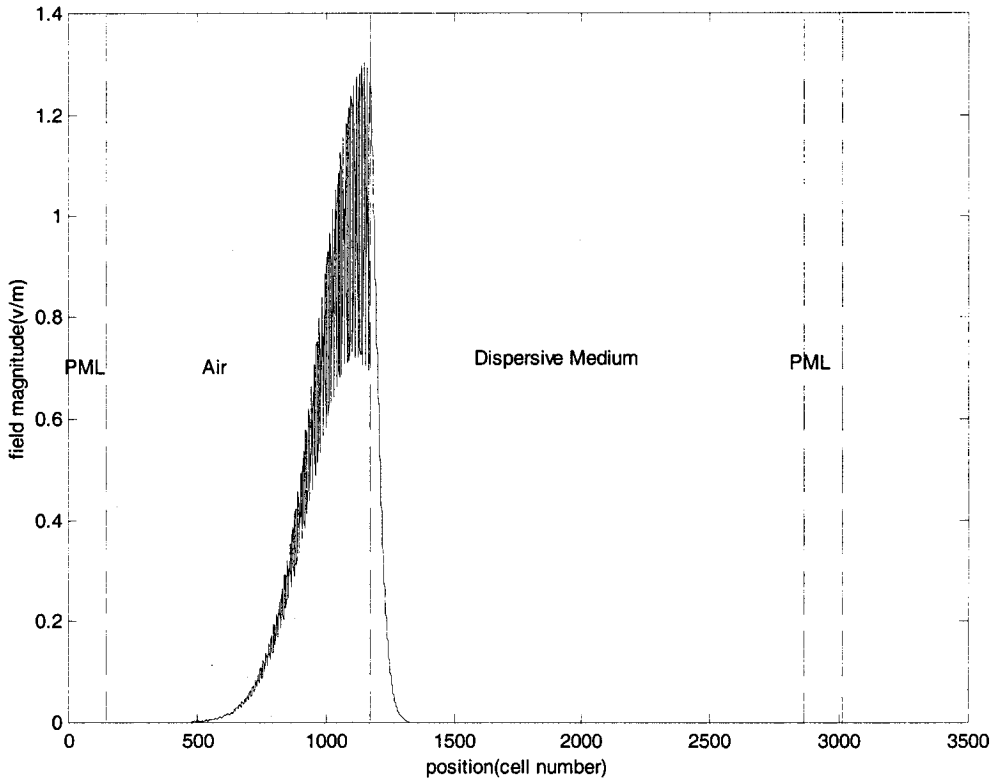

Figure 4.30 : The Total Electric Field Envelope $|u^{total}|(x,t=0.248ns)$ for the Second Validation Problem

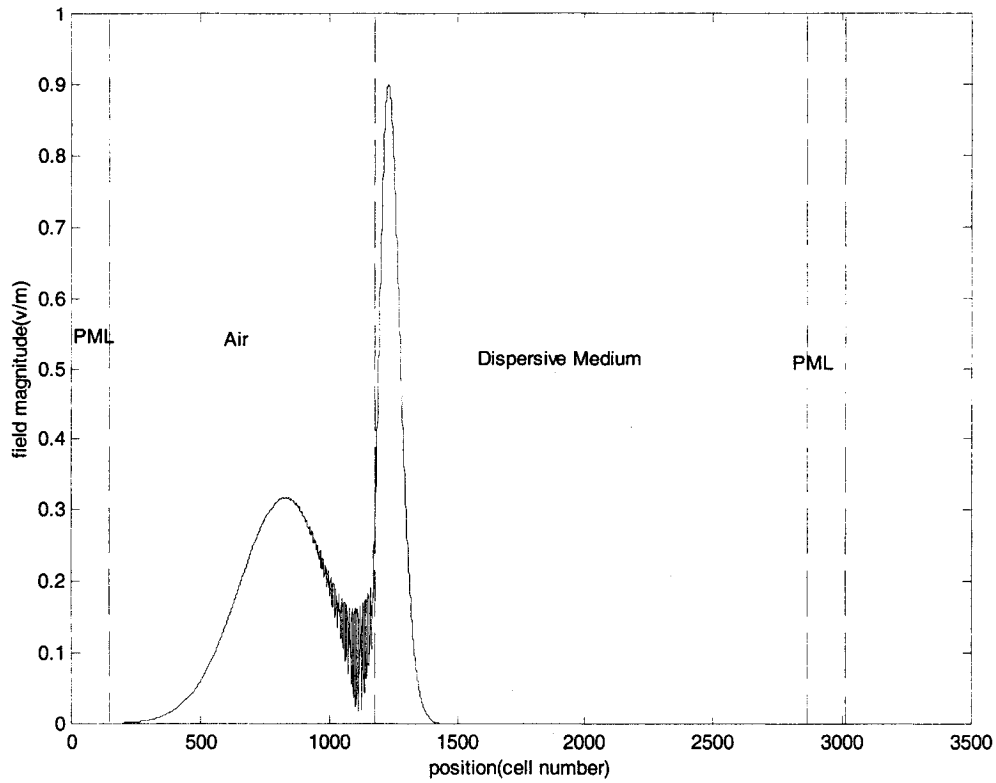

Figure 4.31 : The Total Electric Field Envelope $|u^{total}|(x, t = 0.310ns)$ for the Second Validation Problem

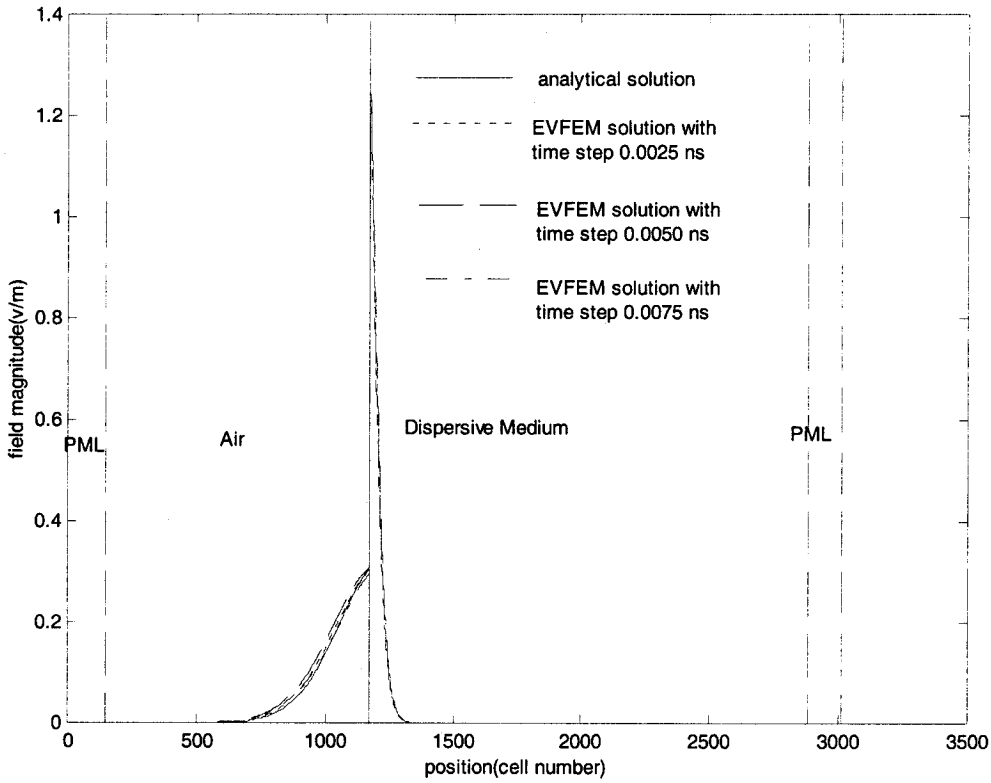

Figure 4.32 : The Reflected & Transmitted Electric Field Envelope at t = 0.248ns for the Second Validation Problem

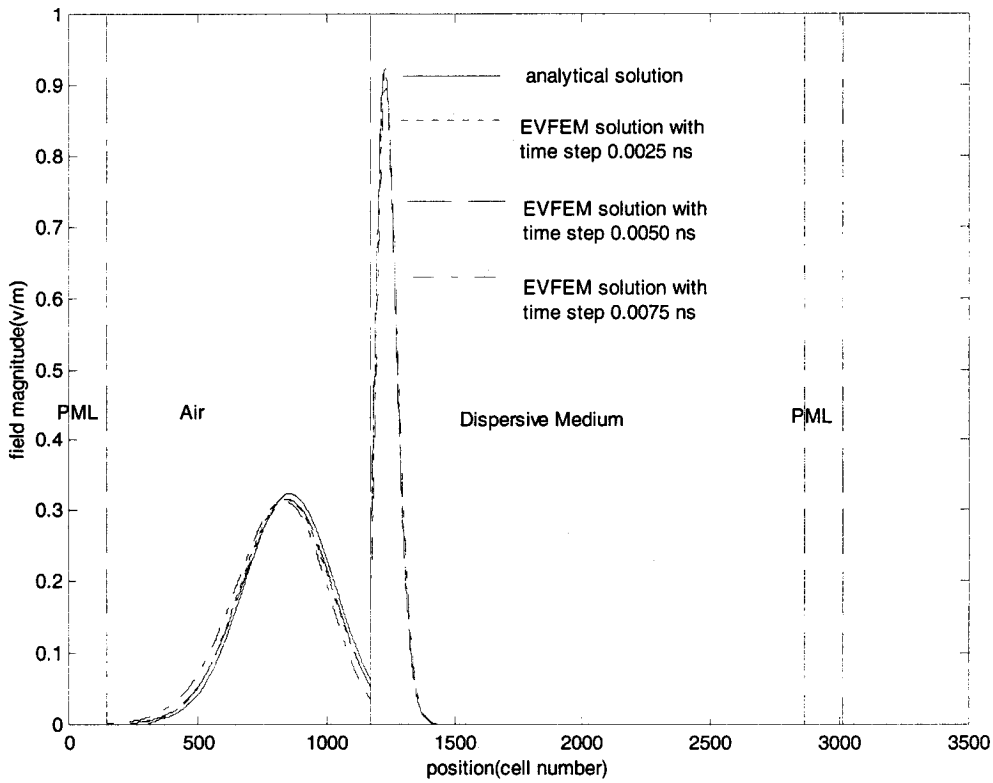

Figure 4.33 : The Reflected & Transmitted Electric Field Envelope at t = 0.310ns for the Second Validation Problem

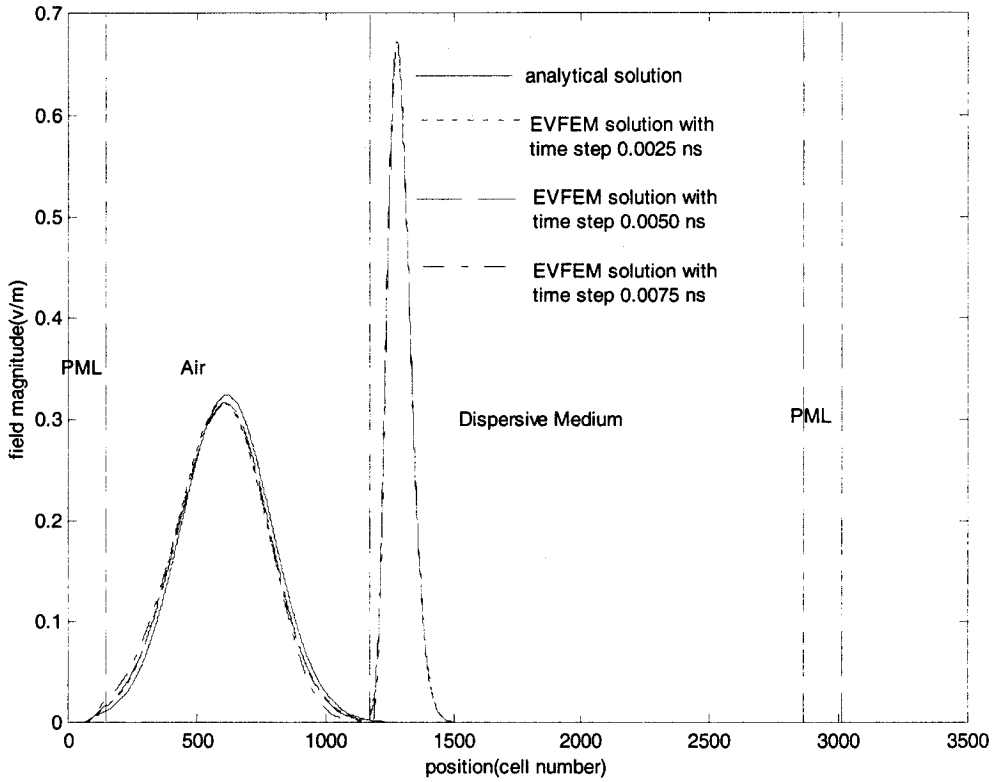

Figure 4.34 : The Reflected & Transmitted Electric Field Envelope at t = 0.350ns for the Second Validation Problem

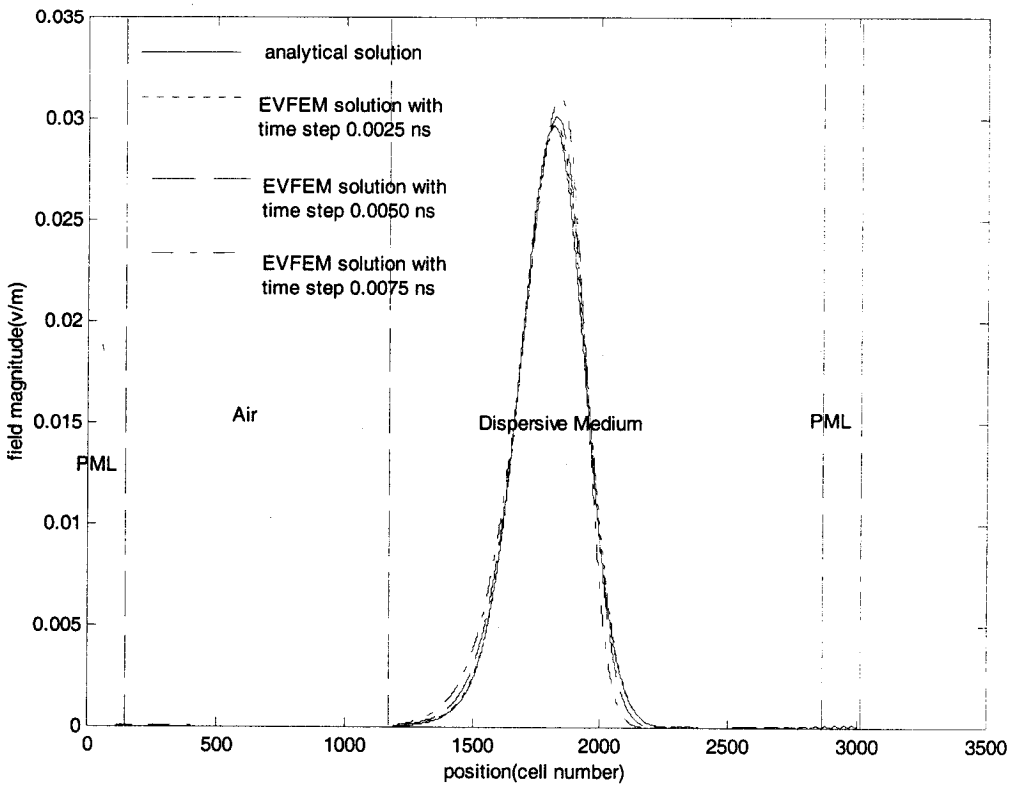

Figure 4.35 : Transmitted Electric Field Envelope at t = 0.748ns for the Second Validation Problem

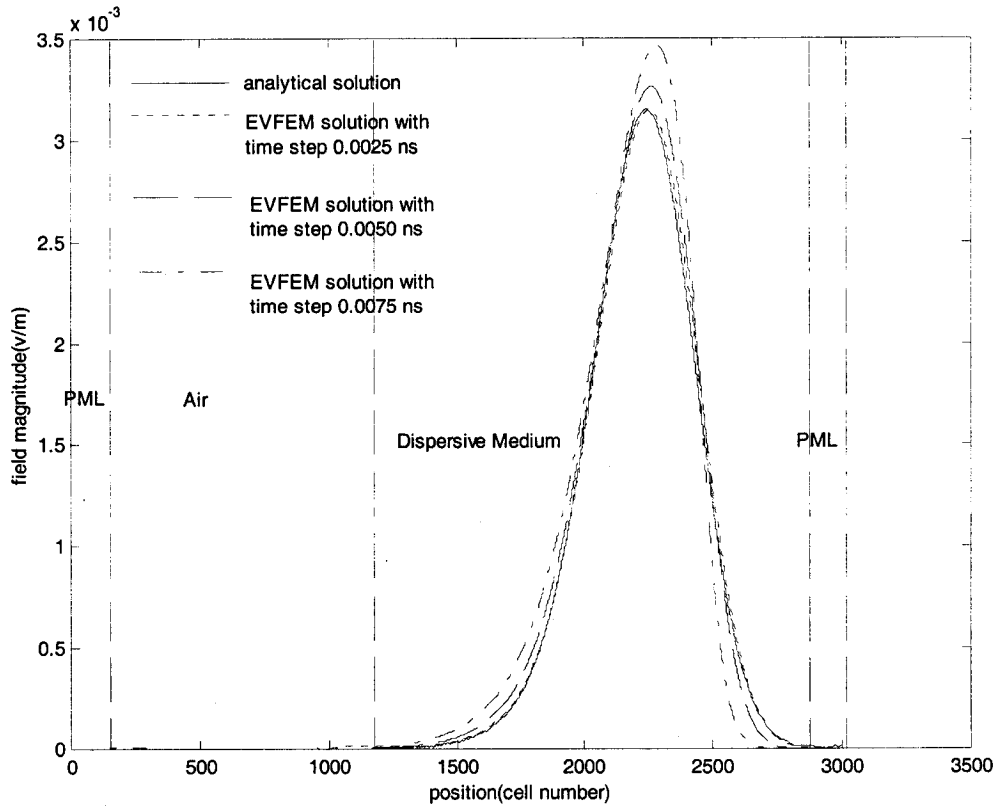

Figure 4.36 : Transmitted Electric Field Envelope at t = 1.060ns for the Second Validation Problem

4.7 CONCLUDING REMARKS

This chapter has described the implementation of the EVFE formulations of Chapter 3. The new formulations permit the treatment of materials with Lorentz-type dispersion in the EVFE framework. In the first validation example the proper working of the PML that can be used adjacent to Lorentz-type material was first confirmed, and then the expected broadening of the envelope of a Gaussian-modulated carrier field as it propagates through Lorentz-type dispersive material was observed. It was verified that all three methods developed in Chapter 3 for including Lorentz-type media in the EVFE method can provide identical results when a sufficiently small time step is used. It was pointed out

that only the first two methods (of Sections 3.3 and 3.4) preserve the larger-time-step advantage of the EVFE over the FETD and are the ones to be used. This was expected, as the third method (intended largely as a reference method for the development work) evaluates the convolution integrals directly, which have to be evaluated using a time-step appropriate for the carrier rather than the envelope. In the second validation reflection and transmission of a Gaussian-modulated carrier at the interface between non-dispersive and Lorentz-type dispersive material was considered and shown to be correctly computed using the EVFE method developed. The validation problems were selected so as to be able to directly compare the EVFE results with those obtained using a semi-analytical method. This comparison served to validate the Chapter 3 formulations.

CHAPTER 5

GENERAL CONCLUSIONS

The principal contributions of this thesis are as follows :

- A computationally efficient method of including materials with Lorentz-type dispersion in the envelope finite-element time-domain (EVFE) method has been presented for the first time.

- A new perfectly matched layer (PML) mesh truncation scheme, which allows the PML to be applied in Lorentz-type dispersive material has also been derived.

- These new formulations have been implemented and applied to specific examples, and the approach validated through comparison with results obtained using alternative semi-analytical methods.

- In particular, it has been demonstrated through the examples that the method developed preserves the large-time-step advantage of the EVFE over the conventional FETD.

Although we have indicated that the method, described here for two-dimensional scalar problems, can be straightforwardly used in more general three-dimensional vector situations, future work might involve the implementation of the formulation to such problems. An important aspect of such work would be to find either experimental results or those obtained from alternative computational methods with which to compare the outcome of the EVFE computations. Such results are still relatively rare in the literature.

APPENDIX A : LINEAR TWO-DIMENSIONAL SCALAR NODAL FINITE ELEMENTS OF RECTANGULAR SHAPE

In this thesis we use the rectangular elements shown in Fig. A.1. The rectangular element is $2l_x$ in length along the x direction and $2l_y$ in width along the y direction. Its center is at (x_c, y_c).

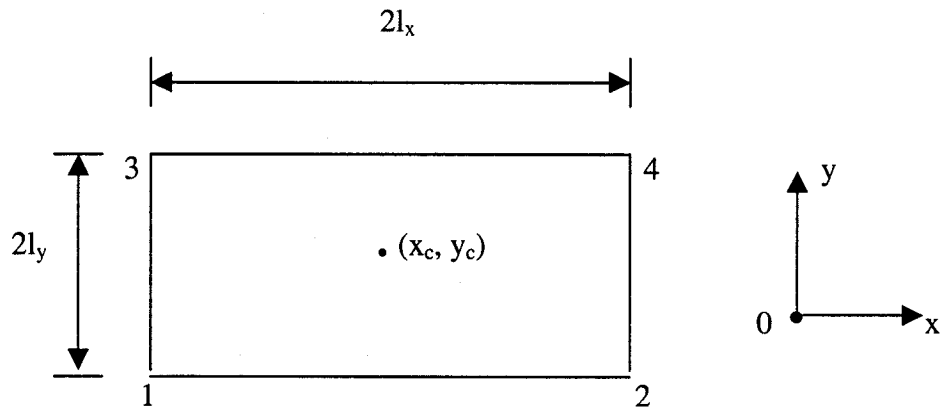

Fig. A.1: Element of Rectangular Shape

If each node is assigned a field component, the field within the element can be expanded the same as in equation (2.3.5)

$$\underset{\sim}{E}^e(x,y,\omega) = \sum_{j=1}^{p_j} N_j^e(x,y)\underset{\sim}{V}_j^e(\omega) \tag{A.1}$$

Using the first order scalar expansion function

$$\begin{cases} N_1^p = \dfrac{1}{4l_x l_y}[l_x - (x - x_c)][l_y - (y - y_c)] \\ N_2^p = \dfrac{1}{4l_x l_y}[l_x + (x - x_c)][l_y - (y - y_c)] \\ N_3^p = \dfrac{1}{4l_x l_y}[l_x - (x - x_c)][l_y + (y - y_c)] \\ N_4^p = \dfrac{1}{4l_x l_y}[l_x + (x - x_c)][l_y + (y - y_c)] \end{cases} \tag{A.2}$$

If we substitute (A.2) into (2.3.11) we can obtain

$$\begin{cases} A_{11}^p = \dfrac{4l_x l_y}{9}, & A_{12}^p = \dfrac{2l_x l_y}{9}, \\ A_{13}^p = \dfrac{2l_x l_y}{9}, & A_{14}^p = \dfrac{l_x l_y}{9}, \\ A_{21}^p = A_{12}^p, & A_{22}^p = A_{11}^p, \\ A_{23}^p = \dfrac{l_x l_y}{9}, & A_{24}^p = \dfrac{2l_x l_y}{9}, \\ A_{31}^p = A_{13}^p, & A_{32}^p = A_{23}^p, \\ A_{33}^p = A_{11}^p, & A_{34}^p = \dfrac{l_x l_y}{9}, \\ A_{41}^p = A_{14}^p, & A_{42}^p = A_{24}^p, \\ A_{43}^p = A_{34}^p, & A_{44}^p = A_{11}^p, \end{cases} \tag{A.3}$$

$$\begin{cases} B_{11}^p = \dfrac{l_x}{3l_y}, & B_{12}^p = \dfrac{l_x}{6l_y}, \\ B_{13}^p = -\dfrac{l_x}{3l_y}, & B_{14}^p = -\dfrac{l_x}{6l_y}, \\ B_{21}^p = B_{12}^p, & B_{22}^p = B_{11}^p, \\ B_{23}^p = -\dfrac{l_x}{6l_y}, & B_{24}^p = -\dfrac{l_x}{3l_y}, \\ B_{31}^p = B_{13}^p, & B_{32}^p = B_{23}^p, \\ B_{33}^p = B_{11}^p, & B_{34}^p = \dfrac{l_x}{6l_y}, \\ B_{41}^p = B_{14}^p, & B_{42}^p = B_{24}^p, \\ B_{43}^p = B_{34}^p, & B_{44}^p = B_{11}^p, \end{cases} \tag{A.4}$$

$$
\begin{cases}
C_{11}^{p} = \dfrac{l_y}{3l_x}, & C_{12}^{p} = -\dfrac{l_y}{3l_x}, \\
C_{13}^{p} = \dfrac{l_y}{6l_x}, & C_{14}^{p} = -\dfrac{l_y}{6l_x}, \\
C_{21}^{p} = C_{12}^{p}, & C_{22}^{p} = C_{11}^{p}, \\
C_{23}^{p} = -\dfrac{l_y}{6l_x}, & C_{24}^{p} = \dfrac{l_y}{6l_x}, \\
C_{31}^{p} = C_{13}^{p}, & C_{32}^{p} = C_{23}^{p}, \\
C_{33}^{p} = C_{11}^{p}, & C_{34}^{p} = -\dfrac{l_y}{3l_x}, \\
C_{41}^{p} = C_{14}^{p}, & C_{42}^{p} = C_{24}^{p}, \\
C_{43}^{p} = C_{34}^{p}, & C_{44}^{p} = C_{11}^{p},
\end{cases}
\tag{A.5}
$$

Select the incident plane at the edge of element therefore

$$D_i = l_y \tag{A.5}$$

where i = 1, 2, 3, 4

APPENDIX B : SOME USEFUL MATHEMATICAL RESULTS

B.1 Leibnitz's Rule for the Differentiation of Integrals

$$\frac{d}{dy}\left\{\int_{\phi_1(y)}^{\phi_2(y)} F(x,y)\,dx\right\} = \int_{\phi_1(y)}^{\phi_2(y)} \frac{\partial F(x,y)}{\partial y}\,dx + F(\phi_1,y)\frac{d\phi_1}{dx} + F(\phi_2,y)\frac{d\phi_2}{dx} \qquad \text{(B.1)}$$

B.2 Convolution Integrals

(a). Definition

If we have two functions *f(t)* and *g(t)*, then the convolution of these two functions is defined by

$$f(t) = \int_{-\infty}^{\infty} g(\tau)h(t-\tau)\,d\tau \qquad \text{(B.2)}$$

which is often written as $f(t) = g(t) \otimes h(t)$.

(b). Implications of Causality

The general form (B.2) can often be simplified. In many physical applications the function *h(t)* is a causal function, meaning that $h(t) = 0$ for $t < 0$. In that case, $h(t-\tau) = 0$ for $\tau > t$, and so we can change the upper limit of integration in (B.2) from ∞ to t, so that we have

$$f(t) = \int_{-\infty}^{t} g(\tau) h(t-\tau)\, d\tau \qquad \text{(B.3)}$$

If the function g(t) is also causal, meaning once again $g(t) = 0$ for $t < 0$, we can replace the lower limit of integration by 0. Thus we end up with

$$f(t) = \int_{0}^{t} g(\tau) h(t-\tau)\, d\tau \qquad \text{(B.4)}$$

(c). Derivative of the Convolution Integral

Sometimes we wish to determine the derivative of the convolution integral, namely

$$\frac{\partial f}{\partial t} = \frac{\partial}{\partial t}\{g(t) \otimes h(t)\} \qquad \text{(B.5)}$$

which is

$$\frac{\partial f}{\partial t} = \frac{\partial}{\partial t}\left\{\int_{0}^{t} g(\tau) h(t-\tau)\, d\tau\right\} \qquad \text{(B.6)}$$

If we apply Leibnitz's Rule we get

$$\frac{\partial f}{\partial t} = \frac{\partial}{\partial t}\left\{\int_0^t g(\tau)\,h(t-\tau)\,d\tau\right\} = \int_0^t \frac{\partial}{\partial t}\{g(\tau)\,h(t-\tau)\}\,d\tau + g(t)h(0) \qquad \text{(B.7)}$$

APPENDIX C : THE ANISOTROPIC PERFECTLY MATCHED LAYER (*PML*) CONCEPT

The discussion provided here is based on [20] and [21]. Figure C.1 shows a uniform plane wave incident from Region#1 (the region in which the computational method being used to determine the unknown fields) onto the surface of the PML half-space (which is Region#2).

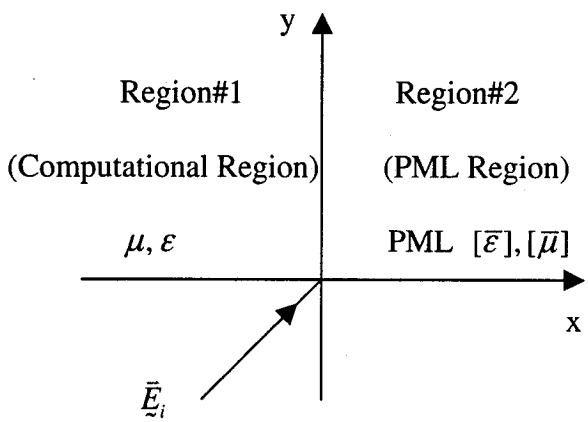

Figure C.1 : Region#1 has Scalar Electromagnetic Properties (μ,ε) While Region#2 has Anisotropic Properties $[\bar{\varepsilon}]$ and $[\bar{\mu}]$

We suppose that PML half-apace is diagonally anisotropic media. In diagonally anisotropic media the general time-harmonic Maxwell's equations are as follow

$$\nabla \times \tilde{H} = j\omega[\bar{\varepsilon}]\tilde{E} \tag{C.1}$$

$$\nabla \times \tilde{E} = -j\omega[\bar{\mu}]\tilde{H} \tag{C.2}$$

$$\nabla \cdot [\bar{\varepsilon}]\tilde{E} = 0 \tag{C.3}$$

$$\nabla \cdot [\bar{\mu}]\tilde{\underline{H}} = 0 \tag{C.4}$$

where

$$[\bar{\varepsilon}] = \varepsilon_0 \begin{pmatrix} \varepsilon_x + \dfrac{\sigma_e^x}{j\omega\varepsilon_0} & 0 & 0 \\ 0 & \varepsilon_y + \dfrac{\sigma_e^y}{j\omega\varepsilon_0} & 0 \\ 0 & 0 & \varepsilon_z + \dfrac{\sigma_e^z}{j\omega\varepsilon_0} \end{pmatrix} \tag{C.5}$$

$$[\bar{\mu}] = \varepsilon_0 \begin{pmatrix} \mu_x + \dfrac{\sigma_m^x}{j\omega\varepsilon_0} & 0 & 0 \\ 0 & \mu_y + \dfrac{\sigma_m^y}{j\omega\varepsilon_0} & 0 \\ 0 & 0 & \mu_z + \dfrac{\sigma_m^z}{j\omega\varepsilon_0} \end{pmatrix} \tag{C.6}$$

In order to match the intrinsic impedance of the medium in Region #1 (computational region) to that in Region # 2 (PLM region) we need to have

$$\frac{[\bar{\varepsilon}]}{\varepsilon} = \frac{[\bar{\mu}]}{\mu} \tag{C.7}$$

Therefore $[\bar{\varepsilon}]$ *and* $[\bar{\mu}]$ should have the forms

$$[\bar{\varepsilon}] = \varepsilon_0\varepsilon_r[\wedge] = \varepsilon_0\varepsilon_r \begin{pmatrix} a & 0 & 0 \\ 0 & b & 0 \\ 0 & 0 & c \end{pmatrix} \tag{C.8}$$

and

$$[\bar{\mu}] = \mu_0\mu_r[\wedge] = \mu_0\mu_r \begin{pmatrix} a & 0 & 0 \\ 0 & b & 0 \\ 0 & 0 & c \end{pmatrix} \tag{C.9}$$

Using (C.8) and (C.9) Maxwell's equations (C.1) through (C.4) can be rewritten as

$$\nabla \times \underset{\sim}{\bar{H}} = j\omega\varepsilon_0\varepsilon_r[\wedge]\underset{\sim}{\bar{E}} \tag{C.10}$$

$$\nabla \times \underset{\sim}{\bar{E}} = -j\omega\mu_0\mu_r[\wedge]\underset{\sim}{\bar{H}} \tag{C.11}$$

$$\nabla \cdot [\wedge]\underset{\sim}{\bar{E}} = 0 \tag{C.12}$$

$$\nabla \cdot [\wedge]\underset{\sim}{\bar{H}} = 0 \tag{C.13}$$

The plane wave solutions of the above forms of Maxwell's equations

$$\underset{\sim}{\bar{E}}(\bar{r},t) = \underset{\sim}{\mathrm{E}}_0 e^{-\bar{\gamma}\cdot\bar{r}} \tag{C.14}$$

$$\underset{\sim}{\bar{H}}(\bar{r},t) = \underset{\sim}{\mathrm{H}}_0 e^{-\bar{\gamma}\cdot\bar{r}} \tag{C.15}$$

where $\underset{\sim}{\mathrm{E}}_0$ *and* $\underset{\sim}{\mathrm{H}}_0$ are constant vectors and $\bar{\gamma}$ is the propagation constant vector

$$\bar{\gamma} = \gamma_x\hat{x} + \gamma_y\hat{y} + \gamma_z\hat{z} \tag{C.16}$$

If we substitute (C.14) and (C.15) into (C.10) through (C.13) yields:

$$\bar{\gamma} \times \underset{\sim}{\mathrm{H}}_0 = -\omega\varepsilon_0\varepsilon_r[\wedge]\underset{\sim}{\mathrm{E}}_0 \tag{C.17}$$

$$\bar{\gamma} \times \underset{\sim}{\mathrm{E}}_0 = \omega\mu_0\mu_r[\wedge]\underset{\sim}{\mathrm{H}}_0 \tag{C.18}$$

$$\bar{\gamma} \cdot [\wedge]\underset{\sim}{\mathrm{E}}_0 = 0 \tag{C.19}$$

$$\bar{\gamma} \cdot [\wedge]\underset{\sim}{\mathrm{H}}_0 = 0 \tag{C.20}$$

From these we can obtain the dispersion relation

$$\frac{\gamma_x^2}{bc} + \frac{\gamma_y^2}{ac} + \frac{\gamma_z^2}{ab} = \gamma_0^2 \tag{C.21}$$

where

$$\gamma_0^2 = \omega^2\varepsilon_0\mu_0\varepsilon_r\mu_r \tag{C.22}$$

The "ellipsoidal" equation (C.21) satisfied by

$$\gamma_x = \gamma_0\sqrt{bc}\cos\theta \tag{C.23}$$

$$\gamma_y = \gamma_0 \sqrt{ac} \sin\theta \cos\phi \tag{C.24}$$

$$\gamma_z = \gamma_0 \sqrt{ab} \sin\theta \sin\phi \tag{C.25}$$

Therefore we can manipulate the propagation constant by choosing a, b and c.

In order to facilitate the calculation of the plane wave reflection coefficient at the Region #1 / Region #2 interface, we choose the coordinates so that the propagation vectors lie in the x-y plane as shown in Fig. C.2

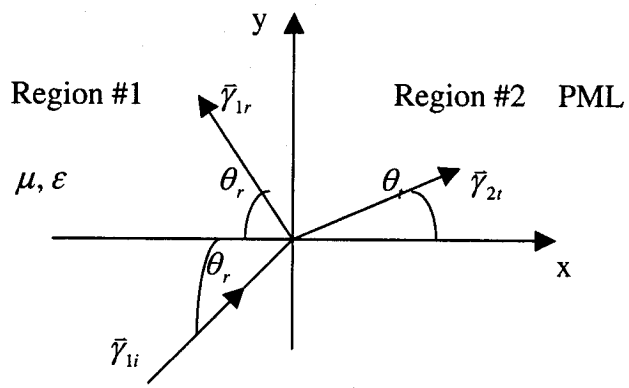

Figure C.2 : The Propagation vectors of the Incident, Reflected and Transmitted Waves at the Interface.

In this case (C.23) to (C.25) reduce to

$$\gamma_x = \gamma_0 \sqrt{bc} \cos\theta \tag{C.26}$$

$$\gamma_y = \gamma_0 \sqrt{ac} \sin\theta \tag{C.27}$$

$$\gamma_z = 0 \tag{C.28}$$

To get the relationship between reflection coefficients and a, b, c, we choose θ to be the angle between propagation constant vector and x-coordinate.

Any arbitrary plane wave can be decomposed to a linear combination of TE and TM modes. For simplicity we consider only TE mode. With the same way we can calculate TM mode. For TE mode we have

$$\tilde{\bar{E}}_i(\bar{r}) = \hat{z}\mathrm{E}e^{-j\gamma_0(x\cos\theta_i + y\sin\theta_i)} \tag{C.29}$$

$$\tilde{\bar{E}}_r(\bar{r}) = \hat{z}R^{TE}\mathrm{E}e^{-j\gamma_0(-x\cos\theta_r + y\sin\theta_r)} \tag{C30}$$

$$\tilde{\bar{E}}_t(\bar{r}) = \hat{z}T^{TE}\mathrm{E}e^{-j\gamma_0(x\sqrt{bc}\cos\theta_t + y\sqrt{ac}\sin\theta_t)} \tag{C.31}$$

$$\tilde{\bar{H}}_i(\bar{r}) = \hat{z}\sqrt{\frac{\varepsilon_0\varepsilon_r}{\mu_0\mu_r}}(\hat{x}\sin\theta_i - \hat{y}\cos\theta_i)\mathrm{E}e^{-j\gamma_0(x\cos\theta_i + y\sin\theta_i)} \tag{C.32}$$

$$\tilde{\bar{H}}_r(\bar{r}) = R^{TE}\sqrt{\frac{\varepsilon_0\varepsilon_r}{\mu_0\mu_r}}(\hat{x}\sin\theta_r + \hat{y}\cos\theta_r)\mathrm{E}e^{-j\gamma_0(-x\cos\theta_r + y\sin\theta_r)} \tag{C.33}$$

$$\tilde{\bar{H}}_t(\bar{r}) = T^{TE}\sqrt{\frac{\varepsilon_0\varepsilon_r}{\mu_0\mu_r}}\left(\hat{x}\sqrt{\frac{c}{a}}\sin\theta_t - \hat{y}\sqrt{\frac{c}{b}}\cos\theta_t\right)\mathrm{E}e^{-j\gamma_{01}(x\sqrt{bc}\cos\theta_t + y\sqrt{ac}\sin\theta_t)} \tag{C.34}$$

where R^{TE} *and* T^{TE} are reflection coefficient and transmission coefficient respectively. According to the boundary conditions the tangential fields should be continue on the interface between region 1 and region 2. Therefore at x = 0 we have

For $\tilde{\bar{E}}_z$

$$\hat{z}\mathrm{E}e^{-j\gamma_0 y\sin\theta_i} + \hat{z}R^{TE}\mathrm{E}e^{-j\gamma_0 y\sin\theta_r} = \hat{z}T^{TE}\mathrm{E}e^{-j\gamma_0 y\sqrt{ac}\sin\theta_t} \tag{C.35}$$

For $\tilde{\bar{H}}_y$

$$\begin{aligned}&\hat{y}\sqrt{\frac{\varepsilon_0\varepsilon_r}{\mu_0\mu_r}}\cos\theta_i\mathrm{E}e^{-j\gamma_0 y\sin\theta_i} - \hat{y}R^{TE}\sqrt{\frac{\varepsilon_0\varepsilon_r}{\mu_0\mu_r}}\hat{y}\cos\theta_r\mathrm{E}e^{-j\gamma_0 y\sin\theta_r}\\ &= \hat{y}T^{TE}\sqrt{\frac{\varepsilon_0\varepsilon_r}{\mu_0\mu_r}}\sqrt{\frac{c}{b}}\cos\theta_t\mathrm{E}e^{-j\gamma_0 y\sqrt{ac}\sin\theta_t}\end{aligned} \tag{C.36}$$

To satisfy (C.35) and (C.36) on the interface $\vec{E}$ and $\vec{H}$ must match both on magnitude and phase. The magnitude matching results in:

$$1 + R^{TE} = T^{TE} \tag{C.37}$$

$$\cos\theta_i - R^{TE}\cos\theta_r = T^{TE}\sqrt{\frac{c}{b}}\cos\theta_t \tag{C.38}$$

The phase matching results in:

$$\sin\theta_i = \sin\theta_r \tag{C.39}$$

and

$$\sin\theta_i = \sqrt{ac}\sin\theta_t \tag{C.40}$$

Solve (C.37) to (C.40) we obtain the reflection coefficient

$$R^{TE} = \frac{\cos\theta_i - \sqrt{\frac{c}{b}}\cos\theta_t}{\cos\theta_i + \sqrt{\frac{c}{b}}\cos\theta_t} \tag{C.41}$$

Impose the condition

$$\sqrt{ac} = 1 \tag{C.42}$$

Therefore from (C.40) we have

$$\theta_i = \theta_t \tag{C.43}$$

Impose anther condition

$$b = c \tag{C.44}$$

From (C.41) we can see that the reflection coefficient R^{TE} will be arbitrarily zero. Thus we can rewrite the condition that make the interface arbitrarily refletionless as follow:

$$[\wedge] = \begin{pmatrix} \frac{1}{s_x} & 0 & 0 \\ 0 & s_x & 0 \\ 0 & 0 & s_x \end{pmatrix} \tag{C.45}$$

where s_x is a complex value. To be agree with (C.5) and (C.6) we define

$$s_x = \alpha + \frac{\sigma_x}{j\omega\varepsilon_0} \tag{C.46}$$

We can extend the condition (C.45) to be a general form [22]:

$$[\wedge] = \begin{pmatrix} \frac{s_y s_z}{s_x} & 0 & 0 \\ 0 & \frac{s_z s_x}{s_y} & 0 \\ 0 & 0 & \frac{s_x s_y}{s_z} \end{pmatrix} \tag{C.47}$$

where

$$s_i = \alpha + \frac{\sigma_i}{j\omega\varepsilon_0}, \qquad i = x, y, z \tag{C.48}$$

For different PML regions as shown in Fig. C.3

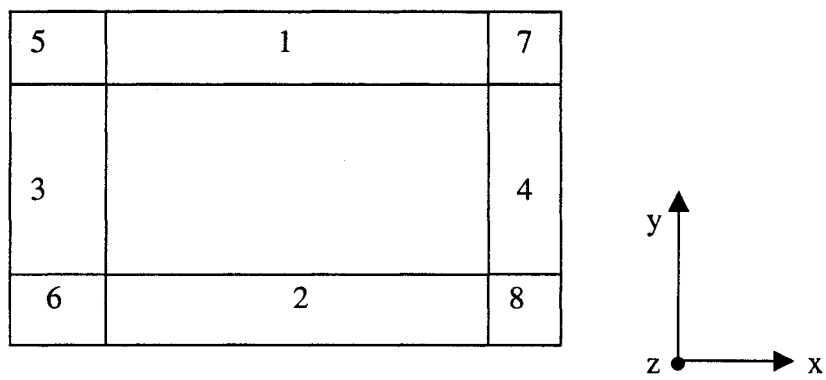

Figure C.3 : Different PML regions

The parameters, s_i, are as follows :

PML Parameters	PML Regions							
	1	2	3	4	5	6	7	8
s_y	s_1	s_2	1	1	s_1	s_2	s_1	s_2
S_x	1	1	s_3	s_4	s_3	s_3	s_4	s_4
S_z	1							

APPENDIX D : SEMI-ANALYTICAL SOLUTIONS FOR TRANSIENT PLANE WAVES IN DISPERSIVE MEDIA

D.1 PLANE WAVES IN AN UNBOUNDED DISPERSIVE

Analytical time-domain solutions for modulated-carrier electromagnetic waves in dispersive media do not appear to be available, even when the electromagnetic waves are plane waves. We therefore use what we have termed "semi-analytical" solutions in order to validate the solutions obtained via the EVFE method.

An expression for the electric field of a time-harmonic (unmodulated) plane wave of frequency ω, in a general lossy medium, is [23]

$$E(\omega, x) = E^{inc}(\omega, x = x_i) e^{j\omega t_{snap}} e^{-\gamma(x - x_i)} \tag{D.1}$$

We have here assumed that the wave is propagating in the x-direction, and that at frequency ω the complex propagation constant is $\gamma(\omega) = \alpha(\omega) + j\beta(\omega)$. The term $E^{inc}(\omega, x = x_i)$ is the complex phasor value of the field (in other words, the Fourier transform of the fields) at some selected reference point $x = x_i$ along the x-axis.

t_{snap} is the time at which the "snapshot" is taken.

This can be converted into the time-domain solution through use of the inverse Fourier transform.

D.2 PLANE WAVE REFLECTION AT A PLANAR INTERFACE BETWEEN NON-DISPERSIVE AND DIEPSERSIVE MATERIAL

In this example the analytical solutions of transmission and reflection wave equations in frequency domain is as follow: [23]

$$E_T(\omega, x) = TE^{inc}(\omega, x = x_R)e^{j\omega t_{snap}}e^{-\gamma(x-x_R)} \tag{D.2}$$

$$E_R(\omega, x) = R\,E^{inc}(\omega, x = x_R)e^{j\omega t_{snap}}e^{\gamma_0(x-x_R)} \tag{D.3}$$

Where

E_T is the transmission field

E_R is the reflection field

T is the transmission coefficient

R is the reflection coefficient

$E^{inc}(\omega, x = x_R)$ is the Fourier transform of the incident field at reflection plane

t_{snap} is the time at which the "snapshot" is taken

γ is the complex propagation constant of dispersive medium and

$$\gamma = j\omega\sqrt{\mu\varepsilon}\sqrt{1 - j\frac{\sigma}{\omega\varepsilon}} \tag{D.4}$$

γ_0 is the propagation constant of vacuum and

$$\gamma_0 = j\omega\sqrt{\mu_0\varepsilon_0} \tag{D.5}$$

With the same way in 6.3 we can use numerical method to compute the inverse Fourier transformation of the solutions to get the solution in time domain.

REFERENCES

[1] A.Taflove and S.C.Hagness, *Computational Electrodynamics: The Finite-Difference Time-Domain Method, 2nd edition* (Artech House, 2000)

[2] S.D.Gedney and U.Navsariwala, "An unconditionally stable finite-element time-domain solution of the vector wave equation" *IEEE Microwave Guided Wave Lett.* Vol.5, pp.332-334, May 1995.

[3] J.F.Lee, R.Lee and A.Cangellaris, "Time-Domain Finite-Element Methods", IEEE Transactions on Antennas and Propagation, Vol. 45, No. 3, March 1997.

[4] D.-K.Sun, J.-F.Lee & Z.Cendes, "The transfinite-element time-domain method", IEEE Trans. Microwave Theory Tech., Vol.51, No.10, pp.2097-2105, October 2003.

[5] J.Jin, *The Finite Element Method in Electromagnetics ,2nd edition* (Wiley, 2002)

[6] J.N.Reddy, *An Introduction to the Finite Element Method* (McGraw-Hill, 1984)

[7] Y.Wang, and T.Itoh, "Envelope-Finite-Element (EVFE) Technique-A More Efficient Time-Domain Scheme", IEEE Transactions on Microwave Theory and Techniques, Vol. 49, No, 12, December 2001.

[8] K.Kundert, "Simulation methods for RF integrated circuits", Proceedings of ICCAD'97, pp.1-14, San Jose, USA, Nov.1997.

[9] H. S.Yap, "Designing to digital wireless specifications using circuit envelope simulation", Asia-Pacific Microwave Conf., 1997, pp. 173-176.

[10] D.Jiao and J.Ming, "Time-Domin Finite-Element Modeling of Dispersive Media", IEEE Microwave and Wireless Components, Vol. 11, No. 5, May 2001.

[11] W.Yao, Y.Wang and T.Itoh, "2-D Envelope Finite Element (EVFE) Technique Implementation of PML and dispersive medium". 2002 IEEE MTT- S CDROM

[12] P. P. Silvester and R. L. *Ferrari, Finite Elements for Electrical Engineering*, Third edition, Cambridge University Press, Great Britain, pp 73-74, 1996.

[13] J. L. Volakis and L. C. Kempel, *Finite Element Method for Electromagnetics*, IEEE Press, New York, pp1-156, 1998.

[14] Edward J. Rothwell and Mchael J. Cloud, Electromagnetics, pp 495, © 2001 by CRCPress LLC.

[15] H. P. Tsai, Y. Wang and T. Itoh, "An Unconditionally Stable Extended (USE) Finite-Element Time – Domain Solution of Active Nonlinear Microwave Circuits Using Perfectly Matched Layers", *IEEE Transactions on Microwave Theory and Techniques*, vol. 50, No. 10, October 2002.

[16] R.Luebbers, D. Steich, and K. Kunz, "FDTD Calculation of Scattering from Frequency-Dependent Materials", *IEEE Transaction on Antennas and Propagation*, pp 1249-1993, vol. 41, No. 9, September 1993.

[17] D.G.Dudley, Mathematical Foundations for Electromagnetic Theory (IEEE Press, 1994)

[18] D. M. Pozar, Microwave Engineering, Second edition, pp 172, New York, John Wiley & Sons, INC, 1998.

[19] The *MATLAB* package of *The MathWorks*, Inc., USA.

[20] Z.S.Sacks, D.M.Kingsland, R.Lee and J.Lee, "A Perfectly Matched Anisotropic Absorber for Use as an Absorbing Boundary Condition", *IEEE Transactions on Antennas and Propagation,* Vol. 43, No. 12, pp.1460-1463, December, 1995.

[21] D.M.Kingsland, J.Gong, J.L.Volakis, and J.Lee, "Performance of an Anisotropic Artificial Absorber for Truncating Finite-Element Meshes", *IEEE Transactions on Antennas and Propagation*, Vol. 4, No. 7, pp. 975-982, July, 1996.

[22] Y. Tsuji, and M. Koshiba, "Finite Element Method Using Port Truncation by Perfectly Matched Layer Boundary Conditions for Optical Waveguide Discontinuity Problems", *J. Lightwave Technology*, Vol. 20, No. 3, pp. 461-468, March, 2002.

[23] D.F.Kelley and R.J.Luebbers, "Piecewise Linear Recursive Convolution for Dispersive Media Using FDTD", IEEE Transaction on Antennas and Propagation, Vol. 44, No. 6, June 1996